THE ROLE OF INDUCIBLE NITRIC OXIDE SYNTHASE IN MACROPHAGE ACTIVATION FOLLOWING ACUTE LUNG INJURY

By

THEA NOREEN GOLDEN

A dissertation submitted to the

Graduate School-New Brunswick

And

The Graduate School of Biomedical Sciences

Rutgers, The State University of New Jersey

In partial fulfillment of the requirements

For the degree of

Doctor of Philosophy

Joint Graduate Program in Toxicology

Written under the direction of

Dr. Andrew J Gow

And approved by

_____

_____

_____

_____

_____

New Brunswick, New Jersey

OCTOBER, 2016

ABSTRACT OF THE DISSERTATION

The Role of Inducible Nitric Oxide Synthase in Macrophage Activation Following Acute Lung Injury

By THEA NOREEN GOLDEN

Dissertation Director:
Andrew Gow, PhD

Macrophage origin and activity is complex in response to acute lung injury. Inducible nitric oxide synthase (iNOS) has a divergent role in the stages following intratracheal bleomycin mediated lung injury (ITB). We hypothesize iNOS is necessary for macrophage activation during the inflammatory and resolution phases that follow ITB. Further, recruited macrophages classically activate during inflammation and resident macrophages alternatively activate during resolution. To test these hypotheses, iNOS was manipulated via scavenge of products, systemic selective iNOS inhibition and chimeric mice in which particular populations were $NOS2^{-/-}$. C57/BL6 mice were intratracheally instilled with bleomycin and samples collected 8 and 15 days following instillation. This work identified oxidants to promote inflammation during the early stages following ITB. Systemic iNOS inhibition reduced classical activation of recruited macrophages during inflammation and alternative activation of recruited macrophages during resolution. Resident macrophage alternative activation was not dependent on iNOS activity. Chimeric mice demonstrated iNOS of a particular cell population is necessary for macrophage activation. Classical activation of recruited cells is dependent

on recruited cell iNOS. Early alternative activation is promoted when recruited macrophages were iNOS incompetent. A pulmonary source of iNOS plays a role in alternative activation during resolution. This work has demonstrated iNOS is important to classical and alternative activation of macrophages. The cell population expressing iNOS determines the effect on activation. The complexity of macrophage populations and effect of iNOS activity on macrophage activation furthers our understanding of the response to ITB and adapted therapeutic approaches have potential for clinical improvement.

ACKNOWLEDGEMENTS

I have been blessed with supportive people in my life who have encouraged me to pursue and complete my PhD. I am incredibly grateful to Dr. Andrew Gow for his investment in my education. While in pharmacy school, Dr. Gow taught Pharmacology. This was the first course I experienced where memorization was not enough and I struggled to comprehend the material. I visited Dr. Gow often to go over exams and review lecture notes. By the second semester of this course I learned how to digest the material and thoughtfully answer exam questions. I also developed an interest in pharmacology and the science behind drug development. It was from this encounter that I started working in Dr. Gow's laboratory. Having an interest in teaching at the collegiate level I spoke with Dr. Gow about pursuing a research career and applying for the PhD program. Dr. Gow supported my application and agreed to have me as a PhD student in his laboratory. While in Dr. Gow's laboratory I was encouraged to explore different areas of lung inflammation and worked with him to develop my thesis project. He has supported many opportunities and projects that afforded me the chance to develop as a scientist. I have been fortunate to attend many conferences and spend a few months visiting a lab at Oxford University. He has also encouraged me to collaborate on projects outside my thesis that helped me develop as an independent researcher. He encouraged me to mentor several students so that I may begin to develop as an educator as well. The support of Dr. Gow has given me the confidence and tools to pursue a research career in academia.

I am grateful to many in the laboratory as well. Dr. Chang Jiang Guo first took me on as a pharmacy student and has continued to support me throughout my time in the laboratory. His enthusiasm for science and desire to make an impact is inspiring. Many fellow graduate students and lab members, past and present, have also supported

me scientifically and emotionally over the past few years; Dr. Debra Laskin, Dr. Helen Abramova, Pamela Scott, Dr. Alba Rossi-George, Dr. Carol Gardner, Dr. Rama Malaviya, Dr. Vasanthi Sunil, Kinal Vayas, Dr. Mili Mandal, Dr. Chris Massa, Dr. Danielle Botelho, Dr. Ashley Pettit, Sheryse Taylor, Dr. Alessandro Venosa, Mary Francis, Richard Sun and Alexa Murray.

I also thank my thesis committee members Dr. Debra Laskin, Dr. Robert Laumbach, Dr. Grace Guo and Dr. Harry Ischiropoulos. I appreciate your time reviewing my thesis and insight into its development.

I am incredibly grateful to the pharmacy school for its financial support. The pharmacy school has supported me through numerous scholarships while a pharmacy student and PhD candidate. It was their development of the PharmD/PhD program and my acceptance into this program that afforded me the right to be granted my F31 grant for PharmD/PhD students. Their financial support has also allowed me to attend many conferences and grow a network that has been and will continue to be useful.

I am grateful for the trust collaborators have had in me in the development of projects. Dr. Elena-Atochina Vasserman and Dr. Vera Krymskaya have given me the opportunity to work on an exciting project that includes human and mouse studies. The tools and skills I learned during this work will continue to serve me as I go forward. I am also grateful to Dr. Anant Madabhushi, Dr. Mirabela Rusu and Dr. Haibo Wang for their efforts in our collaborative project.

Many undergraduate and high school students have worked with me over the past few years. They have reminded me with their excitement and curious minds of my own scientific curiosity and desire to pursue an academic career. Working with them also taught me the hard lesson of managing time and organization. Much of their work resulted in analysis and data useful for projects. I thank Emily Do, SoHyun Rhee, Shivani Gupta, Eunice Jang, Seo Yung Lee, Dae Ho Lee and Emma Frenchu.

I am also incredibly grateful to my family and friends. My parents have supported me emotionally and financially to pursue this career. My sister has pulled me out of the lab and my science world to remind me there is so much more to life. The toxicology program is filled with great students; they have entertained me at every makeshift party we've thrown. I am incredibly grateful to Jamie and Allison for our late night M&M eating study dates that turned into weekly dinners with Kara, Brian and Kristin. I am thankful despite our busy schedules we kept them a priority. I also thank my pharmacy friends, Kaly, Rachel and Liz, who despite thinking me crazy for staying in school supported me and kept me in the loop on changes to pharmacy laws and deadlines for CE credits and license renewals. Finally, I thank Ashley for being a second pair of hands for my crazy dog and reminding me it's ok to care so much about my career. The people in my life have made me believe this was possible and reasonable.

ACKNOWLEDGEMENT OF PUBLICATIONS

CHAPTER 2

Shi, JD.,* **Golden, TN.,*** Guo, CJ., Tu, SP., Scott, P., Lee, MJ., Yang, CS. and Gow, AJ. Tocopherol supplementation reduces NO production and pulmonary inflammatory response to bleomycin. *Nitric Oxide*. 2013 Nov 1; 34:27-36.

CHAPTER 3

Golden, TN. and Gow, AJ.

In preparation for submission

CHAPTER 4

Golden, TN., Crabtree, MJ., Channon, K. and Gow, AJ.

In preparation for submission

APPENDIX 1

Atochina-Vasserman, EN., Guo, CJ., Abramova, E., **Golden, TN**., Sims, M., James, ML., Beers, MF., Gow, AJ. and Krymskaya VP. Surfactant dysfunction and lung inflammation in the female mouse model of lymphangioleiomyomatosis. *Am J Respir Cell Mol Biol.* 2015 Jul;53(1):96-104

APPENDIX 2

Rusu, M., **Golden, T**., Wang, H., Gow, AJ. And Madabhushi, A. Framework for 3D histological reconstruction and fusion with in vivo MRI: Preliminary results of characterizing pulmonary inflammation in a mouse model. Med Phys. 2015 Aug;42(8):4822-32

TABLE OF CONTENTS

LIST OF FIGURES

LIST OF TABLES

.

CHAPTER 1: BACKGROUND

1.1 Pulmonary Innate Immunity

The lung is populated by resident macrophages uniquely positioned to deal with environmental stimuli. These myeloid cells are derived from the yolk sac in 2 successive hematopoietic waves (Orkin and Zon, 2008). A F4/80+ Mac2- macrophage population is present in the interstitial space at E10.5 and this population is joined by F4/80- Mac2+ macrophage population by E15.5 (Tan and Krasnow, 2016). The Mac2+ population moves into alveoli from the interstitium during postnatal week 1. Adult resident alveolar macrophages are embryological in origin (Schulz et al., 2012; Yona et al., 2013).

Resident macrophage population turnover depends on the anatomical location of the population. In the mouse, alveolar macrophages live for as long as 8 months (Murphy et al., 2008). Without injury, alveolar macrophages self-renew and are not blood derived (Tarling and Coggle, 1982; Landsman and Jung, 2007; Hashimoto et al., 2013; Yona et al., 2013). Local proliferation is possible via granulocyte macrophage colony stimulating factor (GM-CSF) and macrophage colony- stimulating factor (M-CSF) through colony stimulating factor 1 receptor (CSFR1) in the lung (Hume et al., 1988; Jenkins et al., 2013) and pleural cavity (Jenkins et al., 2011). Monoclonal antibody to CSFR1 results in depletion of alveolar macrophages (MacDonald et al., 2010). However, interstitial macrophages replace from the blood (Zaynagetdinov et al., 2013) and the number is not dependent on CSFR1 (MacDonald et al., 2010). Some evidence suggests the interstitial macrophage can serve as an intermediate to alveolar macrophages but under what conditions has yet to be fully understood (Landsman and Jung, 2007). Interestingly, the source of resident macrophage population turnover depends on the population in need of replacement.

Resident macrophages also have different roles depending on their location in the lung. As a reflection of these roles their phenotype also varies by location. Alveolar

macrophages are highly phagocytic and immuno-tolerant (Toews et al., 1984; von Garnier et al., 2005; Bedoret et al., 2009; Guth et al., 2009; Zaynagetdinov et al., 2013) as these are the macrophages to first respond to inhaled substances. Consistent with their function, alveolar macrophages express high levels of macrophage markers, F4/80, Cd68 and Siglec F, scavenger receptors, Cd206 and Cd204, pulmonary integrin, Cd11c, and low levels of MHCII (von Garnier et al., 2005; Bedoret et al., 2009; Guth et al., 2009; Misharin et al., 2013; Zaynagetdinov et al., 2013). Interstitial macrophages are less phagocytic and immune-tolerant and thereby express lower levels of scavenger receptors, Cd204 and Cd206, and higher expression of MHCII and CD2 (Bedoret et al., 2009; Zaynagetdinov et al., 2013). These macrophages express F4/80 and Cd68 but not pulmonary integrin Cd11c (von Garnier et al., 2005; Bedoret et al., 2009; Zaynagetdinov et al., 2013). The combination of these proteins allows for immunophenotyping to determine macrophage location in lung digest. Digest of the BALB/C mouse using expression of these proteins identifies the ratio of macrophage populations to be 2:1 alveolar to interstitial (Bedoret et al., 2009).

Resident macrophage phenotype is influenced by the environment. Extra pulmonary macrophages, bone marrow derived (BMDM) or peritoneal, express pulmonary integrin Cd11c if instilled in the lung (Guth et al., 2009). GM-CSF and surfactant protein D (SPD) are key proteins in regulating the expression of Cd11c on BMDMs intratracheally instilled into the lung (Guth et al., 2009). The epithelium influences alveolar macrophages to suppress T cell stimulation via TGFβ and prostaglandins (Roth and Golub, 1993). FoxP3 expression on naïve T cells in culture and in-vivo is stimulated by TGFβ and retinoic acid thereby promoting tolerance (Coleman et al., 2013; Soroosh et al., 2013). This demonstrates the interaction of alveolar macrophages and epithelial cells is influential in maintaining phenotype.

Resident macrophage turnover is seen post injury to the lung. Sterile and infectious caused injury leads to different turnover of resident macrophages. Lethal radiation depletes alveolar macrophages leading to replacement from either a pulmonary or blood source (van oud Alblas and van Furth, 1979; Tarling et al., 1987; Kennedy and Abkowitz, 1998; Landsman and Jung, 2007; Hashimoto et al., 2013). The source and dose of radiation influences the extent of turnover. Patients that have undergone irradiation for bone marrow transplant were studied to determine the extent of resident macrophage turnover. Bronchoalveolar lavage was performed 50 days after transplant and cells were found to be of the recipient's genetics and similar in number to pre-radiation (Nakata et al., 1999). LPS treatment has been shown to deplete alveolar macrophages and replacement is from Gr1 low monocytes (Maus et al., 2006; Landsman and Jung, 2007). On the other hand, toxoplasmosis infection depletes resident alveolar macrophages but replacement is via self-renewal over 4 weeks (Hashimoto et al., 2013). Resident macrophages turnover in response to injury is a dynamic process capable of replacing from pulmonary or blood sources.

1.2 Recruitment

Circulating murine monocytes are divided into 3 populations based on expression of Ly6C. Ly6C+ monocytes are similar to human CD14+ CD16- monocytes (Burke et al., 2008). Ly6C+ monocytes express CCR2 and inflamed tissue most commonly recruits these monocytes (Sunderkotter et al., 2004). Ly6C+ monocytes move between bone marrow and blood (Sunderkotter et al., 2004; Varol et al., 2007) and have a half-life of 1-3 days (Yang et al., 2014). Ly6C- monocytes are comparable to human CD14-CD16+ monocytes (Burke et al., 2008). Ly6C- monocytes arise from Ly6C+ in circulation (Sunderkotter et al., 2004; Landsman et al., 2007; Varol et al., 2007; Geissmann et al., 2010; Yang et al., 2014) and the number of Ly6C+ monocytes

determines their half-life (Yona et al., 2013). Maturation from Ly6C+ to Ly6C- monocytes is under the control of CSF1R (Hume et al., 1988; MacDonald et al., 2010). Ly6C- monocytes express CX3CR1 and move via LAF-1/ICAM1 to patrol blood vessels (Auffray et al., 2007; Yang et al., 2014). These monocytes migrate into tissue experiencing Th2 inflammation. For instance, Ly6C- monocytes are the first to migrate into the peritoneum infected with *Listeria monocytogenes* (Auffray et al., 2007). Ly6C intermediate monocyte population has been identified but less is known about this population. Ly6C intermediate monocytes express CCR7 and CCR8 and participate in lymph node trafficking (Yang et al., 2014). Monocytes are a diverse population and their phenotype determines recruitment.

Monocytes are recruited to tissue in response to chemokines. C-C chemokine receptor 2 (CCR2) is a chemokine receptor necessary for monocyte egress from the bone marrow and migration to the lung in times of inflammation. CCR2 is necessary for bone marrow egress with and without inflammation (Tsou et al., 2007). Epithelial cells release C-C chemokine ligand 2 (CCL2) signaling for monocyte recruitment. Influenza leads to TNFα release by alveolar macrophages signaling epithelial CCL2 secretion (Herold et al., 2006). CCR2 knockout mice have reduced monocyte recruitment to the lung following intratracheal LPS (Maus et al., 2002) or bleomycin (Tighe et al., 2011). Enhanced expression of CCR2 increases the number of monocytes recruited to the lung following intratracheal bleomycin (Liang et al., 2012) or without injury (Srivastava et al., 2005). CCR2 also participates in neutrophil chemotaxis and changes to recruitment are similar to monocytes (Maus et al., 2002; Dhaliwal et al., 2012). In many models, knockout or enhancement of CCR2 expression, there is evidence of a role of CCR2 in monocyte recruitment.

Monocytes use Cd11b to migrate to inflamed tissue (Kirby et al., 2006). Monocytes express Cd11b (Prieto et al., 1994) and expression is increased in response

to CCL2 (Liang et al., 2012). Loss of Cd11b, via diphtheria toxin administration, reduces the number of neutrophils and monocytes recruited to the lung post LPS (Dhaliwal et al., 2012).

The intricacy of the chemokine system specifically recruits monocyte populations. For instance, CCR2 expressing monocytes become exudative macrophages in the lung following LPS instillation (Herold et al., 2011). Monocytes that take on the phenotype of alveolar macrophages following Streptomyces pneumonia are dependent on Cd11b (Kirby et al., 2006). Additionally, interferon type 1 recruits Ly6C+ monocytes to the lung post influenza infection (Seo et al., 2011). Chemokines specifically recruit monocyte populations that will further activate to particular phenotypes in tissue.

1.3 Macrophage Differentiation and Activation

Upon recruitment to tissue, monocytes differentiate into macrophages. Generally speaking, Ly6C+ mature into classically activated macrophages and Ly6C- monocytes mature into alternatively activated macrophages (Auffray et al., 2007). There are exceptions to this rule (Arnold et al., 2007; Saederup et al., 2010; Rivollier et al., 2012; Egawa et al., 2013) supporting the complexity of macrophage biology. Endothelial cells participate in monocyte maturation (Randolph et al., 1998). Upon differentiation to macrophage from monocyte, macrophages express surface protein F4/80 (Austyn and Gordon, 1981; Morris et al., 1991). F4/80 is important to macrophage function as an antigen presenting cell but is universally expressed upon maturation (Lin et al., 2005).

Upon entry to inflamed tissue, macrophages activate based on the environment and signals. Originally, macrophage activation was described as linear polarization with activation to one of two endpoints classical or alternative activation (Gordon, 2003). Recently, Dr. Gordon and Martinez reviewed the literature of activation and explain activation is complex and should be thought of as a spectrum (Martinez and Gordon,

2014). Mosser and Edwards similarly refer to macrophage activation along a spectrum as depicted below (Mosser and Edwards, 2008). They point out environmental influences further influence macrophage activation and use a pie chart to illustrate the complexity caused by interaction with cells of the environment.

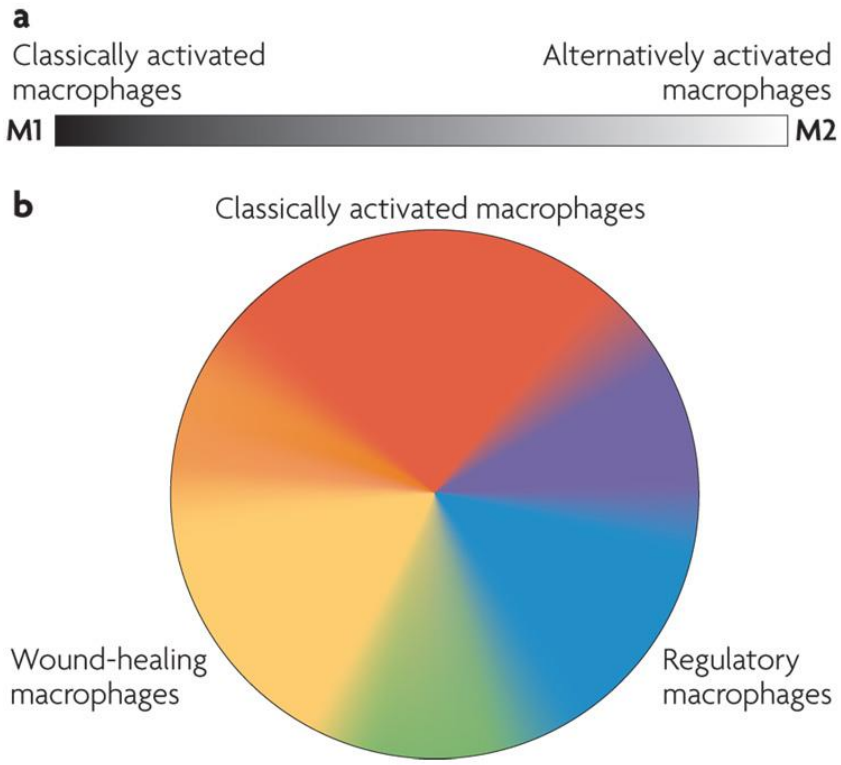

Activation allows macrophages to participate in processes such as phagocytosis, endocytosis, secretion, microbial killing, chemotaxis, adhesion and release of trophic factors (Mantovani et al., 2004). Classical activation was first termed by Mackaness in 1962 for macrophage microbial activity towards *Listeria* and *bacillus calmette-guerin* (BCG) (Mackaness, 1962). Decades later, alternative activation was identified in-vitro after stimulation with IL4 and IL13 (Stein et al., 1992; Doyle et al., 1994) and in-vivo in a nematode infection (Loke et al., 2002). Mills and colleagues termed these activation states as M1, classically activated, and M2, alternatively activated based on T cell nomenclature (Mills et al., 2000). They also identified an important difference between the two activation states, their use of arginine. M1 macrophages metabolize arginine to

nitric oxide and M2 to trophic polyamines thus demonstrating one mechanism by which polarization accomplishes its goal of microbial killing and tissue repair, respectively. Mantovanni later reformed the M2 nomenclature to assign different alternative activation pathways a, b or c notation (Mantovani et al., 2004). This early work established a clear, yet admittedly over simplified, manner to distinguish activation states.

There are key stimuli that promote classical or alternative activation pathways. Depending on the stimuli, downstream pathways vary thus tweaking activation to achieve the goal at hand. For instance, classical activation in response to IFNγ leads to activation of Janus kinase 1 and 2 adaptors thus stimulating Signal transducers and activators of transcription (STAT) 1 (Nau et al., 2002; Martinez et al., 2006). LPS also classically activates but through recognition by toll like receptor (TLR) 4. TLR4 leads to release of cytokines, chemokines and antigen presenting molecules controlled by activation of nuclear factor of kappa light polypeptide gene enhancer (NFκB), activator protein 1 (AP1), STAT 1 and early growth response (EGR) (Nau et al., 2002). Another key classical activator is GM-CSF. GM-CSF receptor activation leads to JAK2 recruitment and STAT5 activation. ERK and NFκB signaling is similarly downstream as is V-Akt murine thymoma viral oncogene homolog 1 (AKT) and IRF5 (Martinez et al., 2013). These are key stimuli of classical activation and show the overlap but distinct downstream pathways.

Alternative activation (M2) has many stimuli resulting in different pro-resolving or repair pathways. IL4, the first identified stimuli of alternative activation, activates JAK 1 and JAK leading to STAT 6 activation and translocation. This induces macrophage fusion, decreases phagocytosis and increases expression of transglutaminase 2, mannose receptor, cholesterol hydrolase CH25H and prostaglandin-endoperoxide synthase (PTGS1) (Martinez et al., 2013). Another stimulus is ligation of FcyRs, for instance on LPS activated macrophages, which turns off IL12 and increases secretion of

IL10 and glucocorticoids (Mantovani et al., 2004). This leads to antigen presentation and Th2 responses (Anderson and Mosser, 2002; Edwards et al., 2006). Lastly, mcsf stimulation leads to nuclear translocation of SP1 and downstream growth promoting pathways like angiogenesis (Curry et al., 2008). Alternative activation is a broad term for diverse pathways macrophages take that are different from classical activation and overall support repair and resolution.

1.4 Nitric Oxide Physiology and Pathology

Nitric oxide (NO) is an important signaling molecule in the lung. NO regulates bronchial tone (Drazen et al., 1995), vasodilatation (Furchgott and Vanhoutte, 1989), branching morphogenesis (Auten et al., 2007), innate and adaptive immunity (Coleman, 2001) and alveolar development (Bland et al., 2005). Nitric oxide is produced by nitric oxide synthase enzymes, endothelial, neuronal and inducible. Inducible NOS (iNOS) differs from other isoforms of NOS in that it is inducibly expressed and produces nitric oxide at a high flux rate while the others are constitutively expressed and produce NO at a low flux rate.

NO plays a role in a number of pulmonary pathologies including pneumonia (Adrie et al., 2001), sepsis (Razavi et al., 2005), chronic lung disease (Munson et al., 2005), cystic fibrosis (Grasemann et al., 1999), asthma (Dweik et al., 2001) and cancer (Masri et al., 2005). In times of inflammation, iNOS expression is induced in pulmonary epithelial cells and leukocytes (Guo and Erzurum, 1998; Guo et al., 2016). NO has a wide range of biological targets including cysteine residues within proteins to form S-nitrosocysteines process termed S-nitrosylation). S-nitrosylation is an important post-translational protein modification and has significant implications for cell signaling (Gow et al., 2004; Gaston et al., 2006; Lee et al., 2011), lymphocyte development (Yang et al., 2010) and apoptosis (Hara et al., 2005). Functional regulation of immunomodulatory

proteins is achieved by S-nitrosylation; NFκB(Kelleher et al., 2007), Keap1 (Buckley et al., 2008), HDAC2 (Malhotra et al., 2011), GAPDH (Hara et al., 2005), Hmgb-1 (Tsoyi et al., 2010) and SP-D (Guo et al., 2008).

1.5 Clinical Acute Lung Injury Pathology

Acute lung injury (ALI) and the more severe form acute respiratory distress syndrome (ARDS) affect many people with and without prior lung disease. ARDS was first termed by Ashbaugh and colleges in 1967 after diagnosing several patients with a similar pathology (Ashbaugh et al., 1967). After decades of case reports, The American-European Consensus conference on acute respiratory distress syndrome agreed upon a definition (Bernard et al., 1994). It includes; acute onset of diffuse bilateral pulmonary infiltrates as identified on chest radiography, a PaO_2/FiO_2 less than 300 for ALI and less than 200 for ARDS, and no clinical evidence of left arterial hypertension (pulmonary artery wedge pressure less than 18). Incidence remains high; 64.2 diagnosed per 100,000 health people from 1996-1999 (Goss et al., 2003) and 78.9 per 100,000 healthy people in 2005 (Rubenfeld et al., 2005). Despite high incidence of ARDS, mortality has decreased. Decades ago mortality was reported 64-70% (Fowler et al., 1983; Villar and Slutsky, 1989; Milberg et al., 1995; Ware and Matthay, 2000) and has declined to 40% (Rubenfeld et al., 2005).

Over the past decades, understanding of the pathogenesis and predisposing clinical factors has improved. Several predisposing clinical factors include pulmonary related, sepsis, pneumonia, aspiration, smoke or toxic gas inhalation and chronic lung disease, and non-pulmonary related, trauma, pancreatitis, blood transfusions, chronic alcohol abuse and multiple co-morbidities (Ware and Matthay, 2000). These predisposing factors cause ALI by disruption of the endothelial and epithelial barrier. Loss of this barrier results in excessive neutrophil migration and release of pro-

inflammatory cytotoxic mediators (Ware and Matthay, 2000; Matthay and Zimmerman, 2005). Upon loss of the barrier, alveolar spaces become overwhelmed with fluid. Down regulation of Na^+/K^+ ATPase pumps leads to poor resolution of alveolar edema (Pugin et al., 1999; Ware and Matthay, 2000). Reduction of surfactant proteins is seen in ARDS, likely due to type II epithelial cell death, and may be the reason for reduced pulmonary compliance (Greene et al., 1999). The initial pathological loss of barrier function therefore results in many downstream effects including inflammation and poor gas exchange.

The release of cytokines is a valuable tool for identifying biomarkers of ARDS. Elevated levels of interleukin 6 (IL6), interleukin 8 (IL8) and tumor necrosis factor alpha (TNFα) are measured in the BAL (Meduri et al., 1995; Pugin et al., 1999) and plasma (Pugin et al., 1999; National Heart et al., 2006) of diagnosed ARDS patients and lower plasma levels correlate with higher mortality (Pugin et al., 1999; Parsons et al., 2005). ARDS patients also have signs of coagulation and fibrinolysis; higher plasma levels of plasminogen activator inhibitor-1 and lower protein C (Meduri et al., 1998; Ware and Matthay, 2000). A sign of endothelial injury and activation, von Willebrand factor (vWf) is elevated in plasma and edema fluid from the lungs of ARDS patients (Ware et al., 2001; Ware et al., 2004; Flori et al., 2007). High levels of intracellular adhesion molecule-1 (ICAM1) are measured in plasma and edematous fluid of the lung from ARDS patients (Flori et al., 2003; McClintock et al., 2008; Calfee et al., 2009). Markers of pulmonary epithelial injury are also detected in the serum of ARDS patients. Surfactant proteins A and B are reduced in the BAL of patients at risk and diagnosed with ARDS and surfactant protein D was reduced in the BAL but elevated in the serum of ARDS patients who died (Greene et al., 1999; Eisner et al., 2003). Transmembrane immunoglobulin expressed on Type I epithelial cells (RAGE) is elevated in the serum of ARDS patients and elevated levels are strongly associated with poor outcomes in high tidal volume

mechanical ventilation (Calfee et al., 2008). These biomarkers in combination are valuable in diagnosing ARDS and following response to treatment.

1.6 Treatment of Acute Lung Injury

Treatment of ARDS and ALI relies heavily on mechanical ventilation in order to improve gas exchange. Ventilator strategies have been adapted over the decades and successfully improved therapy. Pharmacologic approaches however are for the most part unsuccessful. In 2000, the Acute Respiratory Distress Syndrome Network published the results of a clinical trial comparing 2 ventilation strategies (Network, 2000). After evaluating 861 patients with ALI or ARDS, the investigators stopped the trial early because of a successful outcome. This trial compared the then current practice of ventilating with a tidal volume of 12mL/kg and plateau pressure <50cm H_2O to 6mL/kg and plateau pressure <30cm H_2O. The investigators reported a reduction in mortality from 40% to 31% using the low tidal volume approach.

Mechanical ventilation causes release of cytokines. IL6 and TNFα are elevated in the plasma and intra-alveolar space following mechanical ventilation (Ranieri et al., 1999). Lower tidal volume attenuates cytokine response and reduces inflammation. Elevated plasma levels of IL6, IL8 and IL10 have been reported reduced in patients ventilated with lower tidal volumes (Parsons et al., 2005). Lower tidal volumes reduce IL6 and TNFα in the plasma but not intraalveolar space (Stuber et al., 2002). This suggests mechanical ventilation potentiates the loss of barrier thus allowing elevated cytokines to be released from the intra alveolar space to systemic circulation.

Fluid management has also recently been revised after the National Health Lung and Blood Institute reported the results of a clinical trial comparing conservative to liberal strategies in 2006 (National Heart et al., 2006). This clinical trial did not have conclusive results but did show conservative fluid management improved oxygenation and

shortened duration of mechanical ventilation. Importantly, conservative fluid management did not increase other organ failure.

Pharmacologic approaches have primarily focus on inhibiting inflammatory pathways. Glucocorticoids were used as early as 1967 when ALI/ARDS was first termed (Ashbaugh et al., 1967). However, despite continued use, their benefits are questionable. When used acutely following diagnosis clinical trials have yet to demonstrate efficacy (Bernard et al., 1987; Luce et al., 1988). However, when started upon initial diagnosis and therapy continued for prolonged periods of time, methylprednisolone was shown to decrease mortality (Meduri et al., 1998). Timing is particularly important as demonstrated by increased mortality in patients started on methylprednisolone 2 weeks after diagnosis (Steinberg et al., 2006). These inconclusive results suggest the inflammatory processes during ALI and ARDS are complicated and thus timing of immunomodulatory drugs like corticosteroids is important.

Many other pharmacologic approaches to modulating the inflammatory response to ALI/ARDS have been attempted without much success. Inhaled nitric oxide initially demonstrated benefit (Dellinger et al., 1998) but later trials have not supported this initial claim (Gebistorf et al., 2016). Replacement of surfactant proteins via aerosolized surfactant was also an approach without success (Anzueto et al., 1996). Long acting beta agonist, salbuterol, was attempted in order to improve lung function but results showed no benefit (Perkins et al., 2006; Singh et al., 2014). Approaches to reduce oxidative stress, such as intravenous administration of N-acetyl cysteine, have also shown no benefit (Domenighetti et al., 1997). Many other treatment approaches have been attempted without benefit and leave doctors without a clear treatment approach. Improvements to therapy rely on a better understanding of the cellular processes of injury and subsequent inflammation.

1.7 Models of Acute Lung Injury

Studying human acute lung injury and acute respiratory distress syndrome has been achieved through many rodent and non-rodent models. Human and rodents have many differences important to understand when modeling ALI. Anatomically speaking, rodents have different branching patterns of airways and pulmonary vasculature. Rodents also breathe at a faster rate than humans through their nose only. Rodents are also far less genetically complex than humans and the complexity of humans is further increased by comorbidities and environmental exposures. However, rodents offer an experimental model that once limitations are understood offers insight to clinical disease.

In 2011, an official report was issued by the American Thoracic Society after a workshop was held between many lead scientists in the field of ALI/ARDS (Matute-Bello et al., 2011). This report identified the clinical components of disease important to be represented by animal models and the main features of experimental ALI. This report is a basis by which animal models can be understood in the context of clinical disease.

The report identifies main features of experimental ALI to appropriately model clinical disease. Firstly, the onset of disease must be acute (less than 24 hours). There must also be at least one of the following: histological evidence of tissue injury, alteration of the endothelial-epithelial barrier, physiological dysfunction or inflammatory response (Matute-Bello et al., 2011). These outcomes can be measured by many endpoints. The authors suggest endpoints such as lung function and histological assessment. Lung function includes both measures of gas exchange, particularly challenging to measure blood levels of a mouse, and lung compliance, made easier by equipment such as SciReq Flexivent to measure pressure volume curves. Histologically, lungs are assessed for diffuse alveolar damage (DAD). DAD was first coined in 1976 and was defined as neutrophil accumulation, deposition of hyaline membranes thus thickening the interstitium and formation of micro thrombi (Katzenstein et al., 1976) . Finally,

permeability of the epithelial-endothelial barrier measured by protein or dye accumulation in the bronchoalveolar lavage or increased ratio of wet to dry lung tissue. The authors suggest a combination of these endpoints, or similar measures, allow for applicability of a rodent model to clinical disease.

Several models are used to study ALI/ARDS and the mechanism of injury varies. The core pathological cause of ALI is loss of epithelial-endothelial barrier and this occurs from either the vasculature or air side. For instance, many models are initially caused by endothelial cell injury leading to acute lung injury. These models include intravenous oleic acid, lipopolysaccharide or intravenously delivered bleomycin. Models also lead to ALI by causing damage directly to pulmonary epithelial cells via acid aspiration, hyperoxia and surfactant depletion by repetitive lavage or intratracheal instillation of bleomycin. A few models also exist that directly damage the epithelial and endothelial cells such as ischemia reperfusion and sepsis following cecal ligation. The choice of model should therefore be based on the particular aspect of ALI/ARDS to be studied.

Being particularly interested in the macrophage role in the inflammatory and resolution phases to follow injury, intratracheal bleomycin was chosen. The intratracheal bleomycin (ITB) model is used by many to study ALI and subsequent fibrosis. ITB causes injury by first damaging pulmonary epithelial cells via production of radical species leading to DNA strand breaks (Burger et al., 1981). Within the first 24 hours of instillation, there is recruitment of neutrophils to the lung and elevation of pro-MMP9, IL6, IL-1β and KC in the BAL (Gasse et al., 2007). TNF and IL-1 are elevated 63 hours post ITB (Cavarra et al., 2004). TGF-β is elevated 6-7 days post ITB (Cavarra et al., 2004; Gasse et al., 2007) and trichrome and collagen elevated 11 days post ITB (Cavarra et al., 2004). Macrophage numbers progressively increase with time and lymphocytes accumulate beginning 7 days post ITB (Cavarra et al., 2004). Overall, the literature identifies clear stages of ITB mediated ALI; early injury and neutrophil recruitment (day

1-3), acute inflammation with increased pro-inflammatory cytokines and macrophage accumulation (day 3-8) followed by indicators of resolution (day 15) and fibrosis (day 21) (Matute-Bello et al., 2008; Guo et al., 2016).

CHAPTER 2: TOCOPHEROL SUPPLEMENTATION REDUCES NO PRODUCTION AND PULMONARY INFLAMMATION IN RESPONSE TO BLEOMYCIN

* as published in the *Nitric Oxide Journal* 2013 November 1;34:27-36

2.1 Abstract

Bleomycin causes acute lung injury through production of reactive species and initiation of inflammation. Previous work has shown alteration to the production of reactive oxygen species results in attenuation of injury. Vitamin E, in particular, γ-tocopherol, isoform, has the potential to scavenge reactive oxygen and nitrogen species. This study examines the utility of dietary supplementation with tocopherols in reducing bleomycin-mediated acute lung injury. Male C57BL6/J mice were intratracheally instilled with PBS or 2 units/kg bleomycin. Animals were analyzed 3 and 8 days post instillation at the cellular, tissue, and organ levels. Results showed successful delivery of tocopherols to the lung via dietary supplementation. Also, increases in reactive oxygen and nitrogen species due to bleomycin are normalized in those mice fed tocopherol diet. Injury was not prevented but inflammation progression was altered, in particular macrophage activation and function. Inflammatory scores based on histology demonstrate limited progression of inflammation in those mice treated with bleomycin and fed tocopherol diet compared to control diet. Upregulation of enzymes and cytokines involved in pro-inflammation were limited by tocopherol supplementation. Day 3 functional changes in elastance in response to bleomycin are prevented, however, 8 days post injury the effect of the tocopherol diet is lost. The effect of tocopherol supplementation upon the

inflammatory process is demonstrated by a shift in the phenotype of macrophage activation. The effect of these changes on resolution and the progression of pulmonary fibrosis has yet to be elucidated.

2.2 Introduction

Bleomycin is currently used clinically as a chemotherapeutic drug, but its use is limited by development of pulmonary fibrosis. As a model of lung injury, intratracheal bleomycin (ITB) causes inflammation and consequent pulmonary fibrosis. Activated bleomycin acts as a redox-cycler causing damage to proteins, lipids and DNA through the production of reactive oxygen species (ROS) (Hay et al., 1991). The inflammatory process that is initiated by ITB also generates ROS. Furthermore, pulmonary inflammation and fibrosis in response to ITB is associated with decreases in antioxidant enzyme expression and activity, in particular superoxide dismutase, catalase and glutathione peroxidase (Santos-Silva et al., 2012; Togeiro et al., 2012). In this regard, it has been shown that increasing antioxidant defenses by supplementation of lecithinized superoxide dismutase, or increasing host injury defenses by over expressing Hsp70, abrogates ITB acute injury and inflammation (Tanaka et al., 2010a; Tanaka et al., 2010b).

Vitamin E is a powerful antioxidant capable of terminating propagation of radical reactions. Due to its antioxidant potential, vitamin E has been studied in many models of inflammation. In particular, α-tocopherol, the most well recognized form of vitamin E, has been extensively studied as an antioxidant. α-tocopherol levels in the lungs are reduced by bleomycin administration suggesting α-tocopherol is consumed in times of oxidative stress (Mert et al., 2009). Intratracheal liposomal α-tocopherol administered to

rats prior to ITB reveals that α-tocopherol successfully normalizes hydroxyproline concentrations 21 days after instillation (Suntres and Shek, 1997).

Unlike α-tocopherol, γ-tocopherol is uniquely capable of scavenging reactive nitrogen species in addition to its antioxidant potential. Due to an unsubstituted carbon at the carbon-5-position, γ-tocopherol interacts with reactive nitrogen species resulting in the formation of 5-nitro-γ-tocopherol. γ -tocopherol also inhibits lipid peroxidation, in particular by sequestering peroxynitrite. (Campbell et al., 2003; Ju et al., 2010)

Nitric oxide plays a significant role in the initiation and mediation of inflammatory signaling. Inducible nitric oxide synthase (iNOS) produces NO at a high flux rate in inflammatory and epithelial cells in times of inflammation. After ITB, loss of functional inducible nitric oxide synthase (iNOS) as demonstrated through inhibition via GW274150 or $NOS2^{-/-}$ knockout mouse, prevents nitrosative stress. Loss of functional iNOS also abrogates the development of fibrosis in CD mice measured 15 days post ITB by hydroxyproline levels and trichrome stain. (Genovese et al., 2005)

Additional models of lung injury and inflammation demonstrate a role of NOS2 in inflammation progression. Intratracheal lipopolysaccharide (LPS) also causes acute lung injury and inflammation with evidence of nitrosative stress. $NOS2^{-/-}$ knockout mice, treated with LPS, experience less nitrosative stress as evidenced by nitrotyrosine stain. $NOS2^{-/-}$ knockout mice also experience less cell infiltrate and edema as seen on histology (Kristof et al., 1998). We have also previously shown the role of iNOS in the initiation and progression of chronic inflammation. Surfactant protein-D knock out mice experience chronic inflammation that can be inhibited with 1400W, an iNOS selective inhibitor, administered early in disease progression or during active inflammation (Atochina-Vasserman et al., 2007).

Nitric oxide is known to play a role in the promotion and progression of inflammation in response to ITB (Genovese et al., 2005). By using a mixture of tocopherols, with a particularly high concentration of γ-tocopherol, within the diet there is the potential to increase the scavenging of reactive oxygen and nitrogen species and hence reduce inflammation. The ITB model is a progressive model of inflammation allowing one to evaluate both early and late responses. Pulmonary injury and inflammation are evident 3 days after instillation of bleomycin and peak after 8 days. Therefore, we examined the effects of tocopherol supplementation at both of these time points. We hypothesized that tocopherols will act early in the inflammatory process by sequestering reactive oxygen and nitrogen species (RONS) thus reduce NO driven inflammation.

2.3 Methods

Animals and Diet. 48 10-week-old male C57BL6/J mice were obtained from Jackson Laboratory (Bar Harbor, ME). Animals weighed between 20-32 grams. Animals were fed ad libitum either control diet (AIN93M) (Reeves et al., 1993) or treatment diet (0.3%**γ**TmT diet) prepared by Research Diets, Inc. (New Brunswick, NJ). **γ**TmT is a tocopherol-rich mixture of tocopherols consisting of (per gram) 130mg α-tocopherol, 15mg β-tocopherol, 568mg γ-tocopherol and 243mg δ-tocopherol (Cognis Corporation Fairfield, NJ). The tocopherol content of the two diets is shown in Table 1. Animal protocols were reviewed and approved by Animal Care and Use Committee, Rutgers University.

Intratracheal Instillation. Animals were anesthetized by intraperitoneal injection of ketamine (300mg/kg) and xylazine (15mg/kg) (Butler Schein). Each mouse was then laid on a tilting rodent work stand (Hallowell EMC Pittsfield, MA) in the supine position. The larynx was visualized using a hemi-sectioned 3mm diameter speculum with

otoscope (Welch Allyn Skaneateles Falls NY). Either LPS-negative sterile phosphate buffered saline (PBS) or LPS-negative sterile bleomycin sulfate (ITB) (Sigma Aldrich St. Louis, MO) was instilled at 2units/kg. No animals died during instillation.

Tocopherol Measurement. Tocopherol concentrations were measured in the serum and lung by high performance liquid chromatography as previously described(Guan et al., 2012). Measurements were made from in 30mg lung tissue and 20μL plasma collected from mice 8 days post instillation.

Cell Count and Protein Measurement. Bronchoalveolar lavage (BALF) was performed with 5 washes of 1mL PBS via an intratracheally-inserted cannula. BALF was centrifuged at 30,000 g for 10 mins and the cells was resuspended in PBS and counted via Multisizer Coutler Counter (Beckman Coulter). Supernatant was analyzed for protein content with Bradford protein assay kit (BioRad, Hercules, CA) reading at 595nm using MAXline Kinetic microplate reader (Molecular Devices, Sunnyvale, CA) with bovine serum albumin as standard.

mRNA Measurement. BALF cells were analyzed by RT-PCR for expression of inflammatory genes using High Capacity cDNA Reverse Transcriptase Kit (Applied Biosystems Foster City, CA). cDNA samples were analyzed on the 7300 Real Time PCR system using Taqman polymerase and primary probes obtained from Applied Biosystems. Samples ran for 40 cycles of 2 minutes at 50^{o}C, 10 minutes at 95^{o}C, and 15 seconds at 95^{o}C. Fold expression was calculated using the $2^{-\Delta\Delta Ct}$ method using β-actin as the control gene and the PBS/AIN93M samples as the control group. Samples from each treatment group were pooled into 2 sets of 4 animals for analysis.

Histochemistry. Lung tissue was inflation fixed with 1mL 3% paraformadehyde, 2% sucrose and 4% sodium cacodylate 0.1M (pH 7.3). Lungs were embedded in paraffin and stained with hematoxylin and eosin. Inflammation scores were generated using a 5-point scale by two blinded and independent observers as previously published (Rudmann et al., 1998). Tissue sections were analyzed for protein expression by immunohistochemistry. Tissue sections were deparrafinized and rehydrated with xylene and ethanol. Antigen retrieval was achieved with sodium citrate followed by endogenous peroxidase quench. Tissue was blocked with 10% goat serum in PBS for 1 hour followed by primary antibody overnight in 1% serum in PBS. Sections were washed with 0.1 to 0.3% tween20 in PBS and incubated with secondary antibody (Vector Laboratories ABC Kit Peroxidase Rabbit IgG Burlingame, CA) in 1% serum in PBS. Following further washing sections were visualized with DAB (Vector Laboratories DAB Peroxidase Substrate Kit Burlingame, CA). Antibody concentrations for the different epitopes are given in the legends of the figures. Hematoxylin was used for counterstain.

Aliquots of BALF cells (30,000 cells) were spun onto slides with Thermo Shandon Cytospin-4 at 800rpm for 3 minutes and stained for identification with KWIK-DIFF (Thermo). Cell differentials were obtained by counting 5 different fields at an optical zoom of 400x. Cytospin slides were also used to quantify the number of cells greater than 25 microns.

Chemotaxis Measurement. 100,000 RAW264.7 cells (American Type Culture Collection, TIB-71 Manassas, VA) (suspended at $1x10^{6}$ cells/mL) in Dulbecco's Modified Eagle Medium were placed in the upper chamber of a 96 well plate microchemotaxis chamber (Neuro Probe Gaithersburg, MD). 30µL of sample or control solution was placed in the lower chamber of the apparatus.. A filter, with a pore size of 5µm was

used. The chamber was incubated for 4 hours at 37 ^{o}C with 5% CO_2. Migrating cells were collected on the membrane and stained with KWIK-DIFF (Thermo), visualized at an optical zoom of 400x and counted in 5 fields on the BX51 (Olympus).

Nitric Oxide Metabolite Analysis Using the first aliquot of BALF supernatant, samples were analyzed with Ionics/Sievers nitric oxide analyzer 280 (NOA 280 Ionics Instruments). Vanadium chloride (Sigma Aldrich) (1M HCl at 95^{o}C) was used as the reducing agent and sodium nitrate as the standard.

Lung Function Testing. Lung function was measured 3 or 8 days after instillation of PBS or bleomycin. Using SciReq flexiVent (Montreal, Canada) baseline function and mechanics were measured. Measurements were taken via Forced Oscillation Technique at increasing Positive End-Expiratory Pressures (0-9 cmH_2O). Matlab software was used for analysis of parameters to calculate overall elastance and resistance profiles. Results are shown at a PEEP of 3cm H_2O, physiological PEEP.

$$\text{Resistance} = \frac{(a + b*f)}{(c + f)}$$

$$\text{Elastance} = E_0 + \Delta E*(1 - e^{(\beta * f)})$$

Statistics Data was analyzed in 2-way ANOVA and unpaired t-test or Mann-Whitney. Pulmonary inflammation scores were analyzed by Wilcoxon-Rank Test. Cell size was

analyzed by Tukey's test and chemotactic potential by Dunn's test. A *p-value* of <0.05 was considered statistically significant.

2.4 Results

Diet increases tocopherol content within the lung

Due to their ability to scavenge ROS, and reactive nitrogen species, we proposed that increasing the tocopherol content within the lung would provide protection against bleomycin-mediated injury. In this study, we manipulated tocopherol content by means of diet. Mice were fed either a control AIN93M diet or one enriched in tocopherols, especially γ-tocopherol. At the conclusion of the study, both serum and lung tissue were analyzed for tocopherol content (Table 2). The tocopherol enriched diet led to an increase in the content within both the serum and the lung with γ-tocopherol increasing 4 fold in the lung. Lung concentrations of α and δ tocopherol were also increased in those fed tocopherol enriched diet. Notably, in the absence of supplementation, ITB reduced γ-tocopherol levels two fold in the serum.

Tocopherol supplementation reduces lung injury and inflammation

Hematoxylin and eosin staining of lung tissue 3 days and 8 days after ITB shows that there is extensive consolidation and peribronchial and perivascular infiltration (Figure 1). As early as 3 days post administration there is evidence of leukocyte invasion within the lung as well as thickening of the pulmonary epithelium (Figure 1B). However, by day 8 these markers are increased in severity as well as increasing tissue destruction (Figure 1E). In the presence of tocopherol, there is still evidence of both injury and inflammation at day 3; however, there is a minimal increase in these markers over the following 5 days. Non-parametric inflammatory scoring (Rudmann et al., 1998) demonstrates that inflammation resulting from ITB is progressive from day 3 to day 8

and appears to be inhibited by the tocopherol-rich diet (Figure 1G). The progressive nature of this injury is reflected in the protein content of the BAL, which increases at both day 3 and, to a greater extent, at day 8; but is largely unaffected by tocopherol supplementation (Table 3).

Effect of tocopherol supplementation on inflammatory protein expression

The production of ROS from ITB-initiated inflammation is thought to contribute to the progress of the pathology. Cyclooxygenase-2 (COX2) and inducible Nitric Oxide Synthase (iNOS) are both key enzymes in the production of reactive oxygen and nitrogen species in the progress of inflammation. Therefore, we examined their production in response to ITB via immunohistochemistry (Figure 2 & 3). COX2 expression was evident in epithelial and invading inflammatory cells as early as 3 days post ITB (Figure 2B). However, the intensity of COX2 staining increased considerably by day 8, especially within the pulmonary epithelium (Figure 2E). In tocopherol-supplemented mice, ITB was still capable of increasing COX2 staining at day 3, however, there was minimal increase in COX2 expression by day 8 when compared to day 3 (Figure 2 C & F).

The time course of changes in iNOS expression, in response to ITB, mirror those observed for COX2 (Figure 3). At day 3 post ITB there is a small increase in iNOS expression throughout the lung parenchyma. Eight days post injury there is a focal increase within invading inflammatory cells and a less pronounced increase in the epithelium than seen for COX2. Similar to the observations with COX2, feeding with the tocopherol-supplemented diet reduced iNOS staining, although this difference was only apparent at 8 days post ITB.

Ym1 is synthesized and secreted by macrophages and is typically associated with alternative activation. In saline treated mice a few Ym1 positive macrophages can be observed (Figure 4 A & D). Following ITB treatment there is an increase in both the

frequency of Ym1 positive cells observed and the intensity of their staining. This is more pronounced at 8 days post ITB than at 3 days (Figure 4 B & E). Tocopherol supplementation reduces the frequency of Ym1 positive cells at both time points (Figure 4 C & F). However, it does not reduce the intensity with which these cells are stained. Indeed at 3 days post ITB the intensity of stain appears greater than in mice fed the control diet (Figure 4C).

Cells in the Bronchoalveolar Lavage Fluid

In parallel with the histological evidence of inflammation, there is an increase in total cell count within the BAL following ITB (Table 3). In this context, tocopherol supplementation appears to alter the kinetics of cellular accumulation, as the increase in cell number was not significant at 3 days post ITB. Examination of cell differentiation showed that ITB leads to early neutrophilia at day 3, which is not altered by the tocopherol-rich diet, with consequent increases in all inflammatory cell types 8 days post injury (Figure 5). Tocopherol supplementation alters the kinetics of the response, as both lymphocytes and eosinophils accumulate later in this condition. Macrophage size, an indicator of activation status, was examined. The number of cells greater than 25 microns is statistically higher in mice treated with ITB; however, ITB treated mice fed control diet have statistically more large cells than those fed tocopherol diet (Figure 6A).

Chemotactic activity of the BALF can be assessed as a means of measuring the pro-inflammatory nature. BALF from ITB treated mice displayed a significantly greater chemotactic potential than that from saline treated animals (Figure 6B). The bleomycin effect was greater in mice fed the control diet than in those fed tocopherol diet. The BAL chemotactic potential was increased in bleomycin treated mice both 3 and 8 days post injury. At both time points, bleomycin increased the chemotactic potential in tocopherol fed mice, however, this increase was significantly less than that seen in mice fed control diet.

To measure the effect of bleomycin injury on the cells of the lung lining we examined the BAL cell pellet for expression of certain key cytokines/enzymes by rt-PCR (Table 4). As one would predict, bleomycin treatment increased expression of a range of inflammation related mRNAs 3 days post injury. In general, expression was lower in mice fed a tocopherol diet. NOS2 expression is not detectable within mice treated with saline, however, it reaches significant levels post ITB. The ratio of ARG1 to NOS2 expression is a marker of classical vs alternative activation (Menzies et al., 2010). The ARG1:NOS2 ratio in mice fed the control diet was 500 while in those fed tocopherol it was 1000, indicating a bias towards alternative activation. At 8 days post injury all markers, with the exception of YM1, remain higher in bleomycin treated vs saline control mice. However, there is a shift in expression with the tocopherol diet. NOS2, PTGS2, IL1B, which are all markers associated with classical activation (Mantovani et al., 2004; Gordon and Taylor, 2005) are more strongly induced in mice fed the control rather than the tocopherol diet. However, ARG1, YM1, RELM-α, and CCL2 are all more strongly induced in tocopherol fed mice, indicating a bias towards alternative activation. Indeed the ARG1:NOS2 ratio is tenfold higher in tocopherol fed mice compared to control diet following bleomycin treatment (125 vs 13).

As the tocopherol diet resulted in a shift in the ratio of ARG1 to NOS2 expression, and as tocopherol can act as a scavenger of NO metabolites, we examined the BAL for NO metabolite content (Figure 7 A & B). Bleomycin instillation caused a significant increase in both nitrite and nitrate levels within the BAL at 3 and 8 days post injury. In mice fed the tocopherol diet there was no significant increase in either metabolite post bleomycin injury at either day 3 or day 8, indicating either minimal NO production or complete scavenging.

Analysis of Pulmonary-Mechanics

Pulmonary function was assessed using a Forced Oscillation Technique and the resulting elastance and resistance spectra fit to an empirical model. At 3 and 8 days post injury ITB results in a significant increase in the elastance spectra of mice fed the control diet (Figure 8). Component analysis reveals that the change in spectrum at day 3 results from a significant increase in □E, the frequency dependent change in elastance (Figure 8D). At 8 days post injury there is an increase both in □E and the inherent tissue elastance (E_0) (Figure 8C). In mice fed the tocopherol diet there was no change in pulmonary elastance 3 days post bleomycin administration, however, at 8 days post there was a significant increase in both □E and E_0 that was similar to that seen in animals fed the control diet.

Despite the significant increase in elastance spectra with bleomycin administration, there was no significant change observed in the resistance spectra at either 3 or 8 days post injury (Figure 9 A & B). However, component analysis demonstrates that, while there is no change in high frequency resistance (b, Figure 9D), there is a significant increase in low frequency resistance 8 days post injury (a/c, Figure 9C). This increase in low frequency, or tissue, resistance is not abrogated by the tocopherol diet.

2.5 Discussion

The goal of this study was to examine whether dietary supplementation with tocopherols was capable of reducing bleomycin-mediated lung injury and inflammation. Here we have shown that α, δ and γ-tocopherol levels are increased in both the lung and serum by dietary supplementation. ITB administration produces a significant pulmonary injury with accompanying early neutrophilia and later inflammatory changes including macrophage infiltration and activation. These changes are accompanied by a significant increase in NO metabolites and reduced lung function, demonstrated by an increase in inherent and frequency dependent elastance. Tocopherol supplementation, while not

appearing to reduce the direct ITB-mediated injury, completely abrogated the increase in NO metabolites, altered the kinetics of inflammation and macrophage activation, while significantly reducing the acute loss of lung function.

Bleomycin is a redox cycling compound that intercalates into DNA, thus it is capable of generating high concentrations of ROS within the nucleus of cells, producing injury and death (Hecht, 2000). As tocopherols can act as ROS scavengers, it is conceivable that by increasing the tissue concentration of these compounds one may reduce ITB mediated lung injury. This appears not to be the case in the present study, as the early accumulation of protein within the BALF (Table 3) and the injury/inflammation score at day 3 (Figure 1) are not altered by tocopherol supplementation. That the injury process itself is not altered by tocopherol is further confirmed by the observation that neutrophilic invasion, a direct correlate of injury, is not altered (Figure 5). As only 10% of intracellular tocopherol is found in the nucleus (McVean and Liebler, 1999) it is not surprising that supplementation is unable to abrogate ITB-mediated injury. However, tocopherols do operate as efficient scavengers of RONS (Campbell et al., 2003; Ju et al., 2010) generated within ITB as there is no significant increase in either nitrite or nitrate in the presence of tocopherol. It is possible that this reduction in NO metabolites results from reduced iNOS activity, as its increase in expression is inhibited by tocopherol supplementation (Figure 3, Table 4). However, there is still increased expression over saline administered mice and there is no increase in metabolites, which does suggest that the tocopherols have acted as efficient scavengers.

From the present data it is clear that tocopherol supplementation has altered both the time course and the pathway of inflammatory activation following ITB. Despite the fact that injury scores at day 3 are unaltered by tocopherol, it is clear that there is a

reduction in inflammation/injury at day 8 (Figure 1). While total cellular invasion of the lung is not significantly reduced 8 days post ITB (Table 3, Figure 5); there is a significant reduction in the lymphocytic and eosinophilic content of these recruited cells (Figure 5). Also at this later time point there is a significant reduction in the size of the macrophages within the BAL, indicating an altered activation state (Figure 6A).

This potential change in activation is further confirmed by examination of RNA expression within BAL cells. Three days post ITB, a range of macrophage activation markers are increased in expression. Tocopherol supplementation reduces this ITB-mediated increase (Table 4). However, this reduction seems to be greatest in the classical activation pathway as reflected by the higher ARG1:NOS2 ratio (Menzies et al., 2010) within tocopherol fed as opposed to control diet mice. At 8 days post ITB, while classical M1 activation markers such as NOS2, PTGS2 & IL1B remain reduced with tocopherol treatment, a number of alternative M2 markers, namely ARG1, YM1, RELM-α & CCL2, are expressed at higher level with supplementation. These data imply that the inflammatory response is altered such that the acute phase is reduced with tocopherol supplementation, but that the later repair signaling pathways may be enhanced. Such an observation raises the possibility that the fibrotic response may actually be increased by tocopherol supplementation. Further studies at later time points, such as 21 days post ITB, would need to be examined to address this possibility.

This shift in inflammatory signaling is further emphasized by the immunohistochemistry. Both iNOS and COX2 are significantly increased in their expression in response to ITB (Figure 2 & 3); however, this increase is modulated by tocopherol supplementation. This difference is most obvious at days post administration, evidenced by increases in iNOS and COX2 expression increase between day 3 and day 8 in control fed ITB treated mice. Such an increase is not seen with

tocopherol supplementation. In contrast, Ym-1, which is only expressed in inflammatory cells in the lung (Hung et al., 2002) and is often associated with alternative activation (Raes et al., 2002), remains elevated in these cells in both tocopherol supplemented and control diet mice (Figure 4).

Using forced oscillation measurements we examined how the observed inflammatory changes relate to both tissue and airway components of lung function. These data are often analyzed using a constant phase model (Hantos et al., 1990), however this model can sometimes fail to adequately fit in heterogeneous lung injury (Ito et al., 2004; Kaczka et al., 2005). ITB is inherently patchy as an injury mechanism as seen in the whole lung sections (Figure 1). Furthermore, that there was significant heterogeneity of response was confirmed by significant alterations in the E_{RS} spectra with minimal change in R_{RS} at three days post ITB (Figure 8A & 9A) (Bates, 2009). At three days post ITB there is no significant alteration in the resistance spectra either with or without tocopherol supplementation. However, there is a clear increase in lung elastance with ITB-treated control diet mice (Figure 8A). Although, the E_0 value appears higher with ITB-treatment this change did not reach statistical significance (Figure 8C). These data indicate that despite the increase in cell number and protein content in the BAL observed with ITB-treatment there was not a significant change in the tissue stiffness. Of note, tocopherol supplementation did not alter cell number, protein content, or injury score at 3 days post ITB and showed no change in E_0 when compared to saline treated animals. The parameter ΔE, which represents the frequency dependent change in elastance, was significantly raised in only ITB-treated animals fed the control diet (Figure 8D). In conjunction with the lack of change in resistance and tissue elastance, this observation can best be explained by an increase in airway stiffness in these mice.

Observation of the histology does show significant airway thickening (Figure 1), which may explain the change in ΔE.

Eight days post-ITB there is a considerable shift in the lung function response. ITB produces a significant increase in E_0 and the low frequency component of the resistance spectrum, a/c (Figure 9D). There is no further increase in ΔE, although it is still significantly higher than in saline-treated mice (Figure 8D). These data imply that the bulk of the functional change that occurs with ITB as the inflammatory process progresses from day 3 to day 8 occurs at the tissue level. Indeed, the protein content within the BAL doubles over this time period as does the number of cells within the lung lining (Table 3). It is reasonable to suppose that the wetter lung with more observable consolidation (Figure 1) 8 days post ITB is what leads to this increased parenchymal stiffness and resistance. In this regard, it is interesting that tocopherol supplementation does not reduce the protein content or the cell number within the BAL, when compared to control diet fed mice (Table 3); and that a/c and E_0 are significantly increased in these mice. Thus although tocopherol diet alters the inflammatory signaling resulting from ITB, it does not reduce the functional changes that occur within the parenchyma 8 days post injury. It will be interesting to observe how these parameters change at later time points in this injury response.

In conclusion, we have demonstrated that the lung tocopherol content can be successfully increased by diet, and that this supplementation can efficiently scavenge RONS generated by the ITB-mediated inflammatory process. This scavenging appears to reduce acute inflammation and to induce a shift towards alternative macrophage activation. These studies show that dietary supplementation with tocopherols can effectively reduce oxidative stress in pulmonary inflammation. Although, we have demonstrated that acutely tocopherol supplementation reduces the functional deficit that

occurs as a result of ITB, we do not know how the resulting signaling change affects resolution and long-term fibrosis in this model. Finally, through the use of an empirical lung functional model we have been able to relate observable inflammatory changes with alterations in airway and tissue function.

2.6 Tables

Diet	α-T	β-T	γ-T	δ-T
AIN93M	79.8	0.4	24.4	7.6
AIN93M +0.3% γ-TmT	439.8	45.4	1764.4	637.6

Table 2-1

Table 1. Composition of diets. Tocopherols are an essential nutrient and therefore a component of control diet, AIN93M. The tocopherol enriched diet, 0.3% γ-TmT, is supplemented with additional tocopherols in particular γ-tocopherol. Diet was initiated 2 weeks prior to instillation of saline or bleomycin. Animals ate ad libitum throughout the course of the study. Tocopherol composition of both diets is listed as mg tocopherol/kg fed.

	g-T	a-T	d-T
Treatment Group	**Serum (μM)**		
PBS/AIN93M	0.13 ± 0.02	7.72 ± 0.51	0.07 ± 0
ITB/AIN93M	0.06 ± 0.01*	7.62 ± 0.81	0.14 ± 0.01*
ITB/0.3%γTmT	0.55 ± 0.04*,+	10.60 ± 0.67*,+	0.08 ± 0+
	Lung Tocopherols (μmol/kg)		
PBS/AIN93M	0.41 ± 0.03	14.83 ± 3.40	0.09 ± 0
ITB/AIN93M	0.72 ± 0.14*	16.47 ± 2.92	0.22 ± 0.06*
ITB/0.3%γTmT	2.9 ± 0.56*,+	28.45 ± 5.80*,+	1.55 ± 0.29*,+

Table 2-2

Table 2. Tocopherol concentration in the lung and serum of mice 8 days after instillation of saline or bleomycin. Tocopherol content was assessed by HPLC as per the methods section. Tocopherols were successfully absorbed and distributed to the lung and concentrations (expressed as mean ± standard error) increased in those fed 0.3%γTmT diet accordingly.

Treatment Group	Days Post Instillation	Protein (mg/mL)	Total Cells
PBS/AIN93M	3	0.177 ± 0.007	94,269 ± 8,923
ITB/AIN93M	3	0.519 ± 0.052*	168,719 ± 15,343*
ITB/0.3%γTmT	3	0.619 ± 0.086*	127,969 ± 20,720
PBS/AIN93M	8	0.185 ± 0.004	120,375 ± 9,446
ITB/AIN93M	8	1.301 ± 0.157*	306,807 ± 289,070*
ITB/0.3%γTmT	8	1.098 ± 0.140*	329,121 ± 128,784*

Table 2-3

Table 3. Protein concentration and cell yield in the BALF. Cells retrieved in the BALF were counted via Multisizer, while protein concentration in the supernatant was measured by the BCA assay.

Treatment Group	Days Post Instillation	*NOS2*	*PTGS2*	*IL1B*	*CCL2*	*ARG1*	*Ym1*	*RELM-α*
ITB/ AIN93M	3	1	17.95	31.35	66.83	465.74	1.06	14.53
ITB/ 0.3%γTmT	3	0.30	10.56	14.41	40.45	275.03	0.44	12.49
ITB/ AIN93M	8	1	12.35	12.57	5.22	170.91	0.39	122.93
ITB/ 0.3%γTmT	8	0.12	5.41	5.06	9.29	192.9	0.53	290.77

Table 2-4

Table 4. Inflammatory gene expression within BALF cells. Results were normalized to β-actin and expressed as fold increase compared to PBS/AIN93M at respective time point by the $2^{-\Delta\Delta Ct}$ method. NOS2 is undetectable at 3 days in PBS/AIN93M therefore data is expressed as fold increase compared to ITB/AIN93M.

2.7 Figures

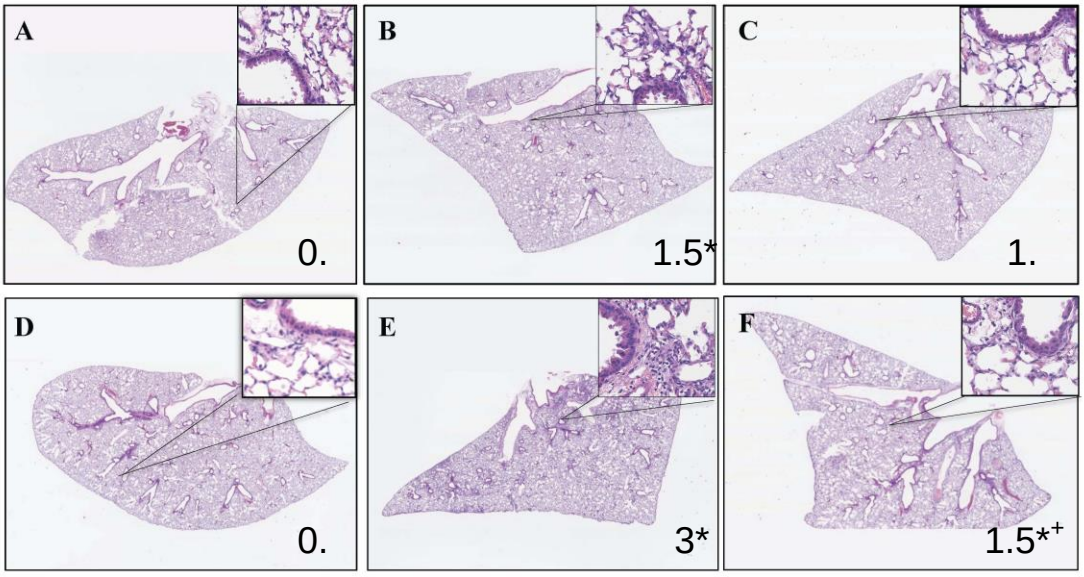

Figure 2-1

Figure 1. Effect of tocopherol diet on progression of inflammation. Lungs were analyzed from mice fed control diet AIN93M (A,B,D,E) or tocopherol enriched 0.3%γTmT (C,F). The right lungs of mice were harvested 3 days (A,B,C) and 8 days (D,E,F) after instillation of PBS (A,D) or ITB (B,C,E,F) and inflation fixed for histology. Representative pictures were taken with Nanozoomer (Olympus) at a magnification of 6.5x and inserts at 100x. Inflammation scores were assigned and the median in bottom corner of each panel. *P<0.05 compared to PBS/AIN93M and + P<0.06 compared to ITB/AIN93M (n=8)

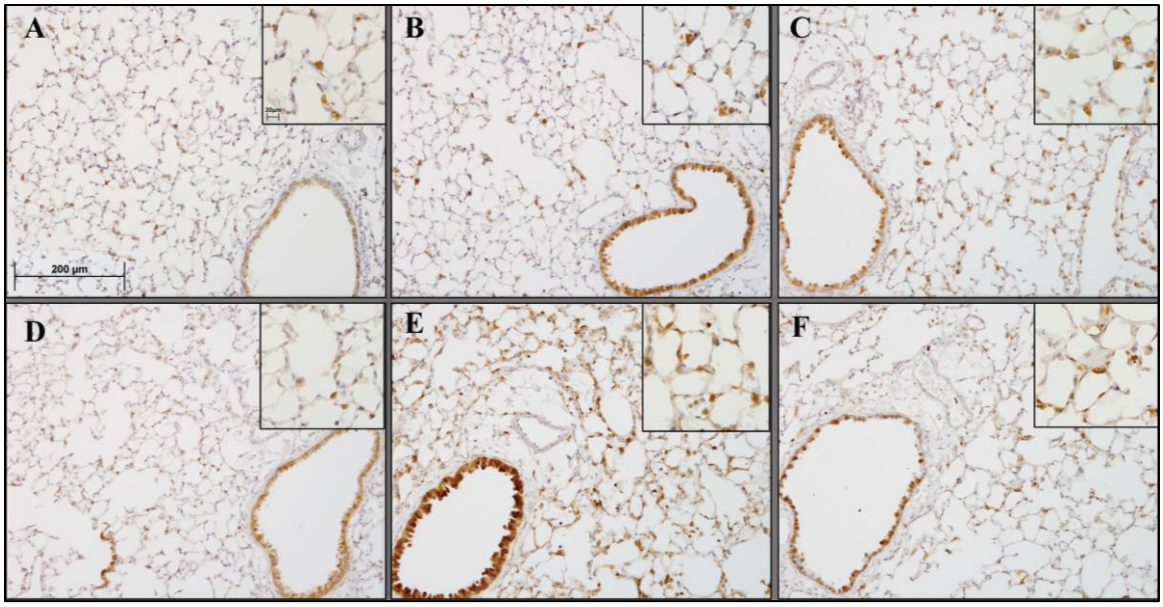

Figure 2-2

Figure 2. COX-2 expression following ITB. Lungs were stained to evaluate cyclo-oxygenase-2 protein expression by immunohistochemistry. Lungs were harvested and sectioned at 3 days (A,B,C) and 8 days (D,E,F) after PBS (A, D) and ITB (B,C,E,F) instillation. Mice were fed control diet AIN93M (A,B,D,E) or tocopherol enriched 0.3%γTmT diet (C,F). Tissue was stained for COX-2; primary antibody dilution 1:2000 overnight (Abcam ab15191 Cambridge, MA) and secondary antibody at 1:2000 for 30 minutes. Representative pictures were taken via the VS120 (Olympus) at an optical zoom 100x and inserts 200x. (n=8)

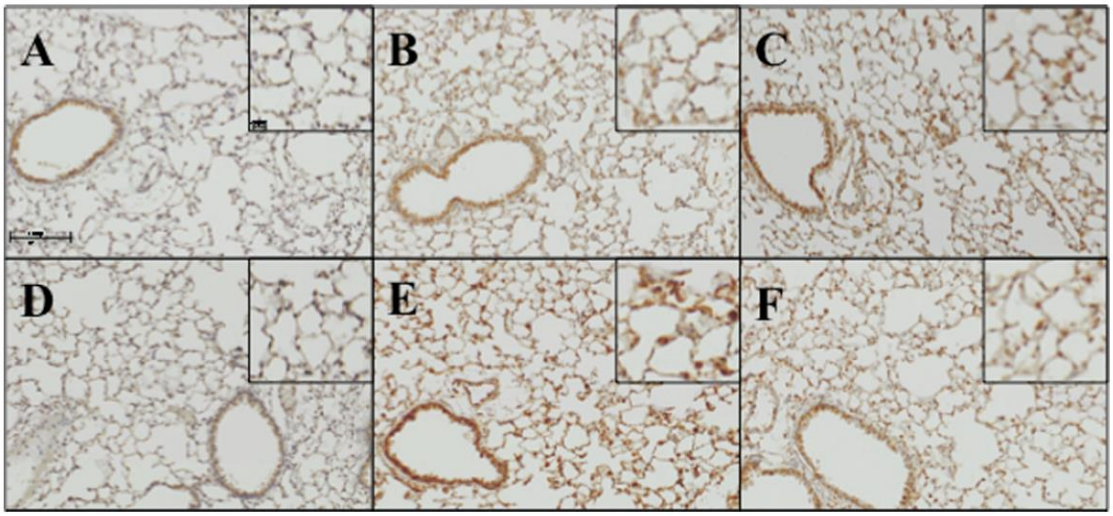

Figure 2-3

Figure 3. Effect of tocopherol diet on increased iNOS expression in response to ITB. iNOS expression was evaluated by immunohistochemistry. Tissues were collected 3 days (A,B,C) and 8 days (D,E,F) after instillation of PBS (A, D) or ITB (B,C,E,F). Mice were fed control diet AIN93M (A,B,D,E) and tocopherol enriched 0.3%γTmT diet (C,F). Tissues were incubated with primary antibody (Abcam, ab15323 Cambridge, MA) at 1:100 dilution overnight followed by secondary antibody at 1:200 for 30 minutes. Representative pictures were taken via the BX51 (Olympus) at an optical zoom 200x and 400x. (n=8) Figure 4. Ym1 expression in response to ITB. Lung sections were stained to evaluate Ym1 protein expression by immunohistochemistry. Lungs were harvested 3 days (A,B,C) and 8 days (D,E,F) after PBS (A, D) and ITB (B,C,E,F) instillation. Mice were fed control diet AIN93M (A,B,D,E) and tocopherol enriched 0.3%γTmT diet (C,F). Tissues were incubated with primary antibody at 1:500 overnight (StemCell Technologies, 01404 Vancouver Canada) and secondary antibody at 1:2000 for 30 minutes. Representative pictures were taken via the VS120 (Olympus) at an optical zoom 100x and inserts 200x. (n=8)

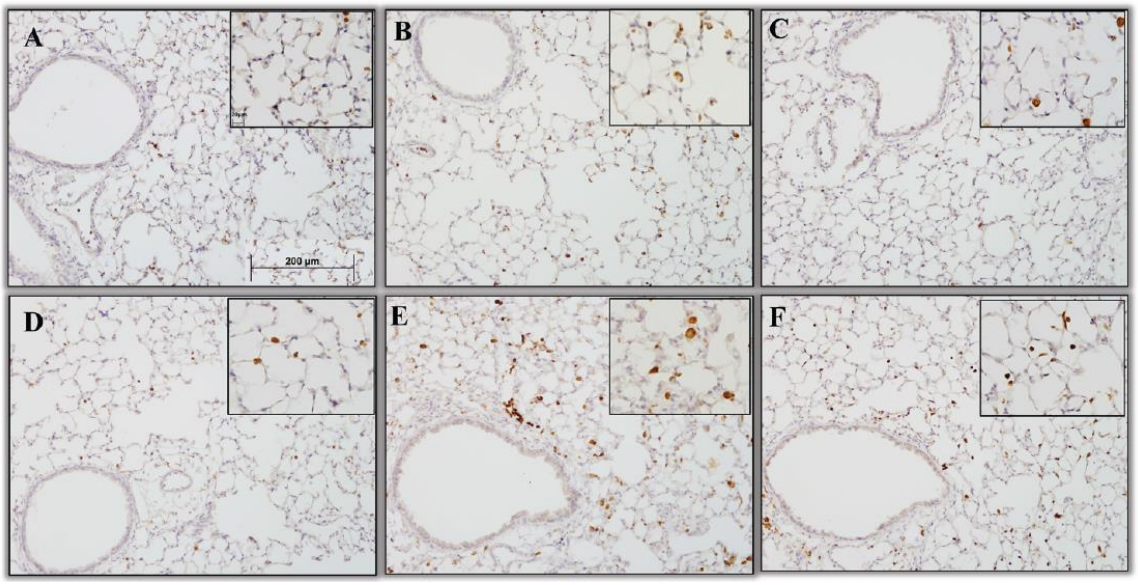

Figure 2-4

Figure 4. Ym1 expression in response to ITB. Lung sections were stained to evaluate Ym1 protein expression by immunohistochemistry. Lungs were harvested 3 days (A,B,C) and 8 days (D,E,F) after PBS (A, D) and ITB (B,C,E,F) instillation. Mice were fed control diet AIN93M (A,B,D,E) and tocopherol enriched 0.3%γTmT diet (C,F). Tissues were incubated with primary antibody at 1:500 overnight (StemCell Technologies, 01404 Vancouver Canada) and secondary antibody at 1:2000 for 30 minutes. Representative pictures were taken via the VS120 (Olympus) at an optical zoom 100x and inserts 200x. (n=8)

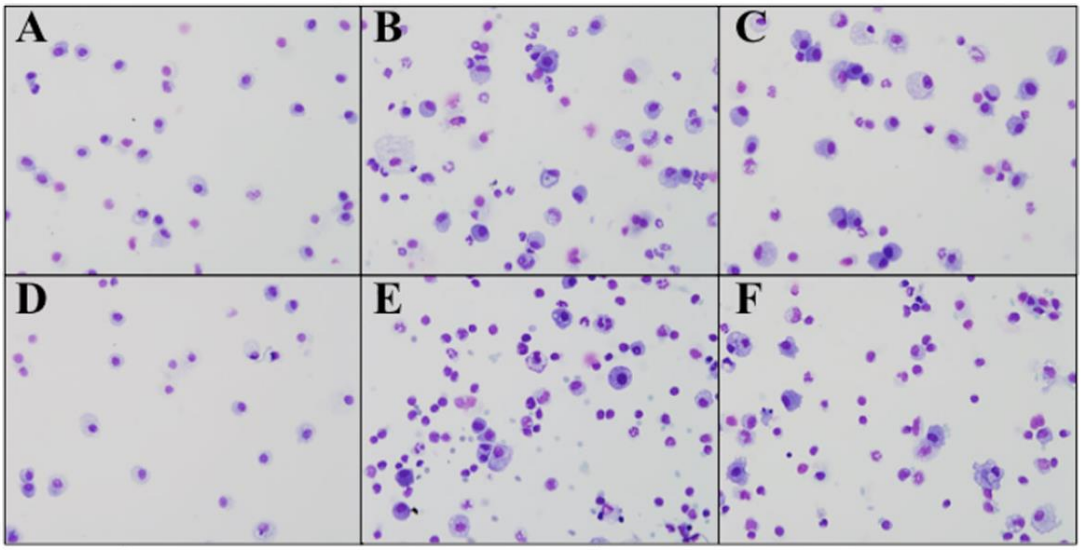

G	3 Days (10^3 cells/mL)				8 Days (10^3 cells/mL)			
Treatment Group	Macrophages	Neutrophils	Lymphocytes	Eosinophils	Macrophages	Neutrophils	Lymphocytes	Eosinophils
PBS/ AIN93M	94.1 ± 7.68	0.6 ± 0.49	3.5 ± 2.16	0	117.4 ± 9.31	0.7 ± 0.29	2.1 ± 0.42	0 ± 0.09
ITB/ AIN93M	112.6 ± 5.42	37.9 ± 12.27*	14.8± 1.97*	3.4 ± 1.78*	187.5 ± 21.10*	71.9 ± 35.45*	38.0 ± 11.78*	9.4 ± 6.71
ITB/ 0.3%γTmT	92.1 ± 12.62	32.4 ± 11.49*	11.1 ± 3.52	0.25 ± 0.25+	201.2 ± 19.85*	92.7 ± 37.47*	28.8 ± 5.15*	4.8 ± 1.46*

Figure 2-5

Figure 5. Effect of tocopherol diet on recruitment of leukocytes. BAL cells were collected from mice 3 days (A,B,C) and 8 days (D,E,F) after PBS (A, D) and ITB (B,C,E,F) instillation. Mice were fed control diet AIN93M (A,D) and tocopherol enriched 0.3%γTmT diet (B,C,E,F). * $P<0.05$ compared to PBS/AIN93M and $P<0.05$ compared to ITB/AIN93M at corresponding duration of exposure. Representative pictures were taken with the BX51 (Olympus) at an optical zoom of 400x. (n=8)

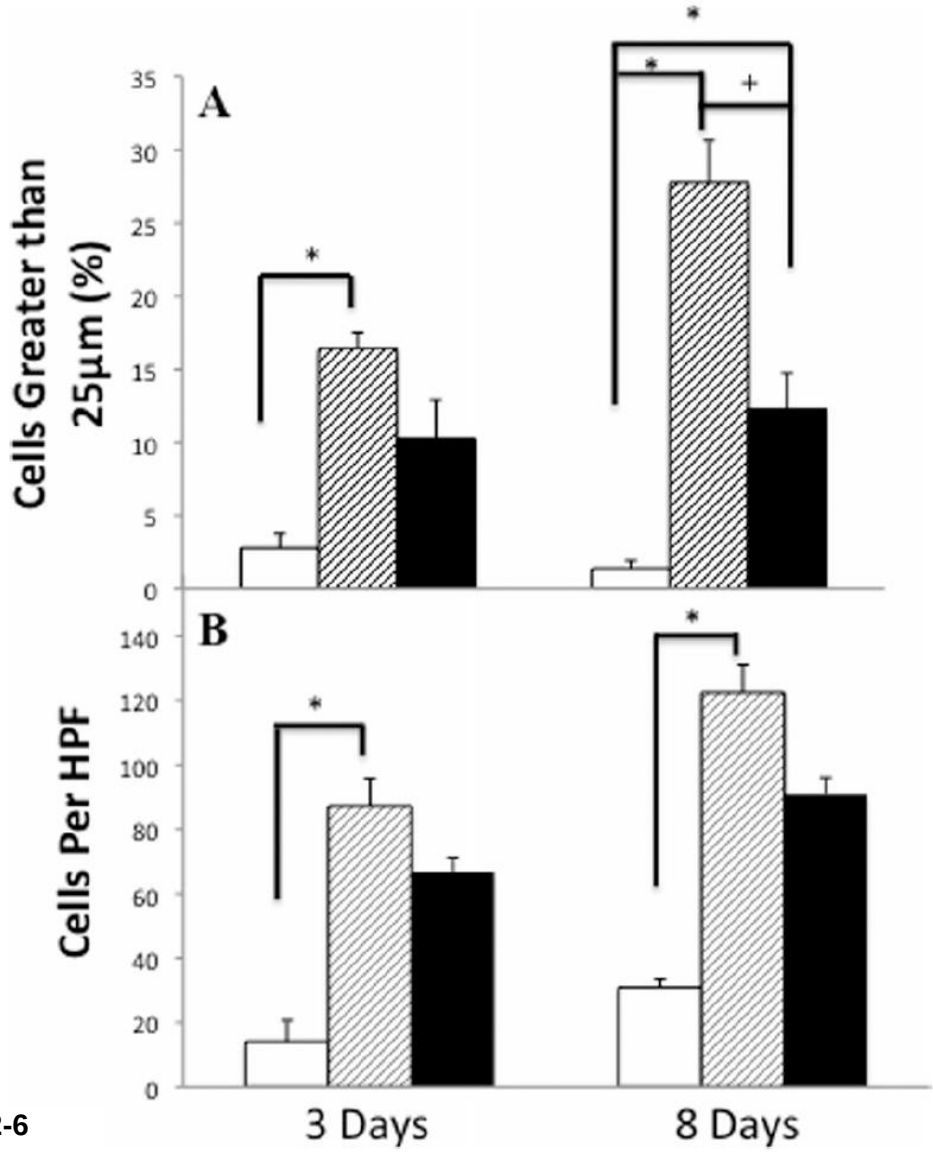

Figure 2-6

Figure 6. Activity of leukocytes post ITB and the effect of tocopherol diet. BALF was collected in mice from the PBS/AIN93M group (white bars), ITB/AIN93M group (dashed bars) and ITB/0.3%γTmT (closed bars). Identification of cells in the BALF greater than 25 microns reveals a population of activated cells (A). Measured in 5 different fields, at an optical zoom of 400x, cells were grouped based on diameter size. The number of cells >25µm is expressed as a percent of total cells counted in the BAL. The chemotactic potential (B) of the BALF is measured by the migration of RAW 264.7 cells in response to BALF. The chemotactic potential is expressed as the mean number of

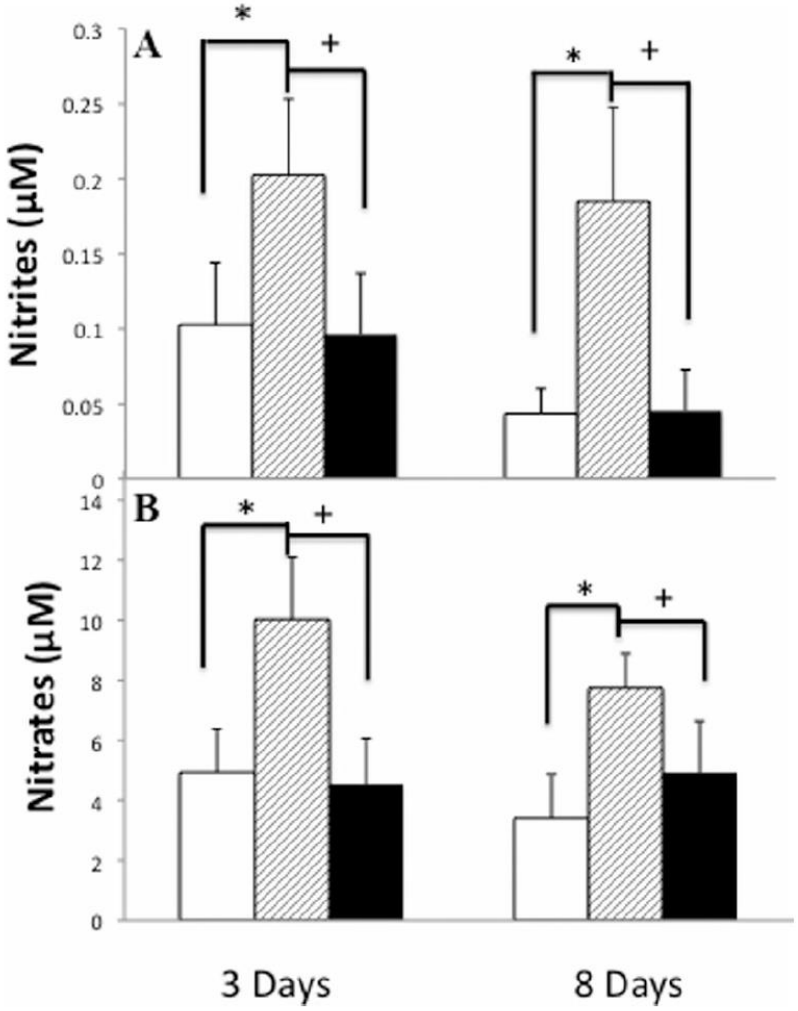

Figure 2-7

Figure 7. Increases in NO metabolites in response to ITB and the effect of tocopherol diet. Nitrites (A) and nitrates (B), metabolites of nitric oxide, were measured in the BALF supernatant at 3 and 8 days post-ITB. Measurements were made in mice from the PBS/AIN93M group (white bars), ITB/AIN93M group (dashed bars) and ITB/0.3%γTmT (closed bars). * $P<0.05$ compared to PBS/AIN93M, $^{+}$ $P<0.05$ compared to ITB/AIN93M ($p<0.05$). (n=8)

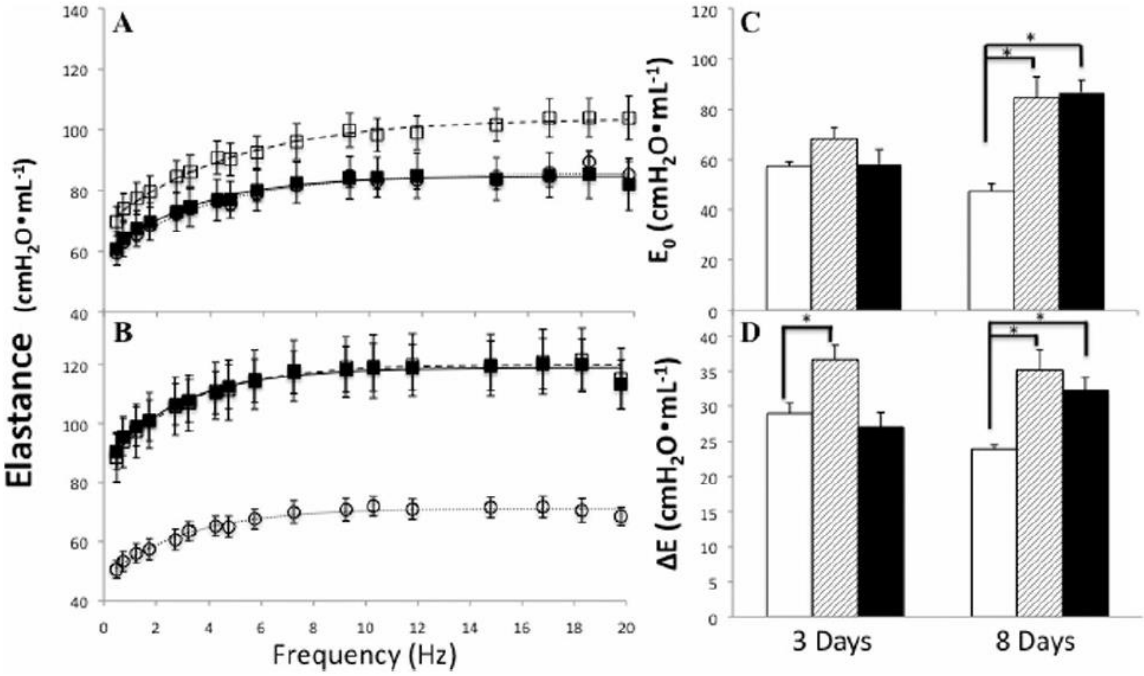

Figure 2-8

Figure 8. Tocopherol effect on pulmonary elastance changes in response to ITB. Elastance spectra 3 days (A) and 8 days (B) post instillation in PBS/AIN93M (○), ITB/AIN93M (□), and ITB/0.3%γTmT (■). Parameters of elastance highlight changes in tissue and airway function; E_0 elastance at the static limit (C) and ΔE the change in elastance with change in frequency ΔE (D); PBS/AIN93M (open bars), ITB/AIN93M (dashed bars) and ITB/0.3%γTmT (closed bars). * P<0.05 compared to PBS/AIN93M.

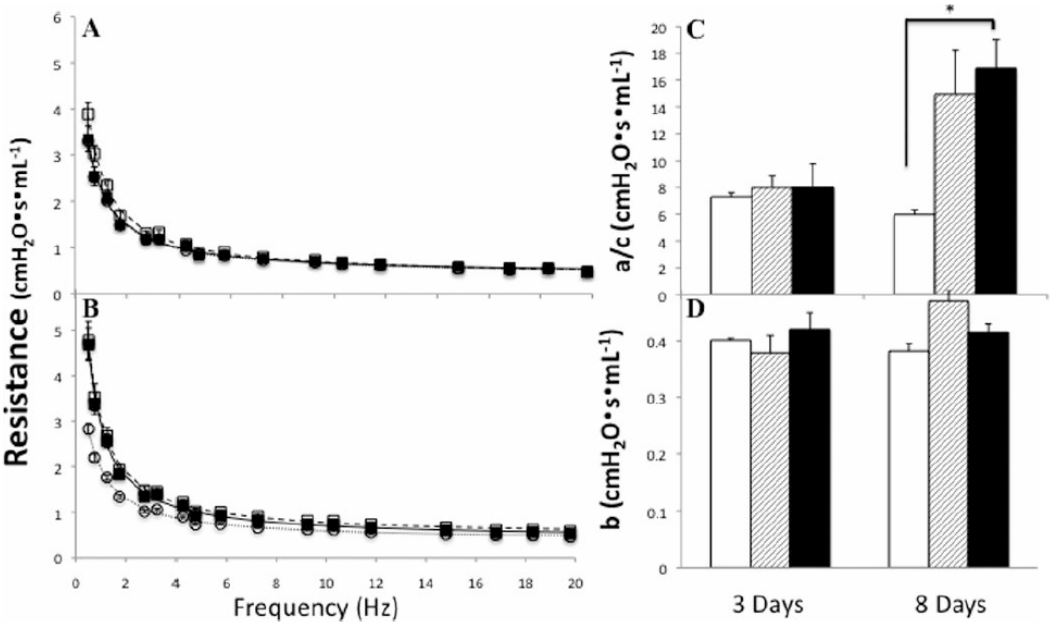

Figure 2-9

Figure 9. Effect of ITB on pulmonary resistance. Resistance spectra was obtained in conjunction with elastance spectra. Resistance is also shown at a PEEP of 3cm H_2O is shown at 3 (A) and 8 (B) days post treatment. PBS/AIN93M (○), ITB/AIN93M (□), and ITB/0.3%γTmT (■). a/c low frequency resistance (C) and b high frequency asymptote (D); PBS/AIN93M (open bars), ITB/AIN93M (dashed bars) and ITB/0.3%γTmT (closed bars). * statistically different from PBS/AIN93M ($p<0.05$).

CHAPTER 3: INDUCIBLE NITRIC OXIDE SYNTHASE ROLE IN MACROPHAGE RECRUITMENT AND POLARIZATION IN ACUTE LUNG INJURY

3.1 Abstract

Inducible nitric oxide synthase (iNOS) has been implicated in the pathogenesis of bleomycin induced acute lung injury (ITB). However, the reason for it's paradoxical role has yet to be studied. Using a chimeric mouse approach, the effect of iNOS inhibition, using 1400W, on resident and recruited macrophage activation was analyzed. C57/BL6 mice underwent lethal radiation followed by adoptive transfer of green fluorescent protein (GFP) expressing bone marrow. Bleomycin was intratracheally instilled and cells were immunophenotyped via flow cytometry 8 and 15 days after instillation. Recruited (GFP+) macrophages classically activated 8 days post ITB and alternatively activated 15 days post ITB. Resident (GFP-) macrophages did not classically or alternatively activate 8 days post but alternatively activated 15 days post ITB. 1400W reduced activation of recruited macrophages 8 and 15 days post ITB without effecting resident cell activation. This work shows iNOS is important to the activation of recruited cells but suggests resident alternative activation is independent of iNOS.

3.2 Introduction

Inducible nitric oxide synthase (iNOS) is involved in many immune driven diseases. iNOS inhibition has been attempted as a therapeutic approach in several immune mediated diseases without success (Singh et al., 2007; Nathan, 2011). Our previous findings demonstrate systemic iNOS inhibition alters the response to ALI. Acute inflammation was reduced but later fibrotic endpoints propagated when mice were treated with ITB and selective iNOS inhibitor 1400W (Guo et al., 2016). This work

suggested iNOS may play a paradoxical role in ITB mediated ALI in that it is detrimental during inflammation but necessary for resolution of inflammation.

Inducible nitric oxide synthase is a unique NOS enzyme as its expression is increased when signaled unlike the other constitutively expressed NOS enzymes. Pulmonary epithelial cells and classically activated macrophages increase iNOS expression in times of inflammation (Guo and Erzurum, 1998; Guo et al., 2016). LPS and IFNγ have been shown to activate macrophages resulting in up regulation of iNOS protein expression.

Macrophages are key players in the response to acute lung injury (ALI). Macrophages activate along a spectrum ranging from classical (M1) to alternative activation (M2) (Martinez and Gordon, 2014). Classically activated macrophages increase production of oxidants via increased expression of proteins such as COX2, LOX, NADPH oxidase and iNOS (Rosa et al., 2014). Classically activated macrophages also increase production of chemokines and cytokines thus creating a pro-inflammatory environment. Macrophages alternatively activated during resolution of inflammation. Proteins such as FIZZ1, Relm1α, Ym1, Arg and mannose receptor are expressed (Gordon and Martinez, 2010).

The intratracheal bleomycin model (ITB) is used to study the various stages of ALI; injury, inflammation, resolution and fibrosis. Bleomycin causes epithelial cell injury that leads to subsequent leukocyte infiltration (Burger et al., 1981). Macrophages predominate during the acute inflammatory stage and are classically activated (Cavarra et al., 2004; Gasse et al., 2007). As inflammation resolves, macrophages favor alternative activation (Cavarra et al., 2004; Gasse et al., 2007).

Previous work evaluating macrophage polarization and involvement in ITB mediated ALI has not considered origin of macrophage. Macrophages during ALI are either resident to the lung, therefore present at time of injury, or recruited to the lung in

response to injury. Resident macrophages phenotype allows for their homeostatic role of interfacing with the environment. Resident alveolar macrophages are M2 biased; highly phagocytic and immune-tolerant (Toews et al., 1984; Guth et al., 2009; Zaynagetdinov et al., 2013). Epithelial cell derived proteins, such as GM-CSF and TGFβ, influence resident macrophage phenotype (Roth and Golub, 1993; Guth et al., 2009). When resident macrophage capacity is exceeded chemokines are released to recruit macrophages to the lung. Recruited macrophages upon entry to the lung are influenced by the environment to activate.

It is our proposal, due to the different nature of resident and recruited macrophages their response to ITB mediated ALI will vary. This may underlie the divergent role of iNOS in the inflammatory and resolution phases following ITB. It is our hypothesis iNOS is required for macrophage activation. In order to study the effect of iNOS inhibition on the recruited and resident macrophage populations we used a chimeric mouse model to study the populations independently.

3.3 Methods

Animals

6 week old male C57/BL6 (Jackson) underwent 12 Grey X-ray radiation using a Torrex irradiator. Bone marrow harvested from C57BL/6-Tg (CAG-EGFP)10sb/J mice was injected 2-4 hours following radiation. Mice were monitored for 6 weeks and fed PicoLab 0.025% Trimethoprim/0.1242% Sulfamethoxazole antibiotic chow for the first 2 weeks (W.F.Fisher and Son Sommerville, NJ).

A set of mice underwent radiation and bone marrow adoptive transfer followed by sham intratracheal instillation to control for the effect of radiation on the lung and resident macrophage population. Histologically mice were evaluated and there was no evidence of inflammation or structural alterations. Cells were harvested by lavage with

or without massage and phenotypically assessed by flow cytometry. Flow cytometry identified a single population of pulmonary macrophages (F4/80+ Cd11c+) that were resident (GFP-) to the lung prior to radiation and subsequent steps (Supplemental Figure 1). Macrophages did not express Ly6C and expressed low levels of Cd206, congruent with alveolar macrophage phenotype. A small number of cells in the lavage was GFP+ ($2.3x10^4$ 8 days post sham instillation and $1.5x10^4$ 15 days post sham instillation). Massage increased the number of GFP+ cells compared to lavage and this number increases with time ($7.7x10^4$ at 8 days and $14.2x10^4$ at 15 days). The total number of GFP- macrophages remains constant with time and is not increased by massage. Others have used this method to genetically alter bone marrow and depending on type and dose of radiation effects on resident population is variable. The X-ray radiation dose used in this experiment allows us to study the unaltered pulmonary resident macrophage population.

Bone marrow was checked for successful adoptive transfer using Gallios flow cytometer to measure GFP fluorescence. Bone marrow cells were gated on forward and side scatter to exclude red blood cells (GFP-). 92±1% of bone marrow is GFP+.

iNOS Inhibition

In order to identify the recruited macrophages from resident, the GFP chimeric mice were used to study the role of iNOS in macrophage activation. 1400W, a specific iNOS inhibitor was chosen instead of NOS2-/- mice in order to use the GFP chimeric mouse approach. 1400W (Cayman Chemical Ann Arbor MI), or saline control, was delivered by osmotic pump (Alzet Cupertino,CA) subcutaneously implanted 3 days prior to intratracheal instillation. Additional 4 days of once daily intraperitoneal injection was required for mice studied at the 15 day time point. 1400W was delivered at 10mg/kg/h or a total dose of 60µg as previously reported (Atochina-Vasserman et al., 2007).

Intratracheal Instillation

Bleomycin (Sigma St. Louis MO) or PBS was intratracheally instilled in isoflurane anesthetized mice. Mice were treated with 3units/kg bleomycin in 50uL PBS or 50uL PBS control. Mice were sacrificed 8 and 15 days post intratracheal instillation by ketamine/xylazine overdose followed by exsanguinations. Hearts were perfused with heparinized saline to clear red blood cells from lungs. Lungs were cannulated and bronchoalveolar lavage (BAL) was completed. For a subset of animals, following BAL a massage (BALM) of lung tissue was performed concurrently with 5 additional 0.5mL washes of the lung. Therefore cells identified as BALM are both lavage and massage collected whereas BAL are only cells collected by lavage. For those mice that only underwent BAL left lungs were inflation fixed with 3% paraformaldehyde 2% sucrose, ethanol dehydrated and paraffin embedded for sectioning.

Cell Analysis

BAL and BALM was centrifuged to collect cell pellets and supernatant stored for protein measurements (Bradford assay). Cells were counted by Multisizer (Beckman Coulter Indianapolis IN). 30,000 cells were spun for cytospin, stained with KWIK-DIFF (Thermo Scientific) and morphologically analyzed for cell type. 200,000 cells (or remaining if insufficient) were immunostained for flow cytometry using the following antibodies: Cd206-PE (Biolegend 141706), Ly6C-PerCP/Cy5.5 (Biolegend 128012), F4/80-PE/Cy5 (Biolegend 123114), Cd11b-APC (Biolegend 101212), Cd11c-AF700 (Biolegend 117320). Manufacturer protocols were followed including 10 minute Fc block (TruStain FcBlock Biolegend 101320) followed by 30 minute antibody incubation at manufacturer suggested concentrations. Viability dye-eFluor780 (eBiosciences 65-0865-14 San Diego, CA) was incubated after antibodies for 30 minutes and washed out before

paraformaldehyde fixing cells. Gallios (Beckman Coulter Indianapolis IN) was used to analyze cell fluorescent expression. Data was analyzed using Kaluza software (Beckman Coulter Indianapolis IN).

Tissue Analysis

Paraffin blocks of left lungs were sectioned for hematoxylin and eosin staining and immunohistochemistry staining. GFP (abcam 290, 1:5000 primary dilution), Cd11b (abcam 133357, 1:3000 primary dilution), COX2 (abcam 15191, 1:2000 primary dilution), Cd206 (abcam 64693, 1:500 primary dilution) and Ym1 (StemCell 01404, 1:500 primary dilution) antibodies were used to evaluate in tissue protein expression by IHC (secondary antibody 1:2000 (Vector Burlingame, CA)). Macrophages were identified in tissue by morphology and GFP expression noted on 20 high power fields (600x). Relative number of GFP positive macrophages were calculated compared to total macrophages identified. Hematoxylin and eosin stained lung sections were scored for inflammation based on previously reported scoring system (Rudmann et al., 1998).

3.4 Results

iNOS inhibition promotes long term inflammation without changing extent of early pulmonary inflammation

Intratracheal bleomycin causes pulmonary inflammation that resolves with time. Following instillation, airways hypertrophy and immune cells infiltrate as seen as increased peribronchial, perivascular and parenchymal cellularity 8 days post ITB. With time cell infiltration persists in the parenchyma and structural changes to the alveoli are evident 15 days post ITB. Inflammation scoring assesses these markers of inflammation. 1400W treatment does not attenuate inflammation at 8 days post ITB.

However, inflammation increases with time particularly persistent peribronchial and perivascular infiltration. ITB increases inflammation score from 0 (PBS) to 2.5 (ITB and ITB+1400W) at 8 days (Table 1). 15 days post ITB, PBS remains 0 while ITB 3 and ITB+1400W 4 (Table 1).

Intratracheal instillation of PBS does not alter resident macrophage phenotype

Cells are collected 8 days post instillation from the airspace by lavage (BAL) and tissue associated compartment by subsequent massage of tissue (BALM). PBS instilled mice have a similar total number of cells in the BAL and BALM as sham treated mice (Table 1, Supplemental Figure 1). These cells also remain constant with time, $22.3x10^4$ ± $2.81x10^4$ (8 days) and 18.3 $x10^4$ ±$1.89x10^4$ (15 days) in the BAL and $51.5x10^4$ ±$8.47x10^4$ (8 days) and $52.3x10^4$ ±$12.20x10^4$ (15 days) in the BALM. Massage increased the number of cells collected from PBS instilled mice.

Macrophage phenotype was not altered by saline instillation compared to sham (Table 1, Supplemental Figure 1). GFP- F4/80+ macrophages make up the majority of cells collected by BAL 8 and 15 days post PBS instillation, $20.1x10^4$ ±2.64 $x10^4$ and 16.3 $x10^4$ ±2.04 $x10^4$. Massage increases the number of GFP- F4/80+ macrophages to 49.9 $x10^4$ ±8.53 and 28.5 $x10^4$ ±2.84 at 8 and 15 days. A similar number of GFP+ macrophages are collected by BAL at 8 and 15 days 1.9 $x10^4$ ±0.37 and 1.8 $x10^4$ ±0.26 and increased by massage only at 15 days to 22.5 $x10^4$ ±8.42 $x10^4$.

Regardless of GFP expression, macrophages collected by BAL or BALM express the pulmonary phenotype F4/80+ Cd11c+ $Cd206^{LOW}$ Ly6C-. Literature supports Cd11c expression and low levels of Cd206 on resident alveolar macrophages(Guth et al., 2009; Zaynagetdinov et al., 2013). BAL GFP- F4/80+ cell Cd11b expression is increased to low expression (MFI 6.1± 0.77) at 8 days and negative expression (MFI 3.1± 0.34) 15

days post PBS instillation suggesting an early but not late migratory phenotype to macrophages post saline instillation.

Macrophages are recruited to the lung and adopt a M1 phenotype 8 days post ITB

Total cell number increases in the BAL 8 days post ITB; 42.4 $x10^4$ ± 4.71 $x10^4$ compared to 22.3 $x10^4$ ± 2.82 $x10^4$ (PBS) (Table 1). The number of GFP+ F4/80+ cells increases 8 days post ITB in the BAL (11.5 $x10^4$ ± 1.82 $x10^4$ compared to 1.86 $x10^4$ ± 0.37 $x10^4$ in PBS instilled) and BALM (22.2 $x10^4$ ± 2.87 $x10^4$ compared to 0.96 $x10^4$ ± 0.27 $x10^4$ in PBS instilled). GFP expression by IHC in the lung, post lavage, is also increased and seen throughout the lung 8 days post ITB but only few cells near the blood vessels of PBS instilled mice are GFP positive (Figure 3, column 1). Cd11b expression by IHC in the lung follows a similar pattern as GFP and is increased following ITB compared to PBS instillation (Figure 3, column 2).

Using antibodies to macrophage markers, the population of GFP+ F4/80+ cells was immunophenotyped. 8 days post ITB, BAL and BALM GFP+ F4/80+ cells make up two populations; Cd11c-$Cd206^{LOW}$ and Cd11c+ $Cd206^{HIGH}$ (Figure 1, Supplemental Figure 2)). Cd11b expression varies in the BAL GFP+ F4/80+ population (Figure 1). GFP+ F4/80+ cells collected with additional massage of tissue show an increase in Ly6C expression (Supplemental Figure 2). COX2 expression in the lung, post lavage, is also increased 8 days post ITB (Figure 4, column 3).

Markers of M2 polarization, Cd206 and Ym1, are increased in a subset of macrophages 8 days post ITB. Cd206 expression is increased on a subpopulation of GFP+ F4/80+ in the BALM 8 days post ITB compared to PBS treated (Supplemental Figure 2). Ym1 expression is induced in the tissue of ITB treated mice 8 days post instillation (Figure 3).

iNOS inhibition prevents recruited macrophage M1 polarization without effecting recruitment 8 days post ITB

The total number of cells collected from mice treated with 1400W 8 days post ITB is not altered by iNOS inhibition (Table 2). The number of GFP+ F4/80+ cells is also unchanged suggesting no difference to recruitment. However, the distribution of Cd11b expressing cells favors Cd11b+ (Figure 1). ITB increased GFP and Cd11b expression in the lung by IHC, post lavage, is also not altered by 1400W administration.

1400W administration decreases polarization of recruited macrophages 8 days post ITB. GFP+ F4/80+ cells in the BALM and tissue that were Ly6C and COX2 positive 8 days post ITB are negative if also treated with 1400W (Supplemental Figure 2 and Figure 3). ITB responsible Cd206 increased expression of GFP+ F4/80+ macrophage population collected in the BALM is also decreased with 1400W (MFI 7.5 ± 1.4 compared to 4.3 ± 0.4) (Supplemental Figure 2). Cd11c expression is decreased with 1400W and there are more Cd11c- Cd206- GFP+ F4/80+ cells in those mice treated with 1400W than without 1400W 8 days post ITB (36 ± 2% vs 17 ±2%, p=0.01). Ym1 expression is present in the tissue but cells are much smaller in size (Figure 3).

Resident macrophages do not polarize 8 days post ITB

The total number of GFP- F4/80+ cells 8 days post ITB is the same as PBS instilled mice in the BAL (20.1 $x10^4$ ± 2.64 $x10^4$, 27.6 $x10^4$ ± 3.85 $x10^4$) and BALM (49.9 $x10^4$ ± 8.54 $x10^4$, 33.5 $x10^4$ ± 6.18 $x10^4$) (Table 2). GFP- F4/80+ cells are $Cd11b^{LOW}$ Ly6C- post instillation of PBS or ITB (Figure 2). The pulmonary phenotype of GFP- F4/80+ cells is altered by ITB in that 46 ±6% are Cd11c-Cd206- (compared to 5± 1%, p<0.001) and the rest Cd11c+ $Cd206^{LOW}$, similar to PBS instilled (Figure 2).

iNOS inhibition does not alter resident macrophage phenotype 8 days post ITB

1400W does not result in polarization of resident macrophages and does not prevent loss of pulmonary phenotype seen 8 days post ITB. Cd11c- Cd206- population constitutes 46 ±6% (ITB) compared to 59 ±5% (ITB+1400W) of total GFP- F4/80+ (p-value >0.05). GFP- F4/80+ cells are $Cd11b^{LOW}$ Ly6C- like that of ITB instilled mice without 1400W (Figure 2).

Resident and recruited macrophages adopt a M2 phenotype during resolution

15 days after ITB instillation, resident and recruited macrophages make up the cell population of the BAL and the number of resident macrophages is increased by massage (Table 2). IHC stain of lung tissue, post massage, demonstrates a decrease in Cd11b expression (Figure 3, 6 column 2). The number of GFP+ F4/80+ cells in the BALM expressing $Cd11b^{HIGH}$ is reduced as well (Supplemental Figure 2, 3). GFP expression, by IHC, is similar to 8 days (Figure 4, 6 column 1) suggesting earlier recruited cells remaining in the tissue.

Recruited and resident macrophages increase Cd206 expression above baseline ($Cd206^{LOW}$) expression of cells collected from PBS instilled mice. Recruited macrophages increase their Cd206 expression (MFI 3.1 ± 0.26 (PBS) compared to 7.7± 0.92 (ITB)) and are predominately Cd11c+ Cd11b- Ly6C- (Figure 4). Resident macrophages are split between Cd11c- Cd206- and Cd11c+ $Cd206^{HIGH}$ (Figure 5) in the BAL and BALM (Supplemental Table 1). GFP- F4/80+ cells are also Cd11b- and Ly6C-. Increased Ym1 expression in the tissue, post lavage, also demonstrates a pro-resolving phenotype of macrophages (Figure 6).

1400W decreases the number of recruited Cd11c+ $Cd206^{HIGH}$ 15 days post ITB

1400W prevents the additional collection of cells by massage seen in both PBS and ITB treated mice without 1400W (Table 2) without changing the number of cells

collected by BAL. GFP+ F4/80+ cells are collected by BAL and more express Cd11b^{HIGH} (Figure 4). Similarly an increased number of Cd11b expressing cells is seen in the tissue of 1400W treated mice 15 days post ITB (Figure 6). GFP+ F4/80+ cells are split into two populations; Cd11c+ Cd206^{HIGH} and Cd11c- Cd206- (Figure 4). 1400W decreases the relative population of Cd11c+ Cd206^{HIGH} cells; 94± 1% compared to 87± 3% ($p=0.03$). GFP- F4/80+ cells are also split between Cd11c+ Cd206^{HIGH} and Cd11c- Cd206- but the ratio is unchanged by 1400W; 72± 6% compared to 61± 8% Cd11c+ Cd206^{HIGH} ($P>0.05$)(Figure 5).

Resident and recruited macrophages adopt a M2 phenotype regardless of 1400W treatment. Those cells F4/80+ Cd11c+ are Cd206^{HIGH} whether GFP+ (Figure 4) or GFP- (Figure 5). Ym1expression is induced 15 days post ITB with or without 1400W, however Ym1 expressing cells in 1400W treated mice are larger (Figure 6).

3.5 Discussion

This work demonstrates inducible nitric oxide synthase is needed for macrophage activation following ITB. Recruited but not resident macrophage activation is depended iNOS. Recruited macrophages classically activate 8 days post ITB. Alternatively activated recruited and resident macrophages populate the lung 15 days post ITB.

Classically activated macrophages increase expression of iNOS but activation has yet to be shown under the control of iNOS. Previously, we have reported a decrease in mRNA levels of pro-inflammatory markers, Ptgs2, IL1β and Ccl2, 8 days post ITB with 1400W (Guo et al., 2016). This work demonstrates iNOS is necessary for classical activation 8 days post ITB. This previous work also reported a reduction in total BAL cell number 8 days post ITB, but this was not observed in this work. This difference is likely due to the varying degree of injury following ITB. The dose given intratracheally

varies by lab a great deal; ranging from 1.25-4units/kg (Moore and Hogaboam, 2008). Also the anesthetic agent can effect the extent of injury (Fortis et al., 2012; Strosing et al., 2016) and in fact varied between these two experiments. It is possible a larger effect on inflammation would have been seen if an earlier time point was evaluated.

Resolution of inflammation was impaired by 1400W 15 days post ITB. 1400W increased inflammation score compared to 8 days and ITB without 1400W at 15 days. Similarly, we previously reported an increase in inflammation score at 21 days post ITB when also treated with 1400W (Guo et al., 2016). The number of recruited $Cd206^{HIGH}$ BAL macrophages was decreased by 1400W. Following 1400W, the number of $Cd11b^{HIGH}$ Cd11c- recruited macrophages was increased suggesting an increase in recruitment or decrease in maturation. Cd11b, a migratory integrin, is shed upon arrival to the site of injury (Gomez et al., 2012). Epithelial influences, such as GM-CSF and SPD, are known to stimulate expression of pulmonary integrin Cd11c (Sunderkotter et al., 2004; Guth et al., 2009).

Radiation is a limitation of the chimeric mouse model as radiation has the potential to cause lung injury. Dose and type of radiation determine the effect on the lung. The dose used in this experiment, 12 Gy by x-ray, has not caused injury to the lung detectable 7 or 8 weeks post radiation. Sham instilled mice, assessed histologically, show no sign of inflammation or fibrosis.

Resident macrophages have different responses to radiation. Alveolar macrophages are particularly resistant to radiation (van oud Alblas and van Furth, 1979; Tarling et al., 1987; Kennedy and Abkowitz, 1998; Landsman and Jung, 2007; Hashimoto et al., 2013). While others have used lung shielding (Janssen et al., 2010), we were limited to whole body irradiation as the length of time required to deliver 12 Gy x-ray radiation, 45 minutes, exceeds the duration of anesthetics. Despite whole body radiation, resident macrophages are collected from the lungs of sham instilled mice. The

phenotype of collected cells is consistent with the pulmonary phenotype, Cd11c+ $Cd206^{LOW}$ Cd11b- Ly6C-. One explanation for the preservation of resident macrophages is the source of radiation; x-ray was used in this work but beta and gamma radiation are more commonly used.

iNOS inhibition reduced only activation of recruited macrophages. It is therefore possible the resident macrophage maintenance of alternative activation is due to a sub-therapeutic dose of 1400W to the airspace. In previous work, we have shown a reduction in NO metabolites in the BAL with this dose of ITB (Atochina-Vasserman et al., 2007). However, the cellular source of NO metabolites cannot be deciphered and therefore may only reduce iNOS activity of blood derived cells.

Several mechanisms by which iNOS inhibition prevents macrophage activation are plausible. NO is known to modify proteins such as NFκB (Kelleher et al., 2007), GAPDH (Hara et al., 2005), Keap1 (Buckley et al., 2008), SP-D (Guo et al., 2008) and Hmgb1 (Tsoyi et al., 2010) via s-nitrosylation. Such protein modifications impact inflammation and resolution pathways. NO also has the potential to influence macrophage activation by directly promoting glycolysis (Erusalimsky and Moncada, 2007) the energy pathway of classically activated macrophages (Kelly and O'Neill, 2015). These NO dependent modifications require evaluation to elucidate the mechanism by which NO activates macrophages.

3.6 Tables

	PBS	ITB	ITB+1400W
8 Days	0	2.5*	2.5*
15 Days	0	3*	4*#

Table 3-1

Table 1. ITB increases pulmonary inflammation and iNOS inhibition potentiates inflammation at later time point. Lungs were prepared for histology 8 and 15 days post instillation after bronchoalveolar lavage. Lung sections were stained with hematoxyllin and eosin, assessed for pulmonary inflammation and assigned scores. $P<0.05$

*compared to PBS, #compared to ITB

Treatment	Collection	Total	GFP+ F4/80+	GFP- F4/80+
8 Days				
PBS	BAL	222,775 ± 28,164	18,567± 3,685	201,376± 26,410
	BALM	515,267± 84,659^{+}	9,625± 2,738	499,436±85,352 $^{+}$
ITB	BAL	424,400± 47,145*	115,275±18,213*	275,849±38,470
	BALM	639,525± 34,419^{+}	221,176± 28,685*$^{+}$	335,140±61,840
ITB+1400W	BAL	393,175± 33,496*	101,854± 9,161*	251,119±29,879
	BALM	853,217± 102,933^{+}	351,406± 55,740*$^{+}$	450,655± 42,522 $^{+}$
15 Days				
PBS	BAL	183,243± 18,899	17,894±2,594	163,303± 20,411
	BALM	522,633± 121,986^{+}	225,369± 84,201 $^{+}$	285,228± 28,355 $^{+}$
ITB	BAL	533,586± 56,669*	190,641± 27,202 *	283,695± 29,766 *
	BALM	925,660± 112,111^{+}	441,431± 61,376	372,787± 52,525
ITB+1400W	BAL	708,025± 57,507*	228,455± 32,118 *	363,290± 24,296 *
	BALM	833,300± 142,041	268,359± 63,044	508,221± 85,424

Table 3-2

Table 2. ITB increased the number of recruited macrophages without altering the number of resident macrophages; *unaffected by iNOS inhibition*. Cells were collected from lungs by BAL and BALM. After counting, GFP and F4/80 expression was measured and macrophage populations calculated. P<0.05 * compared to PBS, #compared to ITB, + compared to BAL

	Markers					8 Days ($x10^4$)			15 Days ($x10^4$)		
	GFP	F4/80	Cd11c	Cd11b	Activation	Saline	ITB	ITB+1400W	Saline	ITB	ITB+1400W
Resident Pulmonary MΦ	-	+	+	-	$Cd206^{Low}$	16.0± 1.87	12.6± 1.38	9.4 ±1.18*	15.4 ± 1.91		
					$Cd206^{High}$					17.9 ± 2.36	17.6 ± 2.77
Resident Non-Pulmonary MΦ	-	+	-	-	-	0.6 ± 0.20	11.2 ±2.82*	13.4 ± 2.59*	0.7± 0.17	8.4 ± 1.83*	14.0 ± 2.79*
Recruited Pulmonary MΦ	+	+	+	-	$Cd206^{Low}$	1.0 ± 0.14			1.5 ± 0.24		
					Ly6C+❖		4.8 ± 1.76	2.5 ± 0.48*			
					$Cd206^{High}$					12.7 ± 1.33*	11.9 ± 1.41*
Recently Recruited Pulmonary MΦ	+	+	+	+	$Cd206^{Low}$				0.13 ± 0.02		
					Ly6C+❖	0.8 ± 0.29	5.3 ± -1.00*	4.6 ± 0.25*			
					$Cd206^{High}$					5.0 ± 1.22*	7.6 ± 1.00*
Recruited Non-Pulmonary MΦ	+	+	-	-	-	0.01 ± 0.00	0.4 ± 0.01*	0.7 ± 0.08*+	0.0 ± 0.00	0.6 ± 0.19*	1.5 ± 0.46*
Recently Recruited Non-Pulmonary MΦ	+	+	-	+	-	0.05 ± 0.00	1.2 ±0.21*	2.5 ± 0.26*+	0.0 ± 0.00	0.2 ± 0.06*	0.7 ± 0.37*

Table 3-3

Supplemental Table 1. Macrophage populations activate in a origin and time dependent manner. Macrophages collected from the BAL are classified based on their origin, pulmonary and migratory integrin expression and activation identified. ❖Recruited pulmonary macrophages ($Cd11b^{+/-}$) are Ly6C positive and Cd206 expression is elevated above low but less than High seen at 15 days. (* p value <0.05 compared to PBS)

3.7 Figures

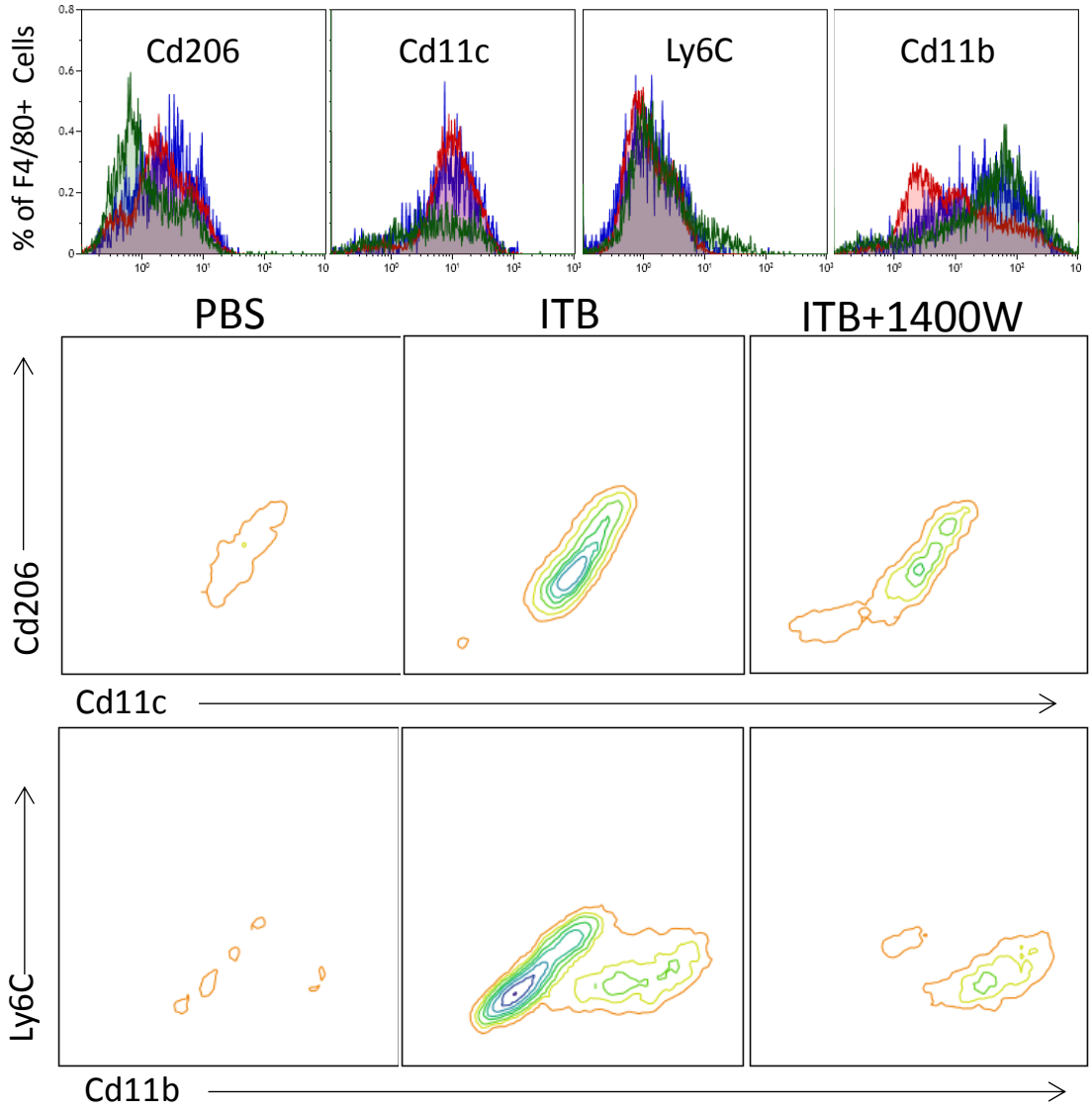

Figure 3-1

Figure 1. ITB leads to recruitment of macrophages that split between recently recruited and pulmonary phenotype; iNOS inhibition increases the portion recently recruited. Mice were intratracheally instilled with PBS (blue), ITB (red) and treated with ITB+1400W (green). Cells were collected 8 days post instillation by bronchoalveolar lavage and immunophenotyped by immunofluorescence using antibodies to Cd206, Cd11c, Ly6C and Cd11b. Data is shown by histogram (A) and contour plot (B).

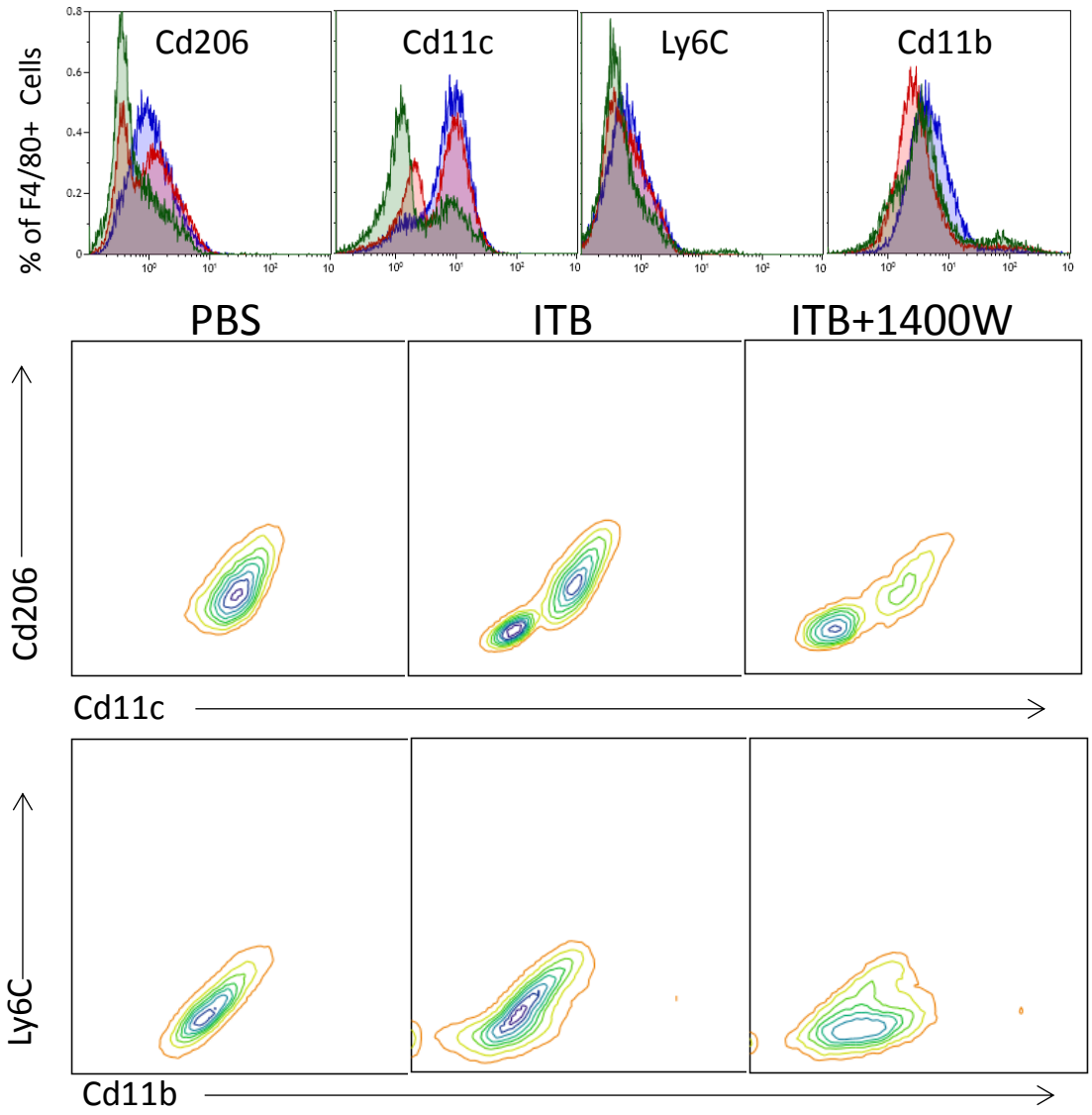

Figure 3-2

Figure 2. Resident macrophages do not polarize 8 days post ITB, unchanged by 1400W. ITB does lead to a subset of resident macrophages with lower Cd11c and Cd206 than saline treated and 1400W promotes this double negative population. Cells were collected by bronchoalveolar lavage from mice 8 days post instillation of saline (blue) or ITB (red, green). 1400W was systemically delivered to a subset of ITB treated mice (green). Flow cytometry was used to measure expression of Cd206, Cd11c, Ly6C and Cd11b on GFP- macrophages. Data is expressed by overlay histograms (A) and contour plots (B).

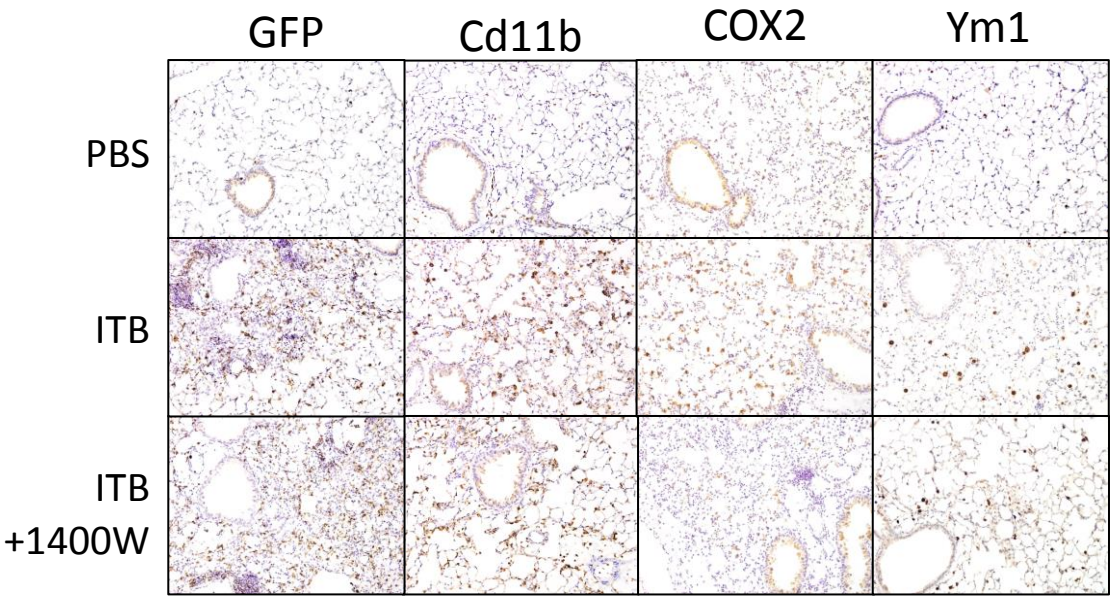

Figure 3-3

Figure 3. Increased expression of COX2 post ITB is inhibited by 1400W treatment. GFP, Cd11b, COX2 and Ym1 are increased 8 days post ITB. Immunohistochemistry was performed to assess protein expression in tissue post lavage. Lungs after bronchoalveolar lavage, were inflation fixed and prepared for histological sectioning. Antibodies to the protein of interest were incubated followed by biotinylated secondary and DAB staining.

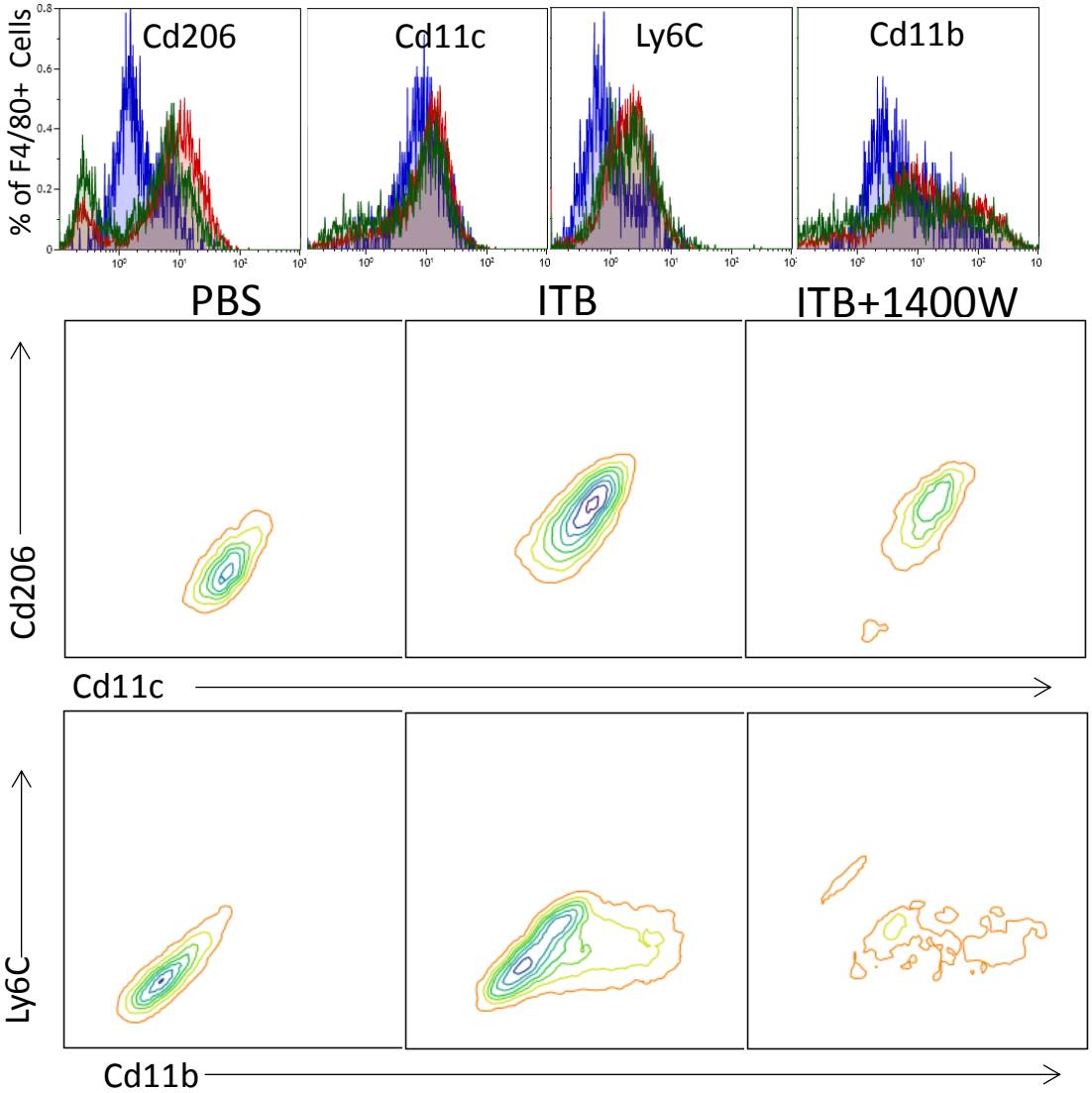

Figure 3-4

Figure 4. Macrophages continue to be recruited to the lung 15 days post ITB, particularly in the 1400W treated mice. Recruited macrophages increase Cd206 expression in response to ITB, population reduced by 1400W. Cells were phenotypically analyzed by flow cytometry after collected from lungs of saline (blue) or ITB (without 1400W (red), with 1400W (green)) using antibodies to F4/80, Cd206, Cd11c, Ly6C and Cd11b.

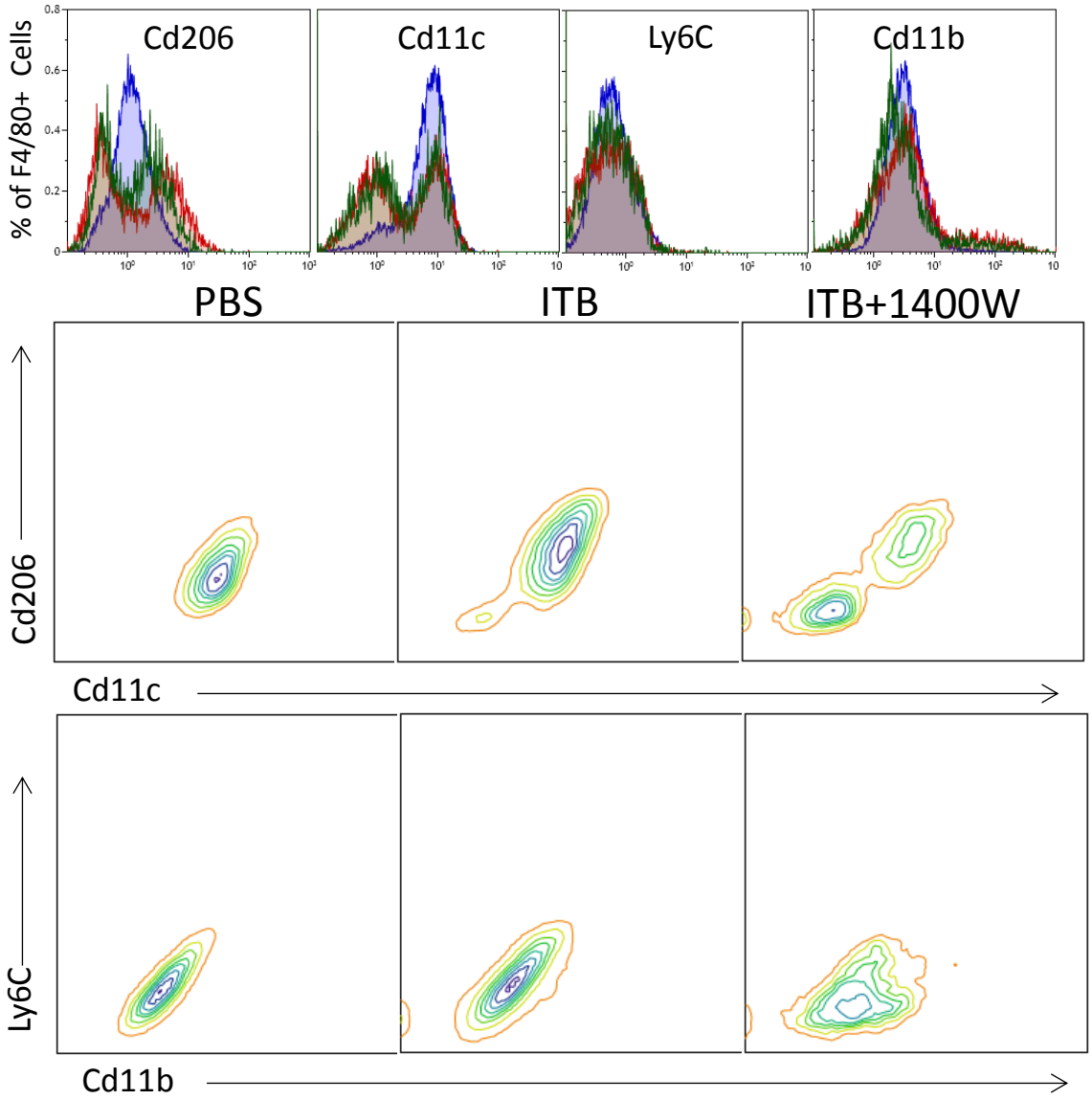

Figure 3-5

Figure 5. Resident macrophages increase their Cd206 expression 15 days post ITB but 1400W promotes a split of resident population into $Cd206^{HIGH}$ Cd11c+ and $Cd206^{LOW}$ Cd11c-. Cells are collected by bronchoalveolar lavage 15 days post instillation of saline (blue) or ITB (red, green). 1400W was administered to a subset of ITB treated mice (green). Resident macrophages were identified as GFP- F4/80+ and phenotypically assessed using antibodies to Cd206, Cd11c, Ly6C and Cd11b.

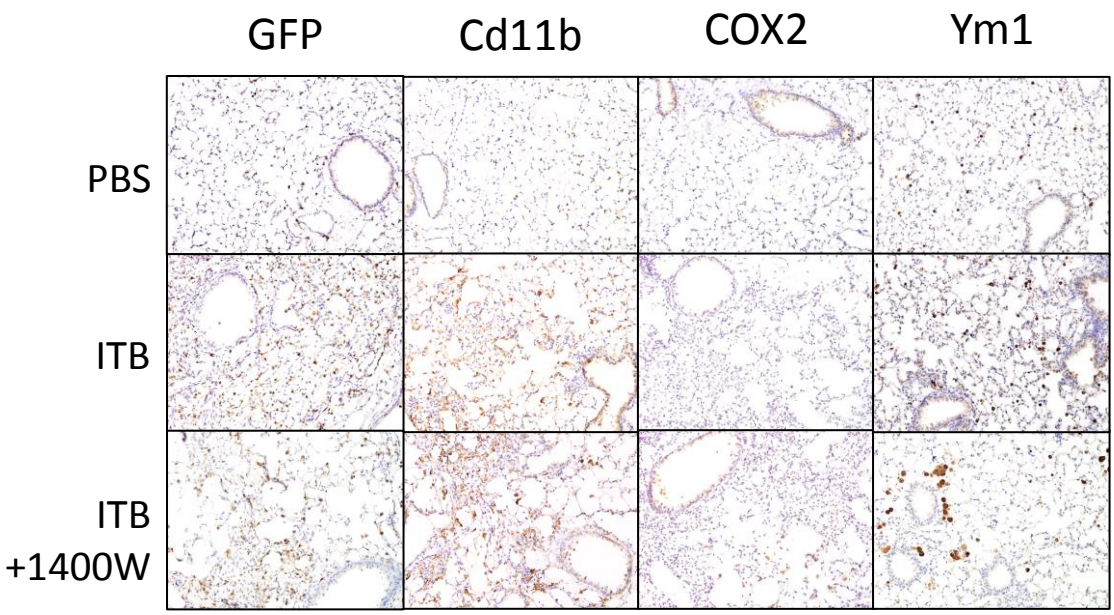

Figure 3-6

Figure 6. GFP expression remains high in tissue 15 days post ITB while Cd11b expression remains high only in ITB+1400W treated mice. COX2 expression is reduced but Ym1 expression induced. Lung tissue was collected for histology after bronchoalveolar and prepared for immunohistochemistry. Antibodies to Cd11b, GFP, COX2 and Ym1 were used followed by biotinylated secondary and DAB stain.

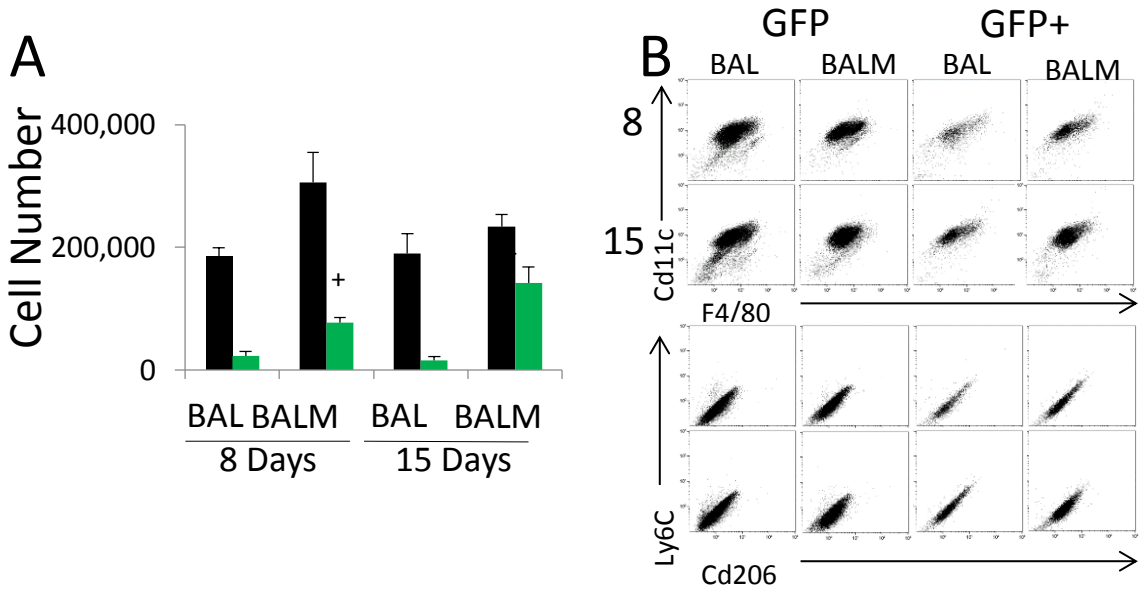

Figure 3-7

Supplemental Figure 1. Resident macrophages predominate the population of macrophages collected by lavage with and without massage following sham instillation. GFP+ macrophages exist in the lavage and increased with massage (+ $p<0.05$ compared to lavage) but phenotypically are identical to GFP- macrophages. Cells were collected from lungs by lavage with (BALM) and without (BAL) massage. Cells counted and identified as GFP+ (green) or GFP- (black) (A) and further phenotypically characterized by flow cytometry (B).

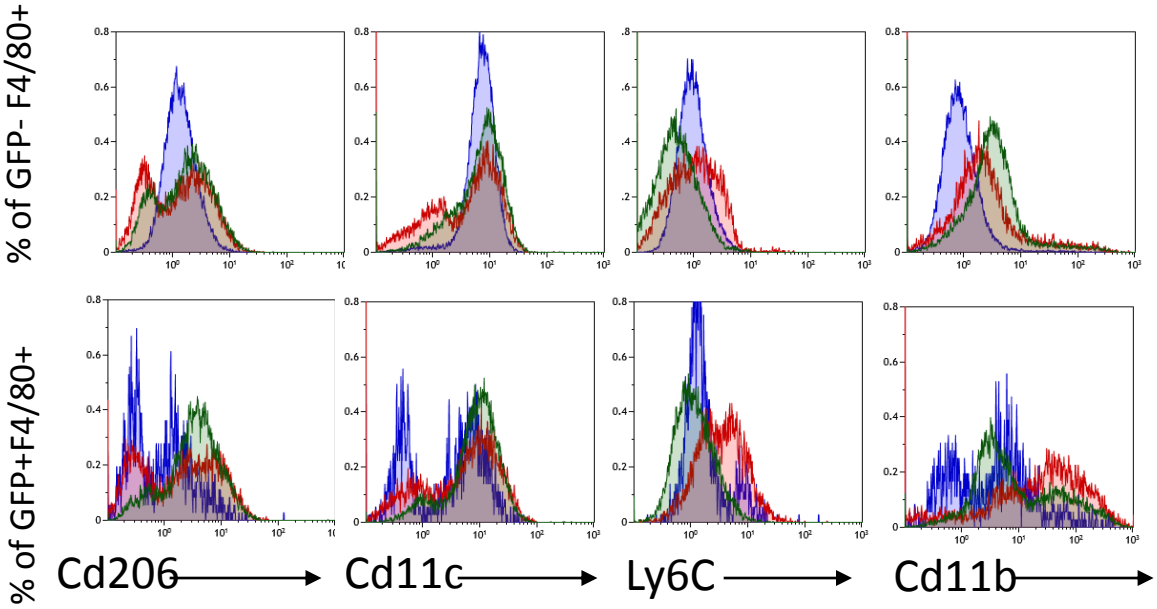

Figure 3-8

Supplemental Figure 2. 8 Day BALM macrophage phenotype (GFP- top, GFP+ bottom) of PBS (blue), ITB (red) and ITB+1400W (green) treated mice.

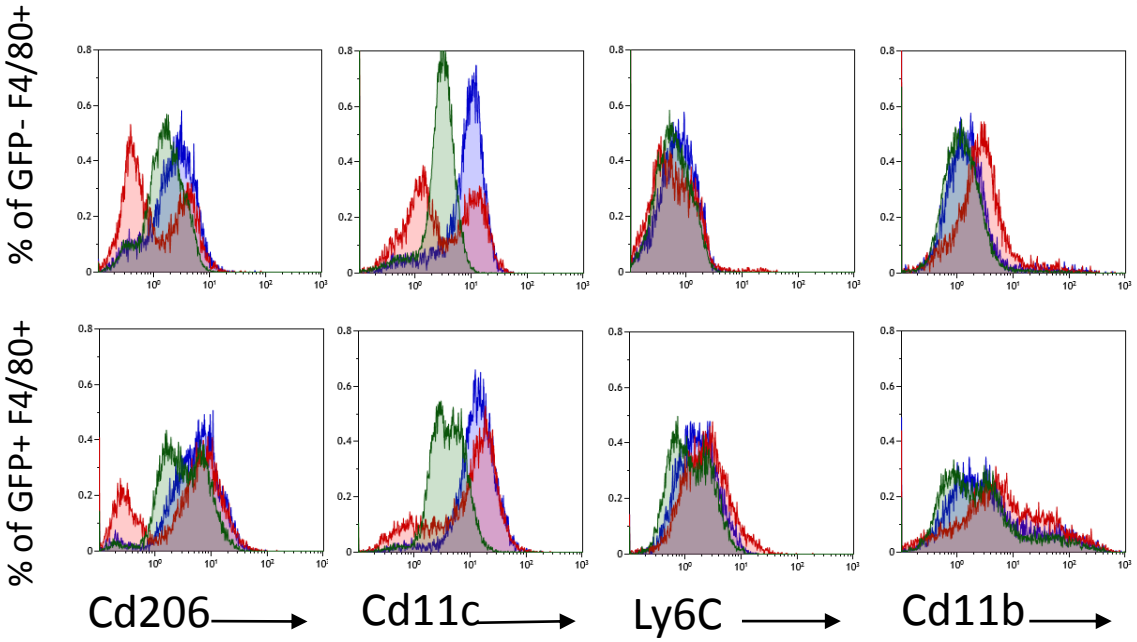

Figure 3-9

Supplemental Figure 3. 15 Day BALM macrophage phenotype (GFP- top, GFP+ bottom) of PBS (blue), ITB (red) and ITB+1400W (green) treated mice.

CHAPTER 4: ORIGIN OF INOS DETERMINES EFFECT ON MACROPHAGE ACTIVATION IN ACUTE LUNG INJURY

4.1 Abstract

Macrophage activation is dependent on inducible nitric oxide synthase in the intratracheal bleomycin model of acute lung injury. This work aims to determine the role of bone marrow cell vs pulmonary derived iNOS. A chimeric mouse approach was employed to create iNOS competent (WT to WT), pulmonary knockout (WT to $NOS2^{-/-}$) and bone marrow knockout ($NOS2^{-/-}$ to WT) chimeras on the C57/BL6 background. Flow cytometry and immunohistochemistry were used to immunophenotype cells 8 and 15 days post ITB. Bone marrow knockout chimeras had reduced classical activation of macrophages and increased alternative activation 8 days post ITB. Alternative activation increased with time in the bone marrow knockout. Pulmonary knockout chimeras had fewer Cd11b positive cells in the tissue 8 days post ITB without altering cell number. Pulmonary knockout chimeras did not alter classical activation 8 days post ITB but did reduce alternative activation 15 days post ITB. Biopterins were also measured and the ratio of reduced to oxidized reduced post ITB. ITB decreases the availability of reduced cofactor 8 and 15 days post ITB. Only the pulmonary knockout chimera has restored levels of available reduced cofactor 15 days post ITB. This work demonstrates iNOS of a particular cell origin influences macrophage activation. These findings could in part explain the divergent role of iNOS previously reported in ITB mediated ALI.

4.2 Introduction

The inflammation and resolution phases of ITB mediated ALI are orchestrated by recruited and resident macrophages in the lung. Previously, we have shown in Chapter

3, macrophages are recruited to the lung 8 and 15 days post ITB while the number of resident macrophages remains consistent. Recruited macrophages classically activate 8 days post ITB while resident macrophages do not activate. 15 days post ITB, recruited and resident macrophages alternatively activate. This work demonstrated macrophage origin determines phenotypic response to ITB mediated acute lung injury. Others have shown cell origin determines response to bleomycin induced lung injury using a chimeric mouse model (Gasse et al., 2007; Sangaletti et al., 2011; Cohen et al., 2015).

Classically activated macrophages increase many pro-inflammatory proteins; one of which is inducible nitric oxide synthase. This enzyme is induced via translocation of NFκB to the nucleus (Robbins et al., 1997). iNOS produces nitric oxide at a high flux rate resulting in the production of high oxides of nitric oxide in the oxidant rich environment following ITB (Rosa et al., 2014). Such radical species have the potential to cause harm to cells thus potentiating the inflammatory response (Ju et al., 2010). Loss of nitric oxide signaling, due to oxidation, is also potentially detrimental as NO has been shown important to many physiological functions (Furchgott and Vanhoutte, 1989; Drazen et al., 1995; Coleman, 2001; Bland et al., 2005; Auten et al., 2007).

iNOS expression is increased during inflammation in macrophages and pulmonary epithelial cells (Guo and Erzurum, 1998; Guo et al., 2016). Therefore there are resident and recruited sources of iNOS. iNOS inhibition, by 1400W, has been shown in Chapter 3 to differentially effect recruited and resident activation. For instance, recruited macrophages classically activate 8 days post ITB and alternatively activate 15 days post ITB, both of which are prevented by 1400W. Resident macrophage activation on the other hand is not reduced by iNOS inhibition and resident macrophages alternatively activate 15 days post ITB with or without 1400W.

4.3 Methods

Animals

6 week old C57/BL6 (Jackson) or NOS2$^{-/-}$ mice were irradiated with 12 Grey (Gy) X-ray radiation using a Torrex irradiator. Bone marrow was harvested from C57/BL6 (Jackson) or NOS2$^{-/-}$ mice and the following chimeras were made; iNOS competent C57/BL6 to C57/BL6, pulmonary knockout C57/BL6 to NOS2$^{-/-}$ and bone marrow knockout NOS2$^{-/-}$ to C57/BL6. Mice were monitored for 6 weeks and fed Picolab 0.025% Trimethoprim/0.1242% Sulfamethoxazole antibiotic chow for the first 2 weeks (W.F.Fisher and Son Sommerville, NJ).

Intratracheal instillation and Sample Collection

After 6 weeks of recovery, mice were either instilled with 50uL saline or 50uL 3units/kg bleomycin (Sigma St. Louis MO) in saline under isoflurane anesthesia. Mice were either sacrificed 8 or 15 days post instillation by ketamine/xylazine overdose followed by exsanguination. Lungs were cannulated and bronchoalveolar lavage (BAL) was completed to collect cells and proteins from airways. Left lungs were then inflation fixed with 3% paraformaldehyde 2% sucrose, ethanol dehydrated and paraffin embedded for sectioning. Another set of mice underwent BAL followed by a massage of lung tissue and subsequent lavage of lung (BALM).

Cell Analysis

Cells collected by BAL and BALM were centrifuged to collect cell pellet and supernatant for protein measurement (Bradford assay). Cells were counted by Multisizer (Beckman Coulter Indianapolis IN). Cytospins of 30,000 cells were prepared and stained with KWIK-DIFF (Thermo Scientific) and morphologically assessed for cell type. 200,000 cells (or remaining if insufficient) were immunostained for flow cytometry using the

following antibodies: Cd206-PE (Biolegend 141706), Ly6C-PerCP/Cy5.5 (Biolegend 128012), F4/80-PE/Cy5 (Biolegend 123114), Cd11b-APC (Biolegend 101212), Cd11c-AF700 (Biolegend 117320). Manufacturer protocols were followed including a 10 minute Fc block (TruStain FcBlock Biolegend 101320), 30 minute antibody incubation and 30 minute viability dye incubation (eBiosciences 65-0865-14 San Diego, CA). Fluorescence was measured using Gallios (Beckman Coulter Indianapolis IN) and data analyzed by Kaluza software (Beckman Coulter Indianapolis IN).

Tissue Analysis

Paraffin blocks were prepared of dehydrated left lungs and sectioned for hematoxylin and eosin (H&E) stain and immunohistochemistry. H&E sections were assessed for extent of inflammation and structural damage. Immunohistochemistry was performed using the following antibodies; Cd11b (abcam 133357, 1:3000 primary dilution), COX2 (abcam 15191, 1:2000 primary dilution), Ym1 (StemCell 01404, 1:500 primary dilution) and (secondary antibody 1:2000 (Vector Burlingame, CA)).

4.4 Results

Cell Number Unaffected by Loss of iNOS in Either Compartment

Total cell number was counted in the BAL and found to be unchanged in either chimeric mouse (Table 1). Cells were identified as macrophages by F4/80 expression and the number of macrophages or other (F4/80-) cells were also unchanged in either chimeric mouse. This is true at 8 and 15 days.

Histological Assessment Reveals Improved Inflammation at Late but Not Early Time Points in the Pulmonary Knockout Chimera

Histology was assessed for signs of inflammation and structural integrity using a scoring system adapted from Rudmann, et al. (Rudmann et al., 1998). 8 days following ITB, all groups had leukocytes in the peribronchial, perivascular and parenchymal areas of the lung. Airway epithelial cells were hypertrophied. There was little septal defect at this early time point. As seen in the top row of Figure 1. there are small areas of consolidation in all chimeric mice. All chimeric groups scored a median of 2. At 15 days there was an increase in median inflammation score to 3 in the iNOS competent and bone marrow knockout mouse, but score remained 2 in the pulmonary knockout mouse. The extent of consolidation is decreased in the pulmonary knockout compared to other groups 15 days post ITB (Figure 1, bottom row). This overall assessment of inflammation suggests loss of pulmonary iNOS improves resolution of inflammation following ITB.

Classical Activation is Prevented and Alternative Activation Promoted in the Bone Marrow Knockout Chimera

Previously reported, in Chapter 3, recruited macrophages increase Ly6C expression in the BAL and COX2 in the tissue suggesting classical activation. Ly6C expression on F4/80+ cells of the BAL showed increased fluorescence in the iNOS competent and pulmonary knockout chimera but not the bone marrow chimera (Figure 2A). COX2 expression of the tissue however was similar in all chimeras (Figure 2B). Markers of alternative activation were also assessed in BAL cells, Cd206 expression, and tissue, Ym1. Cd206 expression of F4/80+ BAL cells was not changed in either chimera (Figure 3). Pulmonary integrin, Cd11c, was also unchanged by loss of iNOS in either compartment (Figure 3). Ym1 expression is not induced in the tissue of iNOS competent mice or pulmonary knockout but expression is increased in bone marrow knockout mice. This suggests loss of bone marrow iNOS prevents classical and

promotes alternative activation of macrophages 8 days post ITB. To confirm, similar recruitment of cells, migratory integrin Cd11b expression was analyzed in the BAL and tissue. Bone marrow knockout mice had similar Cd11b in the BAL and tissue compared to iNOS competent mice. However, pulmonary knockout mice had fewer Cd11b expressing cells in the tissue (Figure 2B).

Alternative activation of Macrophages 15 days post ITB is decreased in pulmonary knockout mice

Cd206 expression is increased on BAL macrophages and Ym1 expression increased on macrophages in the tissue (Figure 4). Bone marrow knockout mice and pulmonary knockout mice have similar Cd206 expression on F4/80+ BAL cells. Bone marrow knockout mice further induce expression of Ym1 in the tissue. Pulmonary knockout mice however do not induce Ym1 expression in the tissue. Classical activation is decreased in chimeras like iNOS competent 8 days post ITB (Supplemental Figure 1).

Cofactor availability is decreased following ITB and only restored in pulmonary knockout chimeras 15 days post ITB

Biopterins were measured by HPLC and the ratio of reduced to oxidized (Figure 5). All groups treated with ITB had significantly decreased levels of reduced co-factor at 8 days compared to saline treated mice. Ratio in saline is similar 15 days post instillation and the ratio remains reduced in iNOS competent and bone marrow knockout chimeras. Pulmonary knockout chimeras restore the ratio to that of saline 15 days post ITB.

4.5 Discussion

Loss of iNOS in either the bone marrow or pulmonary compartment results in distinct changes to macrophage activation but not recruitment. Bone marrow knockout mice decrease classical activation of macrophages collected by BAL and promote alternative activation. Alternative activation persists with time and is similar to iNOS competent mice at 15 days. Pulmonary knockout mice have fewer Ym1 expressing cells in the tissue but similar Cd206 expression on macrophages collected by BAL at 15 days without changing activation at 8 days.

Bone marrow knockout mice experience less classical activation during the inflammatory stage following ITB. Macrophage number and Cd11b expression are unchanged ruling out the possibility recruitment is responsible for fewer Ly6C+ BAL macrophages. Previously, we have shown (Chapter 3) recruited macrophages and not resident macrophages classically activate 8 days post ITB. In the bone marrow knockout chimera, recruited macrophages are $NOS2^{-/-}$. Therefore this finding suggests iNOS of the recruited cell is necessary for classical activation of that cell. Post translational modification of pro-inflammatory proteins is one possible mechanism. For instance, s-nitrosylation of surfactant protein D and HMGB1 lead to classical activation of macrophages. It is possible these proteins are critical to the adoption of the pro-inflammatory phenotype.

Pulmonary knockout mice experience less alternative activation of tissue associated macrophages. BAL Cd206 expression is increased on F4/80+ cells in pulmonary knockout mice like those cells in iNOS competent mice. However, Ym1 expression in the tissue is reduced. In these chimeric mice the resident alveolar macrophages and epithelial cells are $NOS2^{-/-}$ and therefore cannot increase iNOS expression in times of inflammation. Therefore alternative activation of macrophages may be in part dependent on either pulmonary epithelial cell or alveolar macrophage

iNOS activity. S-nitrosylation of KEAP1 and the subsequent release of nrf2 for nuclear translocation and antioxidant response element gene transcription is one possible mechanism by which alternative activation is promoted (Buckley et al., 2008; Jensen et al., 2013).

Tetrahydrobiopterin (BH4) is a necessary cofactor for NOS enzyme production of nitric oxide. Without BH4, NOS functions in an uncoupled manner to reduce molecular oxygen directly rather than its substrate arginine (Stroes et al., 1998; Hurshman et al., 1999). Others have shown loss of macrophage BH4 synthesis decreases NO production, increases reactive oxygen species production and reduces NRF2 dependent gene expression (McNeill et al., 2015). In times of inflammation, BH4 synthesis is increased via upregulation of GTP cyclohydrolase (Gch1)(Hattori et al., 1996; Starr et al., 2014). In oxidative environments BH4 becomes oxidized to BH2 a competitive inhibitor of NOS (Vasquez-Vivar et al., 2001; Alp and Channon, 2004). Oxidized biopterins are capable of binding at the biopterin binding site of NOS but cannot participate in electron transduction (Vasquez-Vivar et al., 2002; Crabtree et al., 2008). This work demonstrates the availability of BH4 is decreased in proportion to the availability of oxidized biopterins. That would suggest iNOS is not only producing NO but superoxide as well. In the pulmonary knockout mouse, the ratio of reduced to oxidized biopterins is restored.

The necessity of radiation in the development of chimeric mice is one limitation to this work. Radiation has been shown to cause lung inflammation. Previously, in chapter 3, we reported the effect of radiation on sham treated mice. Macrophages collected from sham treated mice 6 weeks after radiation were resident pulmonary macrophages (F4/80+ Cd11c+). This supports a significant body of literature demonstrating alveolar macrophage resistance to radiation (van oud Alblas and van Furth, 1979; Tarling et al.,

1987; Kennedy and Abkowitz, 1998; Landsman and Jung, 2007; Hashimoto et al., 2013).

4.6 Tables

Cell Number 10^4	**Total**	**F4/80+**	**F4/80-**
8 Days			
iNOS Competent	42±4.7	41±4.5	1.8±0.41
Pulmonary KO	33±5.3	32±5.1	1.3±0.39
Bone Marrow KO	30±9.4	30±9.2	0.4±0.13
15 Days			
iNOS Competent	53±5.7	50±4.9	3.4±1.12
Pulmonary KO	45±8.1	44±8.0	1.1±0.16
Bone Marrow KO	47±5.3	46±5.5	1.1±0.23

Table 4-1

Table 1. Total, macrophage and non-macrophage cell number is not altered in chimeric mice. Cells were collected by BAL and counted on Multisizer. Flow cytometry was used to identify F4/80 expression.

	Reduced	**Oxidized**	**Total**
8 Days			
PBS	3.4±0.22	28.7±3.78	32.1±3.62
iNOS Competent	3.9±0.76	63.1±10.05	67.0±10.63
Pulmonary KO	2.5±0.17	39.9±2.77	42.4±2.90
Bone Marrow KO	2.0±0.31	46.3±5.75	48.3±6.05
15 Days			
PBS	3.4±0.46	30.2±4.12	33.7±4.52
iNOS Competent	2.7±0.43	55.7±2.96	58.4±3.10
Pulmonary KO	4.5±1.91	55.7±14.86	60.1±16.28
Bone Marrow KO	2.23±0.32	45.8±2.55	48.1±2.36

Table 4-2

Supplemental Table 1. Total biopterins, particularly oxidized, are increased post ITB. Reduced (BH4) is restored to saline levels in pulmonary knockout chimeras 15 days post ITB.

4.7 Figures

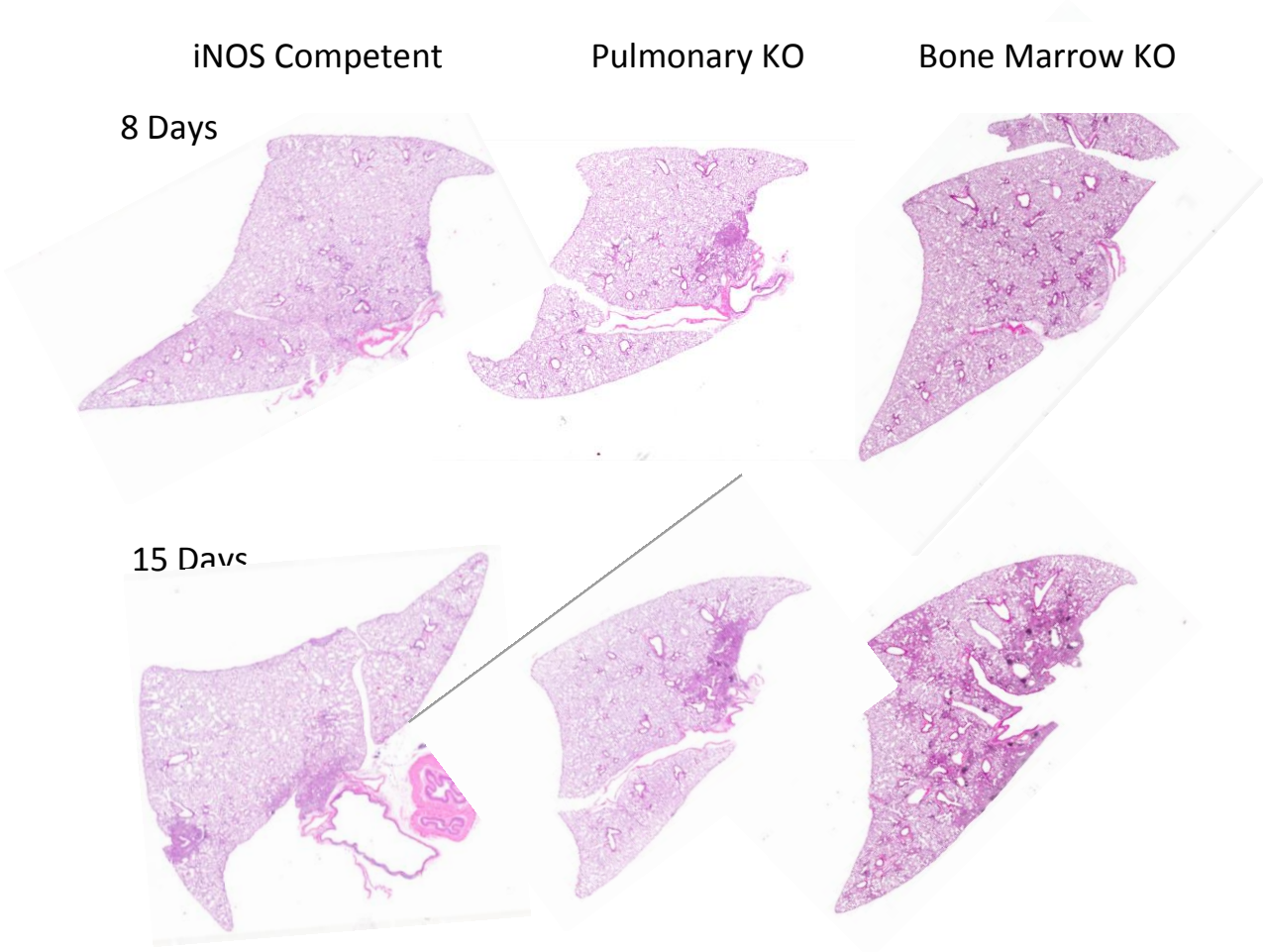

Figure 4-1

Figure 1. Histological assessment of lungs post ITB demonstrate pulmonary knockout mice have less inflammation 15 days post ITB while bone marrow knockout mice have similar to iNOS competent. Left lungs were histologically prepared and stained with H&E. Lungs were compared by histological scoring and representative lungs shown.

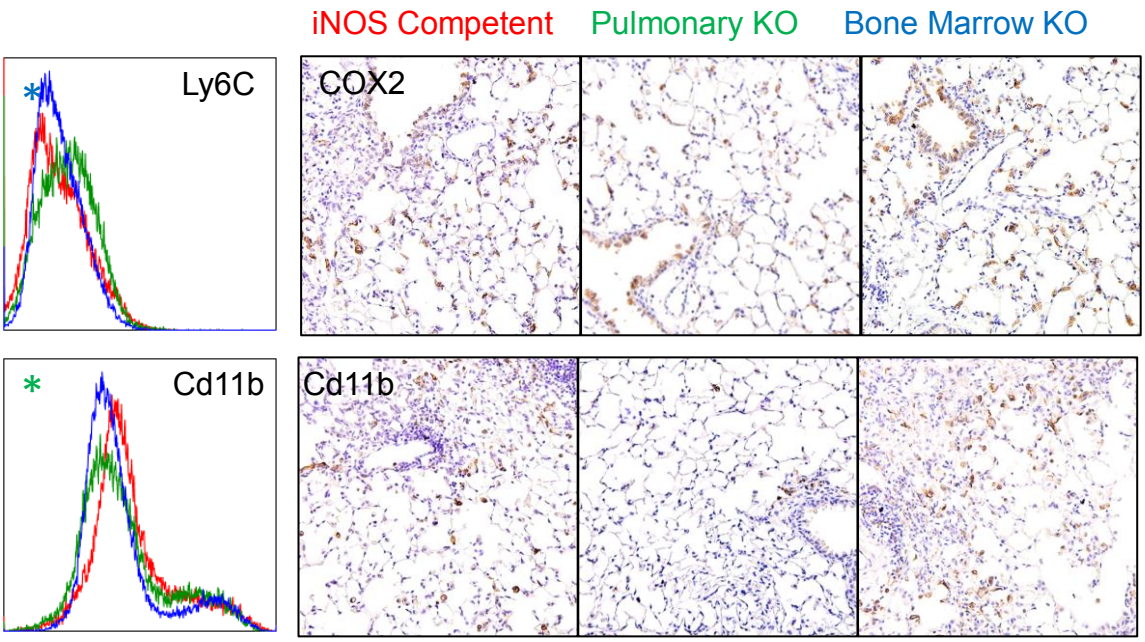

Figure 4-2

Figure 2. Classical activation 8 days post ITB is reduced in bone marrow knockout chimeras BAL but not tissue associated cells. Cd11b expression is decreased in pulmonary knockout chimeras. Cells were collected by BAL and Ly6C and Cd11b expression of F4/80+ macrophages are shown. Lung tissue was stained by IHC for COX2 and Cd11b.

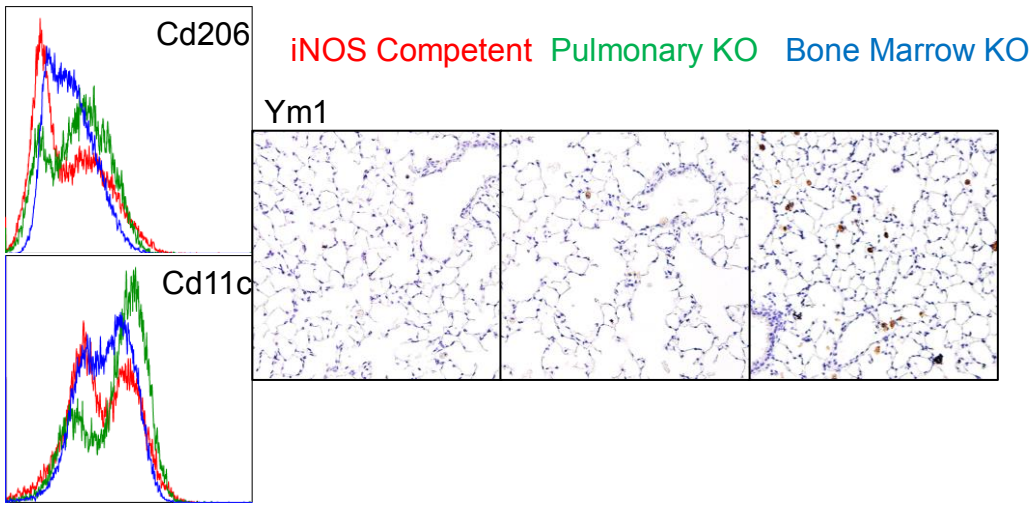

Figure 4-3

Figure 3. Alternative activation of tissue associated macrophages is increased 8 days post ITB in bone marrow knockout chimeras. Cd206 and Cd11c expression on BAL F4/80+ macrophages is shown in histograms and does not differ between chimeras. Ym1 stain in the tissue is only induced in bone marrow knockout chimeras.

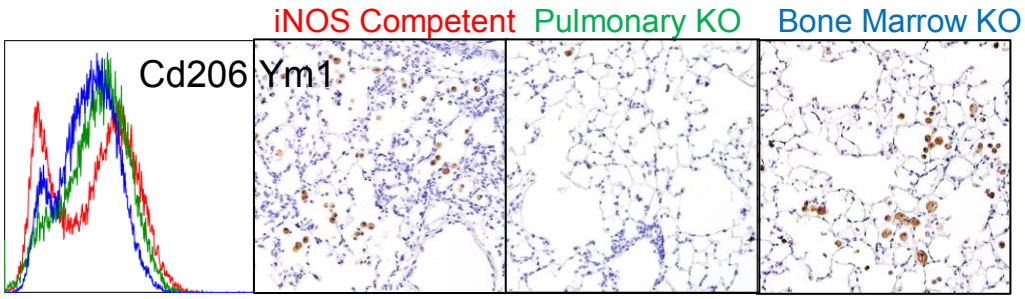

Figure 4-4

Figure 4. Tissue associated macrophages do not alternatively activate in pulmonary knockout chimeras as seen by a decrease in Ym1 positive stain. iNOS competent and bone marrow knockout mice induce Ym1 expression in the tissue and Cd206 expression of the BAL F4/80+ cells.

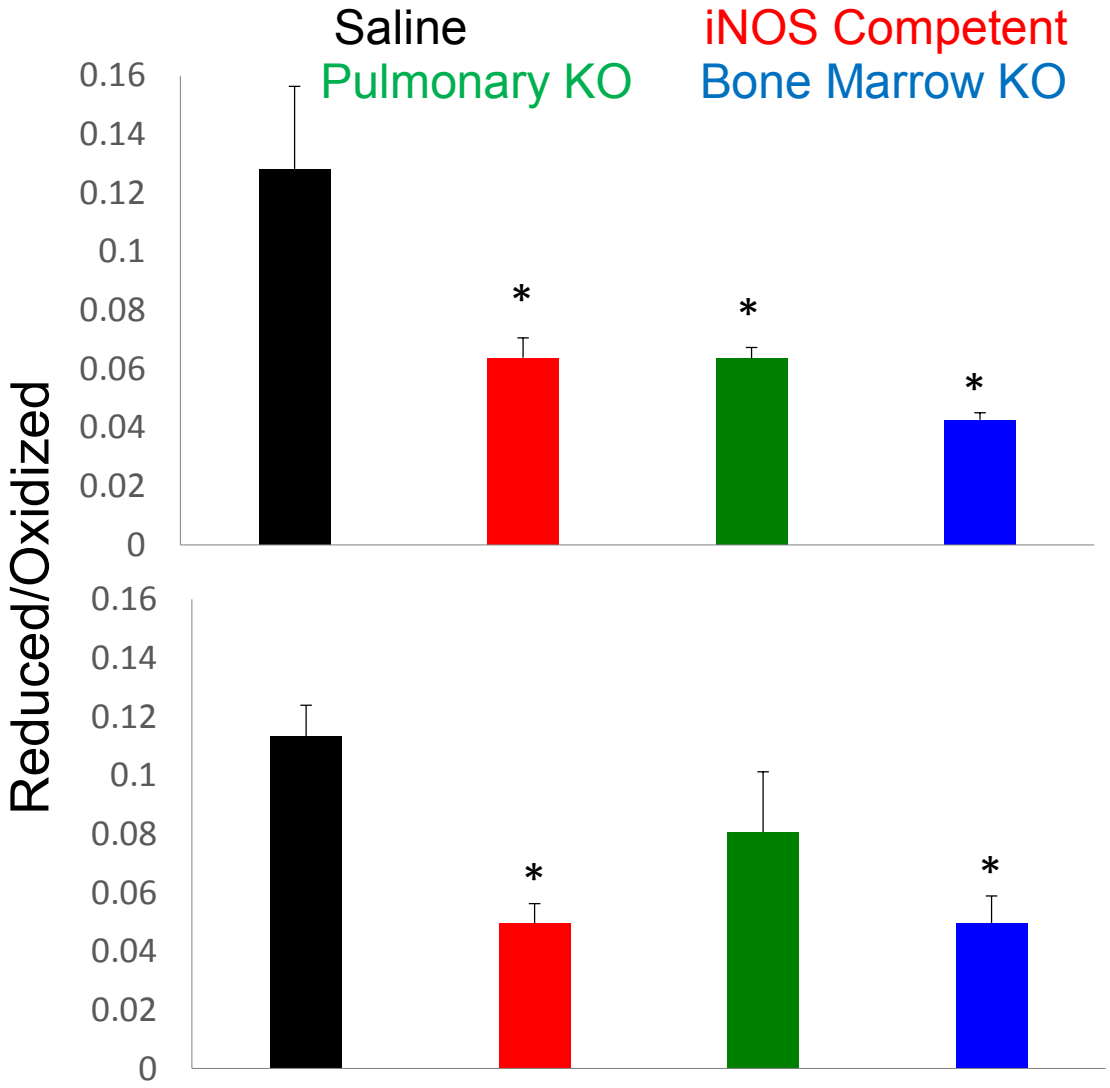

Figure 4-5

Figure 5. Tetrahydrobiopterin (BH4) availability is limited following ITB at 8 and 15 days. Pulmonary knockout chimera restores the ratio to that of saline treated mice 15 days post ITB. Biopterins are measured by HPLC and the ratio of reduced (BH4) to oxidized reported.

CHAPTER 5: SUMMARY, DISCUSSION AND CONCLUSION

5.1 Summary

Macrophages are diverse cells in origin and activation phenotypes. Reactive species are important to macrophage activation and early inflammatory processes. During the inflammatory phase that follows bleomycin mediated ALI, recruited macrophages classically activate. During resolution, recruited and resident macrophages alternatively activate. iNOS is important to recruited macrophage activation during the inflammatory and resolution stages that follow bleomycin mediated ALI. Chimeric mice identify recruited macrophage iNOS necessary for classical activation of the recruited macrophage. Pulmonary cell derived iNOS is necessary for alternative activation 15 days post ITB. Therefore the source of iNOS determines the effect on activation.

5.2 Discussion

iNOS expression is increased downstream of NFκB directed transcription. Classically activated macrophages express high levels of iNOS and have been shown to produce nitric oxide (Mantovani et al., 2004). The role of iNOS in macrophage adoption of pro-inflammatory phenotype has yet to be identified. In chapter 2, scavenge of radical species resulted in reduced macrophage activation and reduced pro-inflammatory mRNA and protein levels 3 and 8 days post ITB. Similar results were published by others in the lab (Guo et al., 2016). In chapter 3, classically activated macrophages were identified as macrophages originating in the bone marrow at the time of injury. 1400W inhibited classical activation of recruited macrophages 8 days post ITB. In chapter 4, it was determined iNOS of the recruited cell is necessary for classical

activation 8 days post ITB. The combination of this work clearly identifies iNOS as a necessary protein in the classical activation of recruited macrophages.

One such mechanism that is capable of resulting in classical activation is through s-nitrosylation of surfactant protein D. The classically activated macrophage expresses high levels of iNOS and therefore produces large amounts of NO. NO diffuses across the cell membrane where it interacts with the oxidative extracellular environment. Higher oxides of nitric oxide have the potential to interact with surfactant protein D to form a trimer leading to NFκB activation.

Alternative activation of macrophages decreases expression of iNOS and substrate, arginine, is instead metabolized by arginase. This work demonstrates iNOS is important to alternative activation. In chapter 3, recruited and resident macrophages alternatively activate 15 days post ITB. iNOS inhibition with 1400W decreases recruited macrophage alternative activation. Pulmonary knockout chimeras used in chapter 4 demonstrate it is iNOS of the pulmonary cells, either resident macrophages or epithelial cells, responsible for alternative activation at 15 days. In fact, when pulmonary iNOS is present but recruited cell iNOS is not, as in the bone marrow knockout chimera, alterative activation is promoted earlier than seen in iNOS competent mice. iNOS of the pulmonary derived cells is responsible for alternatively activating macrophages 15 days post ITB and if unopposed by classical activation, macrophages alternatively activate earlier.

During resolution, there are fewer classically activated macrophages and therefore the expression of iNOS and oxidant producing enzymes is reduced. Less radical species are present in the cellular environment. However, the pulmonary knockout chimera demonstrates lack of iNOS in the resident macrophage population and epithelial cells, reduces macrophage alternative activation. Therefore pulmonary derived iNOS, in either the resident macrophage population or epithelial cell, plays a role in

alternative activation. S-nitrosylation of several proteins, such as GAPDH, p65/p50 and Keap1, lead to pro-resolving pathways. These proteins are intracellular and suggest intracellular NO promotes pro-resolution and anti-inflammatory pathways. It is possible one or more of these pathways are enlisted in order to promote alternative activation during resolution.

iNOS is not a major determinant of recruitment. The earliest time point evaluated was 3 days post ITB in Chapter 2. Total cell number at this time point was reduced by tocopherol supplementation. However, BAL protein was also reduced suggesting the alveolar-capillary barrier less damaged. This effect is lost with time, as both BAL protein and BAL cell number is the same 8 days post ITB with or without tocopherol. Similarly, in chapter 3 1400W does not change the number of cells collected by lavage or lavage with massage. More specifically, the number of GFP+ cells is not decreased 8 or 15 days post ITB. Chimeric mice also have similar numbers of cells and specifically macrophages in the BAL. Neither chapter 3 or 4 looked at the early time point of 3 days. Therefore we cannot confirm the 3 day finding in chapter 2 with systemic or specific loss of iNOS.

This work primarily used flow cytometry and immunohistochemistry to phenotype the macrophages. Immunophenotyping defines populations based on their protein expression. However, this work needs to be followed by measures of cell population activity. For instance, cell populations could be sorted in order to measure mRNA or protein levels. This becomes particularly difficult in mouse models as the number of cells is limited. Newer techniques such as RNAseq or single cell analysis could be employed. The function of these populations would further our understanding of their role in inflammation and resolution of ALI.

The chimeric mouse model relies on radiation to kill bone marrow cells. Radiation has the potential to injure the lung (Jackson et al., 2012; Groves et al., 2015;

Malaviya et al., 2015). Sham instilled mice were used in Chapter 3 in order to account for the effect of radiation and chimeric mouse development on the lung. Mice were sacrificed 7 and 8 weeks (8 and 15 days post sham instillation) and cells taken by BAL, BALM and tissue for histology. As demonstrated in Chapter 3, there was no sign of inflammation or injury in sham instilled mice. Cells collected by BAL and BALM were immunophenotyped by flow cytometry and were F4/80+ Cd11c+ $Cd206^{LOW}$ Cd11b- Ly6C-. The vast majority of these cells were GFP- and therefore resident to the lung. This supports others evidence that resident pulmonary macrophages are radiation resistant (van oud Alblas and van Furth, 1979; Tarling and Coggle, 1982; Kennedy and Abkowitz, 1998; Landsman and Jung, 2007; Hashimoto et al., 2013).

Studying resolution of inflammation in the intratracheal bleomycin model of acute lung injury is complicated by subsequent fibrosis. Early signs of fibrosis can be seen 15 days post ITB and fibrosis 21-28 days post ITB (Matute-Bello et al., 2008). Therefore it is with caution to think of alternatively activated macrophages to be pro-resolving and beneficial only. It is indeed possible the early subset of macrophages responsible for fibrosis is reported in these findings. Without following the macrophage populations to later time points the identification of this population is not possible. The histological findings in Chapter 4 suggest the pulmonary source of iNOS may play a part in fibrosis as this lung has reduced inflammation compared to iNOS competent and bone marrow knockout chimeras. It would be interesting to follow these chimeras out to 21 days and measure fibrotic endpoints.

5.3 Conclusion

Classical and alternative macrophage activation is dependent on iNOS activity. The amount of iNOS protein expressed is likely a determinant of effect. When large quantities of nitric oxide are made quickly, nitric oxide has the potential to diffuse to the

extracellular compartment where it elicits a pro-inflammatory response. When low levels of nitric oxide are made the effect is internal and leads to pro-resolving and repair pathway activation. This work suggests this delicate balance is controlled by macrophage origin in that recruited macrophages classically activate during the inflammatory phase and resident macrophages and/or pulmonary epithelial cells orchestrate resolution through iNOS dependent manners.

5.4 Future Directions

The work I have detailed in this dissertation has focused on the inflammatory response and its resolution in response to acute lung injury. Fibrosis is a long term endpoint of ALI and it would be an extension of my work to consider how iNOS function, within recruited and resident macrophages, alters the fibrotic response to ITB. Fibrosis is thought to develop in consequence to the inflammation at earlier time points following ITB. From the work presented in this thesis, we hypothesize the pulmonary knockout chimera will experience less fibrosis than the iNOS competent and bone marrow knockout chimera. Resolution is improved in the pulmonary knockout chimera and alternative activation of macrophages remaining in the lung after lavage 15 days post ITB is reduced in the pulmonary knockout chimera. If fibrosis is a consequence of inflammation, improved resolution of inflammation will reduce fibrotic endpoints. One of the main ways I would assess fibrosis in this situation would be through Trichrome staining of collagen fibers as well as directly measuring hydroxyproline within lung tissue (an indirect measure of collagen content).

From my studies it appears that iNOS is serving different roles within different cell types, which predominate at different times post ITB. This may explain the failure of iNOS inhibitors to have improved outcome in humans in response to injury. However,

these observations also indicate that the timing of iNOS inhibition offers a manner to improve therapy. It appears that iNOS is important to classical activation during inflammation and alternative activation during resolution. Therefore, it would be interesting to test the effect of iNOS inhibition during either the inflammation or resolution phases following ITB. I would propose that iNOS inhibition in the inflammatory phase will reduce inflammation and improve resolution/fibrosis, however, during the resolution phase it would produce a negative effect. This approach would also evaluate the dependence of resolution on processes during inflammation; for instance is resolution improved or impeded by reduction of early inflammation?

iNOS has been identified as a regulator of macrophage activation through studies that inhibited iNOS or eliminated gene expression of *NOS2*. One of the downstream targets of NO-derived from iNOS are the protein thiols, which can be nitrosylated to produce S-nitrosothiol. Through manipulations of S-nitrosoglutathione reductase (GSNOR), S-nitrosylation of proteins is increased due to decreased reduction of SNO proteins. Thereby manipulations of GSNOR serves as an inverse manipulation to iNOS inhibition. GSNOR inhibition potentially increases SNO proteins of which many are immunomodulatory proteins. GSNOR can be manipulated by conditional or full body knockout or inhibitors currently undergoing testing in clinical trials. I would contend that reducing GSNOR function could lead to enhanced inflammation, if given early, or increased resolution, if given late.

The role of reactive oxide species in contrast to nitric oxide in macrophage activation could also be further explored. This work has studied the role of iNOS in macrophage activation but iNOS can produce nitric oxide and superoxide depending on cofactor availability. As reported in Chapter 4, biopterins are oxidized 8 and 15 days post ITB. Oxidized biopterins bind to iNOS but do not function as cofactor. Therefore iNOS was likely functioning in an uncoupled manner producing superoxide instead of

nitric oxide. Only in the pulmonary knockout mouse 15 days post ITB, was the balance of reduced to oxidized biopterin levels restored to control levels. It would be interesting to study if iNOS functions in a nitric oxide dependent or independent manner to activate macrophages.

INTRODUCTION TO APPENDICES

While working in Dr. Andrew Gow's laboratory I have been interested in studying inflammation and resolution of the lung. My first interest arose after following a patient in the ICU during pharmacy rotation. A 46 year old female presented post colon surgery to the ICU after being diagnosed with acute respiratory distress syndrome (ARDS). She was ventilator dependent and over the following weeks remained ventilator dependent and lung function continued to deteriorate. Her past medical history lacked lung disease and I was surprised risk factors for developing ARDS were largely unknown. In learning about ARDS, I was discouraged to know treatment options are limited and doctors rely on corticosteroids despite their lack of overall success. This patient was a clear example of the clinical therapy's dependence on basic research.

While working in Dr. Andrew Gow's laboratory, I used the bleomycin model of acute lung injury to study macrophage activation in the inflammatory and resolution stages following intratracheal instillation of bleomycin (ITB). I also had the opportunity to study inflammation in other contexts. For instance, myeloid derived cell activation was evaluated in lymphangioleiomyomatosis (LAM). LAM is a progressive disease that develops almost exclusively in women due to loss of *tuberous sclerosis complex* (tsc) 1 or 2. In humans with LAM and mouse models, parenchyma structure is affected and cystic development occurs. Destruction of alveolar spaces also occurs in other diseases, such as emphysema, and is largely due to macrophage activation. Using techniques such as flow cytometry and immunohistochemistry we identified myeloid derived cell populations also involved in LAM. Similar myeloid derived cell populations were also identified in clinical samples from diagnosed patients. These populations were affected through drug treatments and iNOS protein knockout. Using bone marrow iNOS knockout chimeras, like that in Chapter 4, we identified a role of iNOS in myeloid

cell activation in the LAM model. This finding supports the role of iNOS in myeloid cell activation including models of pulmonary inflammation. I have also extended these studies to another rare disease, multi-centric Castleman's, which appears to involve an altered circulating inflammatory phenotype (although this work has been only preliminary in nature).

Intratracheal bleomycin causes a diffuse yet patchy inflammation and fibrosis of the lung. We worked to develop a model in which inflammation could be viewed on a whole lung level using magnetic resonance imaging (MRI). Using co-registration of histological sections and in-vivo MRI a MRI signature for inflammation was developed as explained in Appendix 2. This signature can be used in further experiments to measure the extent and location of inflammation in the entire lung. Effect of treatment on inflammation can therefore be measured using this MRI signature. Animals can also be followed across the multi-stage response to ITB without the need to sacrifice animals at each time point. I have extended the idea of small animal imaging and co-registration to make precise measurements of airway diameter and length that can be incorporated into lung functional models. These studies have been highly collaborative and have pushed me to consider more team-based approaches to solving complex problems.

APPENDIX 1

Lymphangioleiomyomatosis (LAM) is a rare lung disease almost exclusively affects women. Mutation in the tumor suppressor genes *tuberous sclerosis complex* (TSC) 1 or 2 is known to cause disease. We show, in the paper below, in a nude mouse model of LAM the immune system is activated. Specifically, myeloid derived populations increase in the lung including macrophages, neutrophils and an immature myeloid cell. The immature myeloid cell is defined as Cd11b+ F4/80+ Ly6G+ and its morphology consistent with immaturity.

The following discusses work in preparation for publication.

The work in the nude mouse identifies a role of the immune system. Patients with disease do not have impaired adaptive immunity, like that of the nude mouse, so it is important to study LAM in an immunocompetent mouse. Therefore we developed the model in the C57/BL6 mouse. Loss of tsc2 in the cells injected into C57/BL6 mice was confirmed by western blot. We also confirmed typical markers of LAM, lymphatic vessel endothelial hyaluronic acid receptor 1 (Lyve1) and smooth muscle actin- alpha (sma-α), in the lungs 3 weeks post injection of tsc2 null cells. Using flow cytometry we identified an immature myeloid derived cell population collected by bronchoalveolar lavage (BAL) (Figure 1). These cells similarly expressed Cd11b F4/80 and Ly6G but also expressed Ly6C. A more monocytic than granulocytic immature cell was identified on cytospin as well. We also found the C57/BL6 mouse developed more circular lesions than that seen in the nude mouse model (Figure 2).

We designed further experiments to study the immature myeloid derived cell population's origin. Using the green fluorescent protein (GFP) chimeric mouse approach as used in Chapter 3, we identified the immature myeloid derived cell population to be recruited from the bone marrow post tsc2 null cell injection (Figure 3). We also identified GFP+ cells in tissue to reside along the outside of lesions.

We approached treatment of LAM via immune modulating drugs. Axitinib, a vascular endothelial growth factor D (VEGFD) inhibitor, and rapamycin, a mammalian target of rapamycin (mTOR) inhibitor, were used in the C57/BL6 model of LAM. Both drugs reduced lesion load in the lung and when combined further reduced the number of lesions (Figure 4A). Additionally, both drugs reduced the number of immature myeloid derived cells collected in the BAL (Figure 4B).

As seen in chapter 3 and 4, iNOS is responsible for macrophage activation. We hypothesized iNOS was also important to the activation of recruited cells to LAM lesions. Using the chimeric mouse approach, we replaced the bone marrow of a C57/BL6 mouse with *NOS2-/-* bone marrow cells. This chimeric mouse was similar to the "bone marrow knockout" discussed in Chapter 4. In this mouse, we found an increase in the number of immature myeloid derived cells collected by BAL (Figure 5). The lesions were less circular if the recruited cells were *NOS2-/-*, suggesting the recruited cell is important to restricting lesion growth.

We also had the opportunity to study patients diagnosed with LAM. As part of a larger clinical trial evaluating the safety of simvastatin in LAM treatment, we collected peripheral blood. After isolation of white blood cells, cells were immunophenotyped using flow cytometry. In LAM diagnosed patient peripheral blood we were able to confirm an immature myeloid derived cell, CD11B+ CD33+ CD14+ CD15+, not present in healthy control blood (Figure 6A). We also identified these cells in a chyle fluid sample collected from the lung of a LAM patient (Figure 6B). Clinical samples support the presence of immature myeloid cells in LAM disease.

This work will continue to study the immature myeloid derived cell population in LAM disease. Further work evaluating the function of the immature myeloid derived cell population via cell sorting followed by gene expression measures would be informative. Additionally, these cells could be approached as if they are myeloid suppressor cells

(MDSC) as seen in other cancers. Their high expression of iNOS and arginase suggests they are similar to MDSCs. It would be interesting to see if inhibition of proteins known to be over expressed in MDSCs, such as arginase and colony stimulating factors, reduced development of LAM lesions and the number of immature myeloid derived cells. Identification of the role of iNOS to immature myeloid derived cell activation suggests increasing the products of iNOS, such as by inhibition of s-nitrosoglutathione reductase (GSNOR), may decrease the number of immature myeloid derived cells. There are many therapeutic approaches that arise from the identification of immature myeloid derived cells in the mouse model and clinical setting of LAM.

ORIGINAL RESEARCH

Surfactant Dysfunction and Lung Inflammation in the Female Mouse Model of Lymphangioleiomyomatosis

Elena N. Atochina-Vasserman[1,2], Chang-Jiang Guo[3], Elena Abramova[3], Thea N. Golden[3], Michael Sims[2], Melane L. James[1,2], Michael F. Beers[2], Andrew J. Gow[3], and Vera P. Krymskaya[1,2]

[1]Airway Biology Initiative and [2]Pulmonary, Allergy, and Critical Care Division, University of Pennsylvania Perelman School of Medicine, Philadelphia, Pennsylvania; and [3]Department of Pharmacology and Toxicology, Rutgers University, Piscataway, New Jersey

Abstract

Pulmonary lymphangioleiomyomatosis (LAM) is a rare lung disease caused by mutations of the tumor suppressor genes, *tuberous sclerosis complex* (*TSC*) *1* or *TSC2*. LAM affects women almost exclusively, and it is characterized by neoplastic growth of atypical smooth muscle–like TSC2-null LAM cells in the pulmonary interstitium, cystic destruction of lung parenchyma, and progressive decline in lung function. In this study, we hypothesized that TSC2-null lesions promote a proinflammatory environment, which contributes to lung parenchyma destruction. Using a TSC2-null female murine LAM model, we demonstrate that TSC2-null lesions promote alveolar macrophage accumulation, recruitment of immature multinucleated cells, an increased induction of proinflammatory genes, nitric oxide (NO) synthase 2, IL-6, chemokine (C-C motif) ligand 2 (CCL2)/monocyte chemotactic protein 1 (MCP1), chemokine (C-X-C motif) ligand 1 (CXCL1)/keratinocyte chemoattractant (KC), and up-regulation of IL-6, KC, MCP-1, and transforming growth factor-β1 levels in bronchoalveolar lavage fluid. Bronchoalveolar lavage fluid also contained an increased level of surfactant protein (SP)-D, but not SP-A, significant reduction of SP-B levels, and a resultant increase in alveolar surface tension. Consistent with the growth of TSC2-null lesions, NO levels were also increased and, in turn, modified SP-D through *S*-nitrosylation, forming *S*-nitrosylated SP-D, a known consequence of lung inflammation. Progressive growth of TSC2-null lesions was accompanied by elevated levels of matrix metalloproteinase-3 and -9. This report demonstrates a link between growth of TSC2-null lesions and inflammation-induced surfactant dysfunction that might contribute to lung destruction in LAM.

Keywords: interstitial lung disease; nitric oxide; surfactant protein-D; tuberous sclerosis complex 2; animal models

Clinical Relevance

This study demonstrates that tuberous sclerosis complex 2–null induced pulmonary inflammation, as defined by increased nitric oxide synthase 2 expression, *S*-nitrosylation of surfactant protein-D, and surfactants dysfunction, might contribute to airspace enlargement and respiratory impairment, key aspects of the pathology of human lymphangioleiomyomatosis.

Pulmonary lymphangioleiomyomatosis (LAM) is a rare, unrelenting parenchymal lung disease characterized by the proliferation of abnormal smooth muscle–like "LAM cells," leading to cystic destruction of the lung parenchyma and progressive respiratory failure (1, 2). LAM cells are low-grade, destructive, and metastasizing neoplasm (3). A key element to the progression of the disease is parenchymal destruction within the lung that can lead to pneumothorax and respiratory failure. The mechanisms by which LAM cells induce lung tissue destruction are unknown.

Although LAM has not been defined as an inflammatory disease, the high

(Received in original form June 5, 2014; accepted in final form November 12, 2014)

This work was supported by National Institutes of Health grants RO1 HL090829 and RO1 HL114085 (V.P.K.), HL86621 (A.J.G), and by LAM Foundation Career Investigator Award (CIA) 560768.

Author Contributions: E.N.A.-V. and V.P.K.—conception and design; E.N.A.-V., C.-J.G., E.A., T.N.G., and M.L.J.—acquisition of data; E.N.A.-V., M.S., A.J.G., M.F.B., and V.P.K.—analysis and interpretation; E.N.A.-V., A.J.G., M.F.B., and V.P.K.—drafting the manuscript for important intellectual content; all authors approved of the final manuscript.

Correspondence and requests for reprints should be addressed to Elena N. Atochina-Vasserman, M.D., Ph.D., Translational Research Laboratory, 125 South 31st Street, Suite 1200, Philadelphia, PA 19104-3403. E-mail: atochina@mail.med.upenn.edu

Am J Respir Cell Mol Biol Vol 53, Iss 1, pp 96–104, Jul 2015

Originally Published in Press as DOI: 10.1165/rcmb.2014-0224OC on May 29, 2014
Internet address: www.atsjournals.org

expression of inflammatory chemokines in bronchoalveolar lavage (BAL) fluid and nodules from patients with LAM (4) suggested the involvement of inflammation in the pathogenesis of LAM. Importantly, airway inflammation was reported in 61% of patients with LAM (5). One-third of patients with LAM with airway obstruction respond to bronchodilators, such as albuterol, a β2-adrenoreceptor agonist, with an increase in FEV_1 of 12% and 200 ml above baseline values (5). We have reported increased levels of proinflammatory cytokines in a female mouse LAM model, suggesting that inflammation may cause the alveolar destruction (6). Published *in vitro* data also demonstrate that the tuberous sclerosis complex (TSC) 2–mammalian target of rapamycin (mTOR) pathway regulates inflammatory responses after bacterial stimulation in mononuclear phagocytes, suggesting that the TSC2–mTOR pathway is a regulator of innate immune homeostasis (7). However, the exact mechanisms of pulmonary inflammation and its contribution to lung destruction in LAM are not well understood.

In the lung, nitric oxide (NO) is a key regulator, controlling varied processes, including airway tone and inflammation (8, 9). In particular, up-regulation of NO production via the inducible isoform of NO synthase (iNOS; coded by NOS2 gene) has been shown to be important in innate immune responses (10, 11), in promoting macrophage activation (12), and in the development of emphysematous and interstitial lung pathologies (13). NO has also been demonstrated to have both pro- and antitumorogenic roles (14). However, whether NO has a role in the pathophysiology of LAM is unclear.

The lung lining fluid, acting as a surfactant, also contains key regulatory elements of the innate immune system. Produced predominantly by type II epithelial cells, there are four surfactant proteins (SPs), SP-A, -B, -C, and -D (15). Whereas SP-B and -C are critical to surface activity and lung function (16), SP-A and -D are collectins, which facilitate pathogen clearance and regulate immune function in the lung. Homozygous depletion of SP-D (*Sftpd*$^{-/-}$) results in an enhanced baseline inflammatory state and increased susceptibility to bacterial and viral lung infection (17–20).

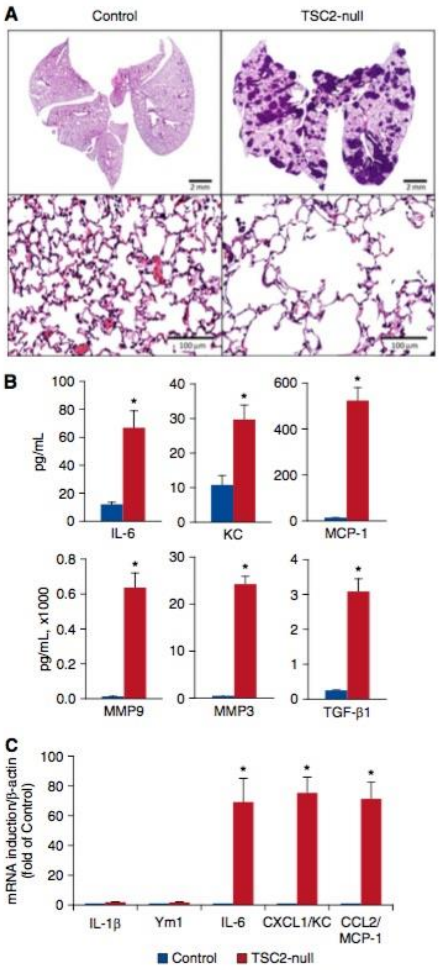

Figure 1. Tuberous sclerosis complex (TSC) 2–null lung lesions induce proinflammatory cytokines and gene activation. (*A*) Representative micrographs of hematoxylin and eosin staining of lung sections from untreated control mice and mice with TSC2-null lesions. (*B*) Bronchoalveolar lavage (BAL) fluid was collected at Day 21 after TSC2-null cell injection and analyzed for cytokine level by the Aushon Searchlight Protein Array multiplex ELISA. Data are expressed as mean values ± SEM; $n = 10$/group. $^*P < 0.05$ versus untreated control mice by *t* test. (*C*) RNA was extracted from BAL cells isolated from lungs of untreated control mice and mice with TSC2-null lesions. Gene markers were quantified by quantitative RT-PCR, as described in the MATERIALS AND METHODS. Threshold cycle (Ct) values obtained were normalized to β-actin signals and further analyzed using the relative quantization (ΔΔCt) method. Data are expressed as fold change (means ± SEM; $n = 5$–8 in each group). Data are expressed as mean values ± SEM; $n = 10$/group. $^*P < 0.05$ versus untreated control mice by *t* test. CCL2, chemokine (C-C motif) ligand 2; CXCL1, chemokine (C-X-C motif) ligand 1; KC, keratinocyte chemoattractant; MCP-1, monocyte chemotactic protein 1; MMP, matrix metallopeptidase; mRNA, messenger RNA; TGF-β1, transforming growth factor β1.

Furthermore, the chronic inflammation seen in the *Sftpd*$^{-/-}$ mice is associated with activation of NOS2 gene expression (10, 19) and parenchymal tissue destruction (13). Importantly, pharmacological inhibition of iNOS or ablation of the NOS2 gene within *Sftpd*$^{-/-}$ mice results in reduction of inflammation (13, 21). We have identified NO-mediated modification of SP-D in a variety of human diseases, including asthma and Hermansky-Pudlak syndrome (22, 23). The link between SPs, their function, and lung destruction in LAM have not been investigated.

In this study, using a female murine LAM model, we demonstrate that TSC2-null lesions activate the innate immune response, resulting in inflammation within the lung lining, impaired SP-B production and surfactant function, activated NOS2 gene expression, NO production, and modification of SP-D. We propose that these events might contribute to lung tissue destruction in LAM.

Materials and Methods

Female Murine LAM Model

The female TSC2-null murine LAM model, previously described and characterized (6), validates metastatic cell dissemination in LAM (3). Briefly, 8-week-old, athymic nude female mice (NCRNU-F; Taconic) were injected with (10^6) TSC2-null cells in PBS into the tail vein. Mice, injected with PBS only, were used as untreated controls. Animals were observed three times per week for signs of pulmonary distress and weight loss. Body weight progressively decreased starting on Day 10, but was not greater than 20% below the initial body weight. At 3 weeks after injection, progressive growth of TSC2-null lesions induced marked airspace enlargement in the lung (Figure 1), in concordance with previous work (6). After 21 days, animals were killed, followed by BAL and tissue collection, and analysis. All animal procedures were approved by the Institutional Animal Care and Use Committees of the University of Pennsylvania (Philadelphia, PA).

BALF Analyses

At 21 days after injection, mice were killed, and lungs were lavaged with 0.5- to 1-ml aliquots of sterile 0.9% saline to a total of 5 ml, as previously described (6). Recovered BAL fluids were centrifuged at 400 × *g* for 10 minutes at 4°C and cell pellets were resuspended in PBS, followed by cell count using a Z1 Counter particle counter (Beckman-Coulter, Inc., Miami, FL). Differential cell counts were performed manually on cytopreparations stained with Diff-Quik. Aliquots of the cell-free BAL fluid were analyzed for cytokine levels by Multiplex (Aushon, Billerica, MA) and NO metabolites by chemical reduction and chemilumnescence using the Ionics/Sievers Nitric Oxide Analyzer 280 (NOA 280; Ionics Instruments, Boulder, CO) (24).

Surfactant Fractionation and Analyses

The cell-free BAL fluids were centrifuged at 20,000 × *g* for 40 minutes at 4°C for separation into two surfactant fractions: the biophysically active large-aggregate (LA) form, and the biophysically inactive small-aggregate (SA) form. The resulting LA pellets were resuspended in saline. Total protein and phospholipid contents within LA and SA surfactant fractions were determined by the bicinchoninic acid method (Pierce, Rockford, IL) and by the method of Bartlett, respectively, as previously described (23). The biophysical activity of recovered LA surfactant was measured in a Capillary Surfactometer (Calmia Medical, Canada) and has been extensively described previously (24, 25). Samples of LA fractions of BAL fluid were diluted with saline to a total phospholipids concentration of 0.5–1.0 mg/ml, and 0.5 μl was deposited into the narrow section of the glass capillary. Data were expressed as percentage of capillary openness, where 100% fully open capillary corresponds to minimum surface tension. Each sample was analyzed in triplicate.

Western Blotting

Detection of SP-B level in LA fraction, SP-A and SP-D levels, and its multimeric structure in BAL was performed as previously described (24, 26, 27) using a polyclonal anti–SP-B (Abcam, Cambridge, MA) or polyclonal in-house anti–SP-D and anti–SP-A antibodies. Detection of *S*-nitrosylated SP-D (SNO–SP-D) in BAL fluid was performed via the biotin switch method, as previously described (11, 23).

Flow Cytometric Analysis

Cells collected in BAL fluid of either untreated control mice or mice with TSC2-null lesions were immunostained for flow cytometry using the following flurochrome-labeled monoclonal antibodies according to manufacturers' protocol: FITC-Cd11b, PE-Ly6C, PE/Cy7- F4/80, AF647-Ly6G (Biolegend, San Diego, CA) and Fixable Viability Dye eFluor 780 (eBioscience, San Diego, CA). Cells were incubated with TruStain FcX (anti-mouse CD16/32) (Biolegend) before antibody incubation. Single stains were used for gating purposes and in accordance with previous measurements using nonimmune IgG controls. Data were acquired with Gallios Flow Cytometer (Beckman-Coulter, Inc.) and analyzed with Kaluza software (Beckman-Coulter, Inc.).

Quantitative RT-PCR

The cells recovered from BAL fluid were analyzed for messenger RNA (mRNA) expression levels by quantitative RT-PCR according to the manufacturer's instructions (Applied Biosystems) as previously described (13). Obtained threshold cycle (Ct) values were normalized to β-actin signals and further analyzed using the relative quantization (ΔΔCt) method.

Statistical Analysis

Data are shown as mean (±SEM). Statistically significant differences between groups of mice were determined by Student's *t* test. Values of *P* less than 0.05 were considered significant.

Results

TSC2-Null Lung Lesions Induce Proinflammatory Cytokines and Genes Activation

We previously established and characterized the mouse LAM model, which manifests by progressive growth of TSC2-null lesions in the lung (6). This experimental LAM model demonstrates the metastatic potential of TSC2-null cells and supports its use as a model for LAM (3). Consistent with our previous observations, the lungs with TSC2-null lesions (Figure 1A, *upper panels*) contain multiple emphysematous-like areas, displaying enlarged airspaces, heterogeneously distributed, and interspersed with interstitial infiltrates

comprised predominantly of mononuclear inflammatory cells (Figure 1A, *lower panels*).

To determine whether TSC2-null lung lesions induce inflammatory cytokine release, a profile of relevant cytokines/chemokines were measured in the BAL fluid from both experimental groups (mice with TSC2-null lesions and littermate untreated controls). The concentration of cytokines, IL-6, chemokine (C-C motif) ligand 2 (CCL2)/monocyte chemotactic protein 1 (MCP-1), chemokine (C-X-C motif) ligand 1 (CXCL1)/keratinocyte chemoattractant (KC), matrix metalloproteinase (MMP) 3, MMP9, and transforming growth factor (TGF)-β1, were markedly increased in BAL from lungs with TSC2-null lesions when compared with untreated control lungs (Figure 1B). The levels of granulocyte/macrophage colony–stimulating factor, IFN-γ, IL-13, and eotaxin were not altered by the development of TSC2-null lesions (data not shown). The increased levels of IL-6, CCL2/MCP-1, and CXCL1/KC suggested classic proinflammatory activation of macrophages. In accordance with these observations, examination of BAL cell mRNA reveals proinflammatory gene expression, IL-6, CXCL1/KC, and CCL2/MCP-1, without increases in alternative activation genes, IL-1β and Ym1 (Figure 1C). The increase in metalloproteinase expression (MMP3 and MMP9) is indicative of inflammation-mediated tissue destruction (6).

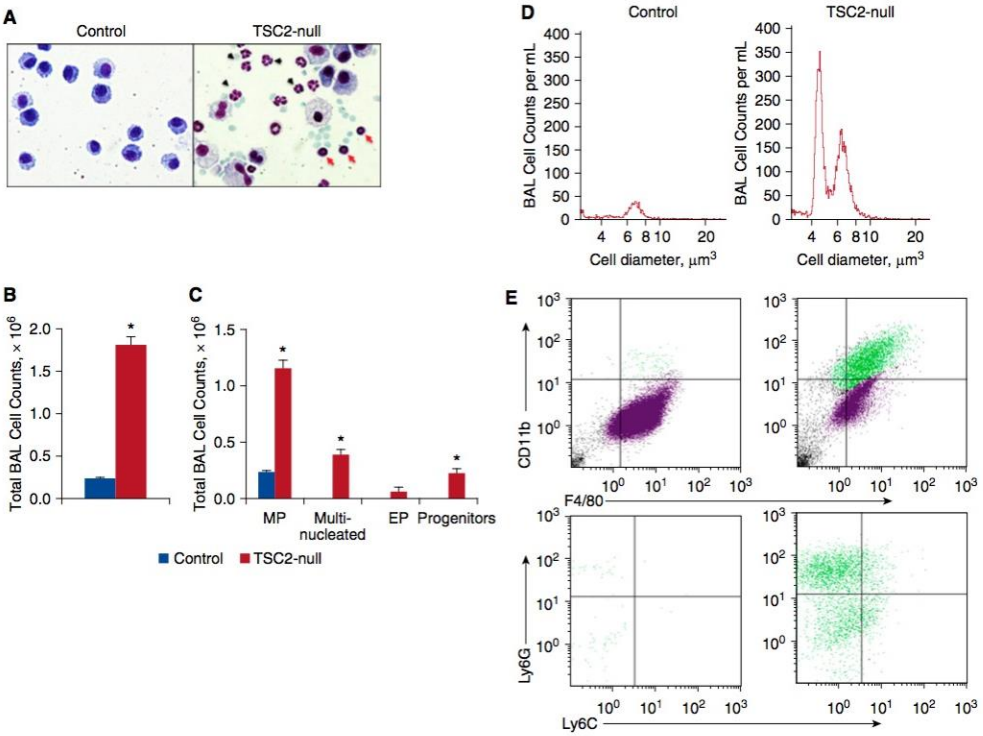

Figure 2. TSC2-null lung lesions promote recruitment of immature myeloid cells. (*A*) Representative micrographs of cells recovered from BAL untreated control mice and mice with TSC2-null lesions. The *red arrows* indicate precursor cells, and the *arrowheads* denote multinucleated cells; magnification, ×20. (*B*) Total BAL cells were determined by Coulter counting. (*C*) Differential cell counts were done using Diff-Quick staining of cytospin slides. Cells were identified as macrophages, eosinophils, multinucleated, or precursors by standard morphology. Values are shown as means ± SEM. $^*P < 0.05$ versus untreated control mice by *t* test; $n = 10$/group. (*D*) Representative micrographs of BAL cell distribution by size. (*E*) Representative flow cytogram of BAL cells stained for CD11b, F4/80, Ly6C, and Ly6G markers. Colors are drawn by population and quadrants by single-stain gating strategy. *Upper panels* show the CD11b and F4/80 expression of viable cells. $CD11b^+/F4/80^+$ cells are *green* in color, whereas *purple color* represents $CD11b^-/F4/80^+$, and *black* is negative for both. *Lower panels* show the Ly6C and Ly6G expression of cells gated on $CD11b^+/F4/80^+$. Flow cytograms are representative of five mice in each group. EP, eosinophils; MP, macrophages.

Interestingly, the profibrotic cytokine, TGF-β1, which can suppress IFN-γ expression (28), was also increased in the lung lining fluid (Figure 1B).

TSC2-Null Lung Lesions Promote Recruitment of Immature Myeloid Cells

The expression of proinflammatory cytokines seen in Figure 1 is generally associated with the recruitment and classical activation of macrophages (12, 13). The BAL cells from mice with TSC2-null lesions and littermate untreated controls were visualized, counted, and analyzed by flow cytometry for surface marker expression. TSC2-null lesions were accompanied by increased total BAL cellularity, which consisted primarily of increased numbers of macrophages (Figures 2B–2D). Morphological differentiation (Figures 2A and 2C) revealed that BAL cells from untreated control lungs contained predominantly macrophages, whereas cells from lungs with TSC2-null lesions were heterogeneous in appearance and contained a variety of immune cells, including macrophages, multinucleated cells, and a large number of smaller cells (Figures 2A and 2D). These smaller cells had band- or ring-shaped nuclei with a higher nucleus-to-cytoplasm ratio than normal alveolar macrophages, features that are consistent with being myeloid progenitors (Figure 2A). To further characterize the cells of the lung lining, we examined surface marker expression by flow cytometry. As seen in Figure 2E (*top panels*), the predominance of cells in the BAL were positive for F4/80, a macrophage marker. A significant portion of cells from mice with TSC2-null lesions, but not from untreated control mice, also expressed CD11b, an integrin that is associated with cellular movement and is an indicator of immaturity. To further characterize their phenotype, the $F4/80^{+}/CD11b^{+}$ cells were further analyzed for expression of the activation markers, Ly6G and Ly6C. As seen in Figure 2E (*lower panels*), these cells were indeterminate in their expression of Ly6C, but there was a clear subpopulation that was positive for Ly6G. These cells represent immature activated myeloid cells that have previously been shown to have immunosuppressive function (29).

TSC2-Null Lung Lesions Induce Dysfunction of Surfactant and Its Activity

Pulmonary inflammation has been shown to alter surfactant component homeostasis and function in both human and animal models (23, 26, 30–33). We examined the total protein and phospholipid contents in the LA and SA surfactant fractions of the BAL from untreated control mice and those with TSC2-null lesions. Table 1 shows that the total protein level in the LA and SA surfactant fractions were proportionately increased (3.7- and 3.3-fold, respectively) in mice with TCS2-null lesions, suggesting an increase in vascular permeability within these lungs. The phospholipid content of the LA fraction was increased by 2.6-fold in mice with TSC2-null lesions (Table 1), whereas the phospholipid level in the SA fraction was unaffected. Measurement of the LA for SP-B content, normalized to total phospholipid, shows that the presence of TSC2-null lesions reduces its expression (Figure 3A). Because SP-B modulates surfactant biophysical activity, we directly determined whether mice with TSC2-null lesions exhibited surfactant dysfunction via capillary surfactometry (24, 25). LA surfactant from lungs with TSC2-lesions produced 45% less capillary opening time when compared with untreated control lungs, indicating a significant reduction in surfactant function. Thus, despite an increase in total phospholipid, the reduction in SP-B, and possibly the increase in vascular leak, as shown by the increased total protein, promoted an increase in the minimum surface tension. A loss of surface-active function within the lung lining would contribute to respiratory impairment as is seen in LAM.

In addition to the surface-active components, type II cells also produce the pulmonary collectins, SP-A and SP-D. To assess whether the reduction of SP-B content in the lungs with TSC2-null lesions was specific and not simply due to global type II cell impairment or dropout, BAL fluids from untreated control mice and mice with TSC2-null lesions were also analyzed for SP-A and SP-D. Total BAL SP-D level was significantly increased in mice with TSC2-null lesions compared with untreated control mice (Figure 3C). In contrast to differential changes in SP-B and SP-D, the SP-A protein content was not significantly altered by the presence of TSC2-null lesions (Figure 3D).

TSC2-Null Lung Lesions Are Associated with Enhanced Pulmonary Nitrogen Oxides Production

Previously, we showed that NOS2 induction and the production of nitrogen oxides accompanies both chronic and acute pulmonary inflammation in a variety of models (11, 22, 24, 34). In addition, NO appears to regulate mTORC1 function and autophagy within breast cancer cells (14). In this context, it is significant that the nitrogen oxide content of BAL fluid, and NOS2 mRNA expression in the BAL cells, were significantly increased in mice with TSC2-null lesions when compared with untreated control (Figures 4A and 4B). Importantly, NOS2 expression was 16-fold higher than ARG1 arginase 1 expression in mice with TSC2-null lesions when compared with untreated control (Figure 4B), confirming a bias toward NO production by pulmonary inflammatory cells within this model of LAM.

Table 1. Tuberous Sclerosis Complex 2–Null Lung Lesions Alter Surfactant Homeostasis

	Protein (μg)		Phospholipids (μg)	
	LA	SA	LA	SA
Control	25 ± 4	310 ± 7	78 ± 13	42 ± 10
TSC2-null	92 ± 5*	1,014 ± 99*	206 ± 29*	67 ± 13

Definition of abbreviations: LA, large aggregate; SA, small aggregate; TSC2, tuberous sclerosis complex 2.
LA and SA fractions from bronchoalveolar lavage fluid of untreated control lungs and lungs with TSC2-null lesions were analyzed by the Bartlett method for phospholipids and by bicinchoninic acid assay for protein contents. Data shown are mean ± SE.
*$P < 0.05$ versus untreated control lungs.

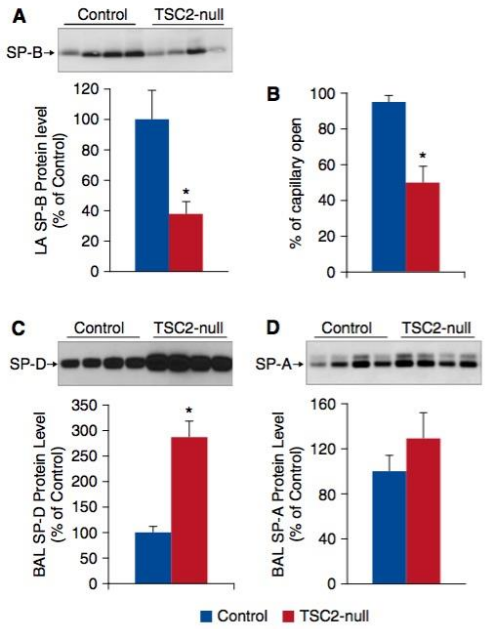

Figure 3. TSC2-null lung lesions induce dysfunction of surfactant and its activity. (*A*) Equal amount of total phospholipids from large-aggregate (LA) fractions of untreated control mice and mice with TSC2-null lesions were subjected to SDS-PAGE under reduced conditions, followed by immunoblotting with anti–surfactant protein (SP)-B antibody. *Upper panel*: representative micrographs of SP-B content. *Lower panel*: densitometric quantification of SP-B content. Mean values of all the samples from untreated control ($n = 10$) and TSC2-null ($n = 10$) groups were calculated and presented as a percentage of untreated control mice. Values are shown as means ± SEM. *$P < 0.05$ versus untreated control mice by *t* test. (*B*) Minimum of surface tension was determined by measuring capillary openness by capillary surfactometer, as described in MATERIALS AND METHODS. Values are shown as a percentage of capillary openness, where 100% is fully open capillary that corresponds to the minimum surface tension (values are obtained by averaging triplicate measurements of each sample; mean + SEM; $n = 10$/group); *$P < 0.05$ versus untreated control mice by *t* test. (*C* and *D*) BAL fluid was collected at 21 days after TSC2-null cell injection and analyzed for SP-D (*C*) or SP-A (*D*) protein content. *Upper panels*: representative micrographs of total BAL fluid SP-A or SP-D content. BAL samples containing equal volume were subjected to SDS-PAGE under reduced conditions, followed by immunoblotting with anti–SP-A or SP-D antibody. *Lower panels*: densitometric quantification of SP-A and SP-D content presented as a percentage of untreated control mice. Values are shown as means + SEM; $n = 6$/group.

TSC2-Null Lesions Induce *S*-Nitrosylation of SP-D

We have previously shown that SP-D is susceptible to post-translational modification by NO via *S*-nitrosylation (SNO–SP-D) and can serve as a biomarker of pulmonary inflammation (35). Therefore, we examined SNO–SP-D levels in BAL fluids of both untreated control and mice with TSC2-null lesions (Figure 5). BAL fluids were normalized for equal total SP-D loading (Figure 5C). There was a significant increase in SNO–SP-D content in mice with TSC2-null lesions (Figure 5A). In agreement with increased level of SNO–SP-D, there was observed disruption of SP-D multimeric structure in the BAL of mice with TSC2-null lesions, as shown by the presence of lower molecular weight bands on native electrophoresis (Figure 5B). These lower molecular weight forms were not observed in untreated control mouse BAL. Previously, we have observed that SNO–SP-D is an activator of macrophage function and that it is associated with a variety of pulmonary inflammatory diseases (11, 22, 23, 36), indicating that NO-mediated modification of SP-D may play a role in the tissue destruction observed in this model of LAM.

Discussion

LAM is a progressive debilitating disease in which neoplastic lesion growth is associated with proliferation of the lymph vessels. However, the disease is also characterized by lung tissue destruction and loss of septation, as has been seen in a variety of pulmonary inflammatory diseases, such as emphysema. Lung inflammation and SPs are key components in dysregulated lung homeostasis, causing emphysematous alveolar changes. Little is known about SPs and their regulation in pulmonary LAM. In this study, using a mouse LAM model, we demonstrated that growth of TSC2-null lung lesions promoted recruitment of activated inflammatory cells, proinflammatory cytokine influx, and surfactant dysfunction.

Chronic inflammation is highly correlated with many types of human cancer, where both tumor cells and stromal cells elaborate chemokines and cytokines (12). In this study, we demonstrated that CCL2/MCP-1 and CXCL1/KC chemokine levels were higher in BAL fluid from lungs with TCS2-null lesions than from untreated control lungs. Moreover, the increase in CCL2/MCP1 and CXCL1/KC chemokine levels is associated with the recruitment of macrophages and neutrophils into the lung lining. This observation is in agreement with recently published data that CCL2/MCP-1 level in BAL fluid from patients with LAM was higher when compared with healthy volunteers (4). It has been recently reported that CCL2/MCP-1 selectively attracts cells with dysfunctional TSC2 and is associated with LAM nodules in roughly 70% of patients, suggesting that this chemokine could be involved in the recruitment of LAM cells to the lung (36).

In addition, the observed increase in TGF-β1 level is consistent with tumorigenesis in the lungs, and may be

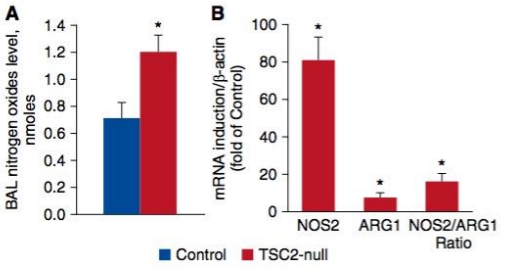

Figure 4. TSC2-null lung lesions enhance pulmonary nitrogen oxides production. (*A*) BAL fluid was collected at 21 days after TSC2-null cell injection and analyzed for NO metabolites by chemical reduction, as described in MATERIALS AND METHODS. Results are expressed as means + SEM; $^*P < 0.05$ versus untreated control mice by *t* test; $n = 5$ for untreated control group; $n = 12$ for TSC2-null group. (*B*) Cells recovered from BAL fluid were analyzed by quantitative RT-PCR for nitric oxide synthase (NOS) 2 and arginase 1 (ARG) gene expression and normalized to β-actin. All samples were run in triplicate; $n = 5$ for untreated control group; $n = 12$ for TSC2-null group.

mechanistically related to the extensive formation and growth of TSC2-null lesions. Examination of the inflammatory cells released to the lung lining reveals a large number of macrophages and recruited multinucleated cells, which are morphologically similar to tumor-associated neutrophils. These observations are indicative of a "left shift" to the young, less well differentiated neutrophils and neutrophil-precursor cells (38, 39). Appearance of neutrophil-precursor cells generally reflects early release of myeloid cells from the bone marrow, due to acute inflammation.

It is likely that distinct differentiation programs of inflammatory cells occur in different states depending on the cytokine milieu. It has been reported that, in the tumor microenvironment, tumor-associated neutrophils and immature myeloid cells support tumor growth by producing angiogenic factors and matrix-degrading enzymes (40, 41), and suppress the antitumor immune response (42). In this study, we found that immature myeloid cells are recruited to the lining of lungs with TSC2-null lesions. Such immature cells could contribute to tumor growth through the inhibition of T-cell function, although in a nude mouse model, this is unlikely to be a significant contribution. The presence of these cells in the lung lining fluid, rather than within the tumor, has implications for the initiation of tissue destruction observed in this model, and warrants further investigation in an immunocompetent mouse model.

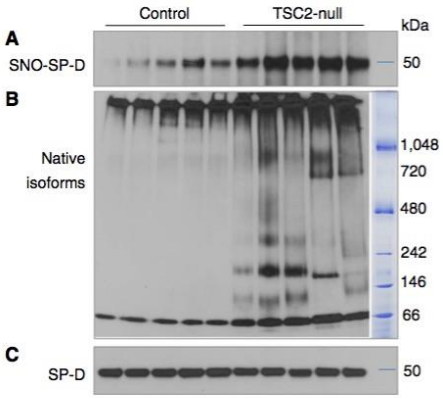

Figure 5. TSC2-null lesions induce *S*-nitrosylation of SP-D. BAL fluid was collected at 21 days after TSC2-null cell injection and analyzed for SP-D protein content. (*A*) Representative micrographs of *S*-nitrosylated SP-D (SNO–SP-D) content. BAL samples containing equal SP-D loading were subjected to Biotin-Switch assay to determine amount of SNO–SP-D. (*B*) Representative micrographs of native SP-D. BAL samples containing equal SP-D loading were subjected to native gel electrophoresis to determine multimeric structure of SP-D. (*C*) Representative micrographs of equal SP-D loading. The net intensity of the samples from Figure 3C (*upper panel*) was calculated for equal SP-D loading.

Inflammatory cells can release various proteases, leading to destruction of the extracellular matrix and subsequent loss of the alveolar units (43). Pulmonary inflammation contributes to respiratory impairment, at least in part, by disrupting the pulmonary surfactant system (24, 44). Pulmonary surfactant is a surface-active mixture of phospholipids and hydrophobic proteins, SP-B and SP-C, secreted by alveolar epithelial type II cells to reduce surface tension at the air–liquid interface to maintain alveolar stability. Our study demonstrates that TSC2-null lesions induced down-regulation of SP-B, which was reflected by an increase in minimum surface tension achievable by the BAL *in vitro*. Because SP-B operates to increase phospholipid incorporation into the surfactant monolayer, it is critical to the reduction of surface tension within the alveoli. Thus, the decreased SP-B level in the lungs with TSC2-null lesions, along with the emphysematous alterations observed in these lungs (6), may lead to alveolar collapse, increased work of breathing, and impaired gas exchange. These data are consistent with the report by Taveira-DaSilva and coworkers (5) that the histological severity of the disease in patients with LAM correlates with the degree of impairment in gas exchange.

We have recently shown that SP-D, a pulmonary collectin and innate host defense protein with well-established immunomodulatory properties (11), can serve as a marker of pulmonary

inflammation (35, 45). We have also demonstrated that, under inflammatory conditions, NO modifies SP-D through *S*-nitrosylation, resulting in disassembling of multimeric SP-D structure and initiates a proinflammatory response through NF-κB activation (11). To determine whether TCS2-null lesions induce *S*-nitrosylation of SP-D, we examined BAL fluids for the presence of SP-D modifications. When controlled for input of SP-D, BAL of the lungs with TSC2-null lesions exhibited a significant increase in SNO–SP-D. Increased SNO–SP-D levels were also associated with the presence of lower molecular weight forms of SP-D, evident by native gel electrophoresis of the BAL fluids, consistent with our previous results in other models of inflammation (11, 22, 24). SP-D multimeric structure was not disrupted within the lungs of untreated control mice, as shown by native gel electrophoresis. Therefore, the balance between multimeric SP-D and trimeric SNO–SP-D forms in the lung with TSC2-null lesions was shifted to favor of trimeric SP-D forms. The increase in SNO–SP-D, as well as in low molecular weight forms of the protein, was associated with increased NO production and NOS2 activity. These results indicate activation of inflammatory processes within lungs with TSC2-null lesions, although we do not know whether SNO–SP-D is cause or effect in this process.

A major limitation in the development of new strategies for LAM treatment has been the lack of a representative animal model (6, 46). In this study, we have further characterized the TCS2-null mouse LAM model established in nude mice to examine the role of inflammation in the pathology. Although an animal model cannot exactly reproduce the pathology and pathophysiology of human LAM, this study has allowed us to make several important observations, namely, that there is significant inflammatory activation, recruitment of activated myeloid cells, disruption of surfactant function, and increased iNOS-related signaling. Bearing in mind that there is inflammatory activation within this model, there is a significant limitation in the use of a nude mouse, namely, a lack of normal T lymphocyte function. T cells are an important aspect of the inflammatory response and play a key role in tumor suppression. Therefore, our future goal is to develop the LAM model into an immunocompetent mouse to understand how T cells may alter this inflammatory activation within LAM and to determine whether the observed lung inflammatory response is specific to TSC2-null lesions. Understanding the role of each type of immune cell, and the relevant signaling pathways involved in LAM initiation and progression, is critical to the discovery of biomarkers specifically targeting cancer inflammation.

Our data using a female murine LAM model have established a link between growth of TSC2-null lesions in the lung, NOS2 activation, and inflammation-induced surfactant alterations. These studies suggest that TSC2-null–induced pulmonary inflammation might directly contribute to increased NOS2 expression, SNO–SP-D levels, and dysfunction of pulmonary surfactant, which, in turn, results in airspace enlargement and respiratory impairment, key aspects of the pathology of human LAM. ■

Author disclosures are available with the text of this article at www.atsjournals.org.

References

1. Johnson SR. Lymphangioleiomyomatosis. *Eur Respir J* 2006;27: 1056–1065.
2. Taveira-DaSilva AM, Moss J. Lymphangioleiomyomatosis. *Cancer Control* 2006;13:276–285.
3. Henske EP, McCormack FX. Lymphangioleiomyomatosis—a wolf in sheep's clothing. *J Clin Invest* 2012;122:3807–3816.
4. Pacheco-Rodriguez G, Steagall WK, Moss J. Chemokine-enhanced chemotaxis of lymphangioleiomyomatosis cells with mutations in the tumor suppressor TSC2 gene. *J Immunol* 2009;182:1270–1277.
5. Taveira-DaSilva AM, Hedin C, Stylianou MP, Travis WD, Matsui K, Ferrans VJ, Moss J. Reversible airflow obstruction, proliferation of abnormal smooth muscle cells, and impairment of gas exchange as predictors of outcome of lymphangioleiomyomatosis. *Am J Respir Crit Care Med* 2001;164:1072–1076.
6. Goncharova EA. Goncharov DA, Fehrenbach M, Khavin I, Ducka B, Hino O, Colby TV, Merrilees MJ, Haczku A, Albelda SM, *et al*. Prevention of alveolar destruction and airspace enlargement in a mouse model of pulmonary lymphangioleiomyomatosis (LAM). *Sci Transl Med* 2012;4: 154ra134.
7. Weichhart T, Costantino G, Poglitsch M, Rosner M, Zeyda M, Stuhlmeier KM, Kolbe T, Stulnig TM, Hörl WH, Hengstschläger M, *et al*. The TSC-mTOR signaling pathway regulates the innate inflammatory response. *Immunity* 2008;29:565–577.
8. Gow AJ. The biological chemistry of nitric oxide as it pertains to the extrapulmonary effects of inhaled nitric oxide. *Proc Am Thorac Soc* 2006;3:150–152.
9. Foster MW, Hess DT, Stamler JS. Protein *S*-nitrosylation in health and disease: a current perspective. *Trends Mol Med* 2009;15:391–404.
10. Atochina EN, Beers MF, Hawgood S, Poulain F, Davis C, Fusaro T, Gow AJ. Surfactant protein-D, a mediator of innate lung immunity, alters the products of nitric oxide metabolism. *Am J Respir Cell Mol Biol* 2004;30:271–279.
11. Guo CJ, Atochina-Vasserman EN, Abramova E, Foley JP, Zaman A, Crouch E, Beers MF, Savani RC, Gow AJ. S-nitrosylation of surfactant protein-D controls inflammatory function. *PLoS Biol* 2008;6:e266.
12. Mantovani A, Allavena P, Sica A, Balkwill F. Cancer-related inflammation. *Nature* 2008;454:436–444.
13. Knudsen L, Atochina-Vasserman EN, Guo CJ, Scott PA, Haenni B, Beers MF, Ochs M, Gow AJ. NOS2 is critical to the development of emphysema in Sftpd deficient mice but does not affect surfactant homeostasis. *PLoS One* 2014;9:e85722.
14. Tripathi DN, Chowdhury R, Trudel LJ, Tee AR, Slack RS, Walker CL, Wogan GN. Reactive nitrogen species regulate autophagy through ATM-AMPK-TSC2–mediated suppression of mTORC1. *Proc Natl Acad Sci USA* 2013;110:E2950–E2957.
15. Wright JR, Dobbs LG. Regulation of pulmonary surfactant secretion and clearance. *Annu Rev Physiol* 1991;53:395–414.
16. Serrano AG, Perez-Gil J. Protein–lipid interactions and surface activity in the pulmonary surfactant system. *Chem Phys Lipids* 2006;141: 105–118.
17. LeVine AM, Whitsett JA, Hartshorn KL, Crouch EC, Korfhagen TR. Surfactant protein D enhances clearance of influenza A virus from the lung *in vivo*. *J Immunol* 2001;167:5868–5873.
18. Schaub, B, Westlake RM, He H, Arestides R, Haley KJ, Campo M, Velasco G, Bellou A, Hawgood S, Poulain FR, *et al*. Surfactant protein D deficiency influences allergic immune responses. *Clin Exp Allergy* 2004;34:1819–1826.
19. Atochina EN, Gow AJ, Beck JM, Haczku A, Inch A, Kadire H, Tomer Y, Davis C, Preston AM, Poulain F, *et al*. Delayed clearance of *Pneumocystis carinii* infection, increased inflammation, and altered nitric oxide metabolism in lungs of surfactant protein-D knockout mice. *J Infect Dis* 2004;189:1528–1539.
20. Madan T, Reid KB, Clark H, Singh M, Nayak A, Sarma PU, Hawgood S, Kishore U. Susceptibility of mice genetically deficient in SP-A or SP-D gene to invasive pulmonary aspergillosis. *Mol Immunol* 2010; 47:1923–1930.

21. Atochina-Vasserman EN, Beers MF, Kadire H, Tomer Y, Inch A, Scott P, Guo CJ, Gow AJ. Selective inhibition of inducible NO synthase activity *in vivo* reverses inflammatory abnormalities in surfactant protein D–deficient mice. *J Immunol* 2007;179:8090–8097.
22. Atochina-Vasserman EN, Winkler C, Abramova H, Schaumann F, Krug N, Gow AJ, Beers MF, Hohlfeld JM. Segmental allergen challenge alters multimeric structure and function of surfactant protein D in humans. *Am J Respir Crit Care Med* 2011;183:856–864.
23. Atochina-Vasserman EN, Bates SR, Zhang P, Abramova H, Zhang Z, Gonzales L, Tao JQ, Gochuico BR, Gahl W, Guo CJ, *et al*. Early alveolar epithelial dysfunction promotes lung inflammation in a mouse model of Hermansky-Pudlak syndrome. *Am J Respir Crit Care Med* 2011;184:449–458.
24. Atochina-Vasserman EN, Gow AJ, Abramova H, Guo CJ, Tomer Y, Preston AM, Beck JM, Beers MF. Immune reconstitution during pneumocystis lung infection: disruption of surfactant component expression and function by S-nitrosylation. *J Immunol* 2009; 182:2277–2287.
25. Enhorning G. Pulmonary surfactant function studied with the pulsating bubble surfactometer (PBS) and the capillary surfactometer (CS). *Comp Biochem Physiol A Mol Integr Physiol* 2001;129:221–226.
26. Guttentag SH, Akhtar A, Tao JQ, Atochina E, Rusiniak ME, Swank RT, Bates SR. Defective surfactant secretion in a mouse model of Hermansky-Pudlak syndrome. *Am J Respir Cell Mol Biol* 2005;33:14–21.
27. Atochina EN, Beers MF, Scanlon ST, Preston AM, Beck JM. *P. carinii* induces selective alterations in component expression and biophysical activity of lung surfactant. *Am J Physiol Lung Cell Mol Physiol* 2000;278:L599–L609.
28. Letterio JJ, Roberts AB. Regulation of immune responses by TGF-beta. *Annu Rev Immunol* 1998;16:137–161.
29. Tam JW, Kullas AL, Mena P, Bliska JB, van der Velden AW. CD11b+ Ly6Chi Ly6G− immature myeloid cells recruited in response to *Salmonella enterica* serovar typhimurium infection exhibit protective and immunosuppressive properties. *Infect Immun* 2014;82:2606–2614.
30. Günther A, Ruppert C, Schmidt R, Markart P, Grimminger F, Walmrath D, Seeger W. Surfactant alteration and replacement in acute respiratory distress syndrome. *Respir Res* 2001;2:353–364.
31. Atochina EN, Beck JM, Scanlon ST, Preston AM, Beers MF. *Pneumocystis carinii* pneumonia alters expression and distribution of lung collectins SP-A and SP-D. *J Lab Clin Med* 2001;137:429–439.
32. Casey J, Kaplan J, Atochina-Vasserman EN, Gow AJ, Kadire H, Tomer Y, Fisher JH, Hawgood S, Savani RC, Beers MF. Alveolar surfactant protein D content modulates bleomycin-induced lung injury. *Am J Respir Crit Care Med* 2005;172:869–877.
33. Glasser SW, Senft AP, Maxfield MD, Ruetschilling TL, Baatz JE, Page K, Korfhagen TR. Genetic replacement of surfactant protein-C reduces respiratory syncytial virus induced lung injury. *Respir Res* 2013;14:19.
34. Shi JD, Golden T, Guo CJ, Tu SP, Scott P, Lee MJ, Yang CS, Gow AJ. Tocopherol supplementation reduces NO production and pulmonary inflammatory response to bleomycin. *Nitric Oxide* 2013; 34:27–36.
35. Atochina-Vasserman EN. *S*-nitrosylation of surfactant protein D as a modulator of pulmonary inflammation. *Biochim Biophys Acta* 2012; 1820:763–769.
36. Atochina-Vasserman EN, Beers MF, Gow AJ. Review: chemical and structural modifications of pulmonary collectins and their functional consequences. *Innate Immun* 2010;16:175–182.
37. Pacheco-Rodriguez G, Moss J. The role of chemokines in migration of metastatic-like lymphangioleiomyomatosis cells. *Crit Rev Immunol* 2010;30:387–394.
38. Fridlender ZG, Sun J, Kim S, Kapoor V, Cheng G, Ling L, Worthen GS, Albelda SM. Polarization of tumor-associated neutrophil phenotype by TGF-beta: "N1" versus "N2" TAN. *Cancer Cell* 2009; 16:183–194.
39. Mantovani A, Sozzani S, Locati M, Allavena P, Sica A. Macrophage polarization: tumor-associated macrophages as a paradigm for polarized M2 mononuclear phagocytes. *Trends Immunol* 2002;23: 549–555.
40. Pekarek LA, Starr BA, Toledano AY, Schreiber H. Inhibition of tumor growth by elimination of granulocytes. *J Exp Med* 1995;181: 435–440.
41. Shojaei F, Singh M, Thompson JD, Ferrara N. Role of Bv8 in neutrophil-dependent angiogenesis in a transgenic model of cancer progression. *Proc Natl Acad Sci USA* 2008;105:2640–2645.
42. Schmielau J, Finn OJ. Activated granulocytes and granulocyte-derived hydrogen peroxide are the underlying mechanism of suppression of T-cell function in advanced cancer patients. *Cancer Res* 2001;61: 4756–4760.
43. Mouded M, Egea EE, Brown MJ, Hanlon SM, Houghton AM, Tsai LW, Ingenito EP, Shapiro SD. Epithelial cell apoptosis causes acute lung injury masquerading as emphysema. *Am J Respir Cell Mol Biol* 2009;41:407–414.
44. Wright K, Kolios G, Westwick J, Ward SG. Cytokine-induced apoptosis in epithelial HT-29 cells is independent of nitric oxide formation: evidence for an interleukin-13–driven phosphatidylinositol 3-kinase–dependent survival mechanism. *J Biol Chem* 1999;274: 17193–17201.
45. Matalon S, Shrestha K, Kirk M, Waldheuser S, McDonald B, Smith K, Gao Z, Belaaouaj A, Crouch EC. Modification of surfactant protein D by reactive oxygen–nitrogen intermediates is accompanied by loss of aggregating activity, *in vitro* and *in vivo*. *FASEB J* 2009;23: 1415–1430.
46. Kwiatkowski DJ. Animal models of LAM and TSC. *Lymphat Res Biol* 2010;8:51–57.

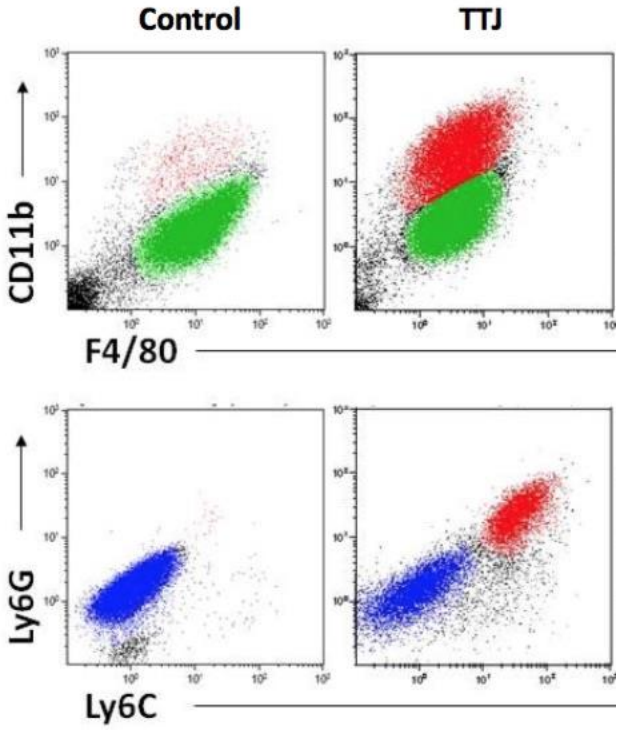

Figure 6-1

Figure 1. Myeloid derived cells are collected by BAL and in control mice are phenotypically consistent with pulmonary macrophages. Activated immature macrophages (red) are present in the BAL following TTJ cell injection (F4/80+ Cd11b+ Ly6C+ Ly6G+).

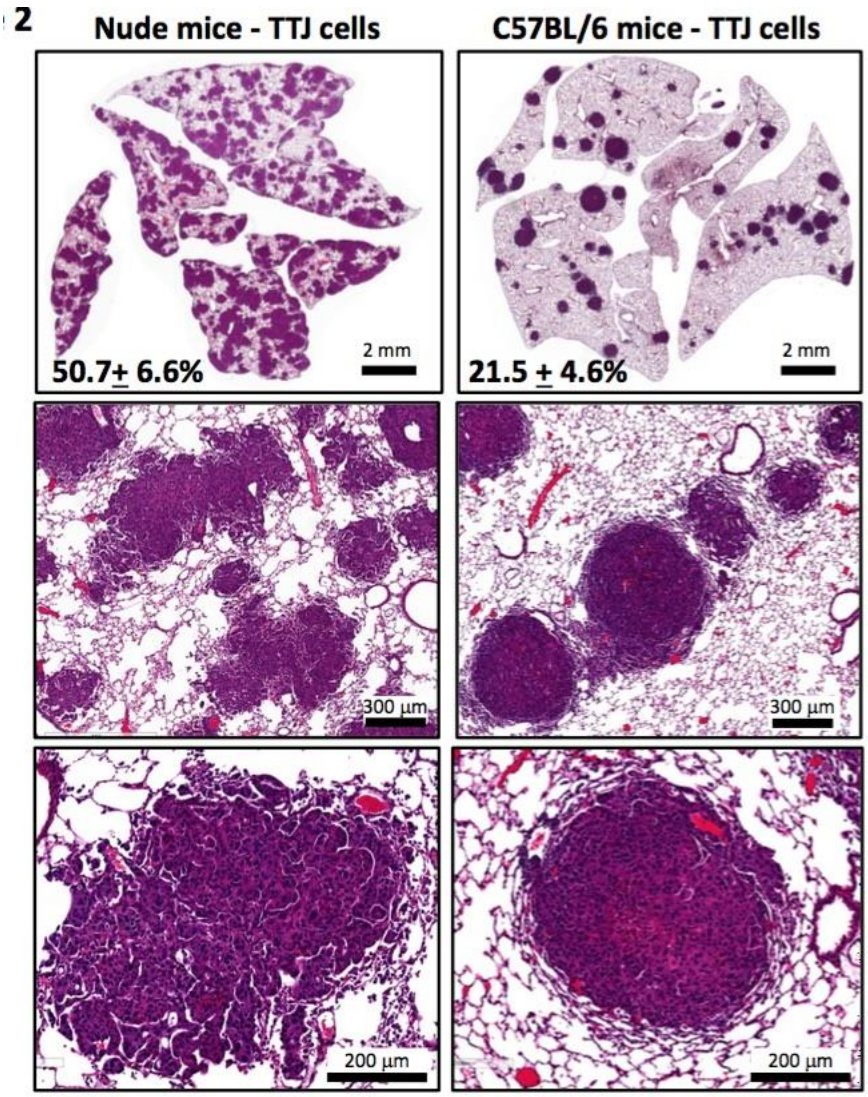

Figure 6-2

Figure 2. Histological assessment of lesions in nude and C57BL/6 mice 3 weeks post tsc2 null cell injection demonostrate differences in lesion dimensions. C57BL/6 mice have rounder lesions with defined borders compared to nude mice.

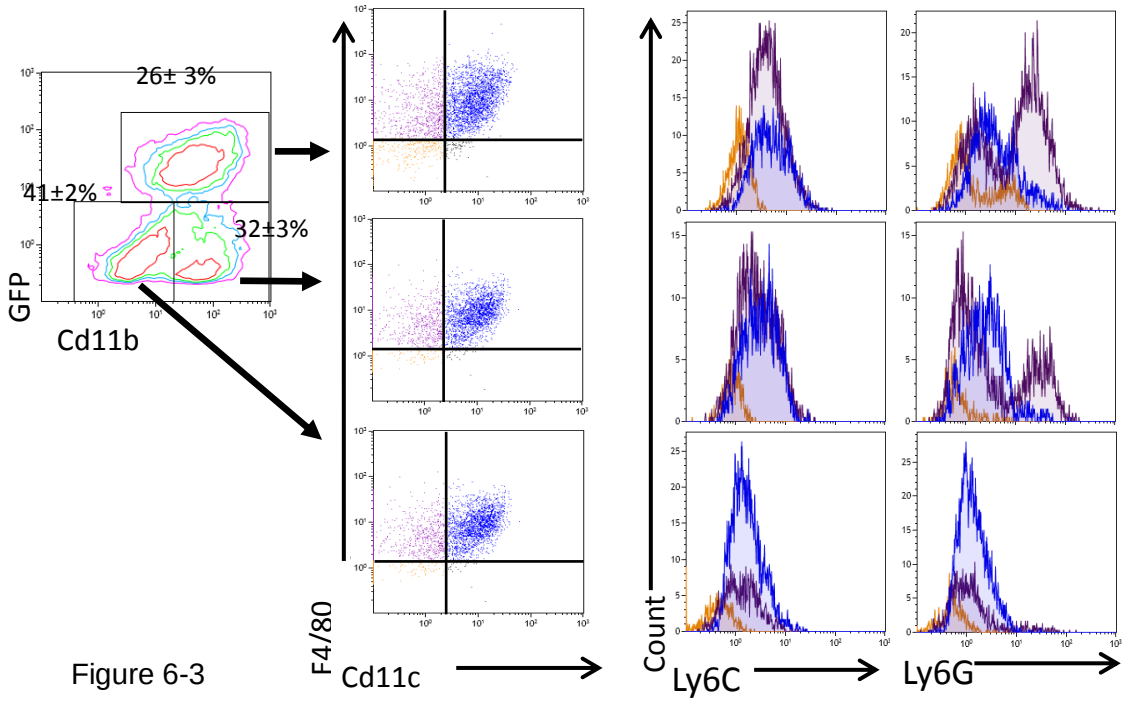

Figure 6-3

Figure 3. BAL cells collected from Tsc2-null cell injected mice were incubated with fluorescently tagged antibodies for cell phenotyping.

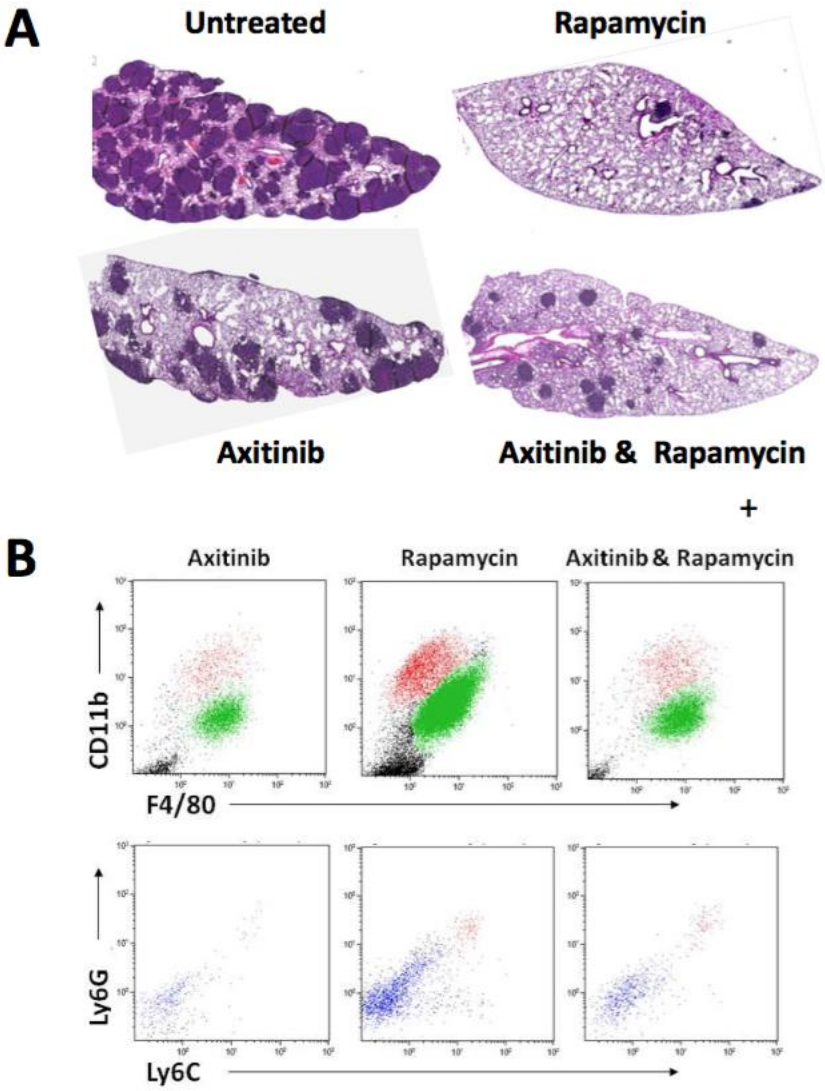

Figure 6-4

Figure 4. Mice were treated with rapamycin, Axitinib or a combination and injected with tsc2 null cells. Histological assessment (A) and cell phenotype (B) were analyzed. Both treatments reduced lesion development and number of immature cells compared to no treatment.

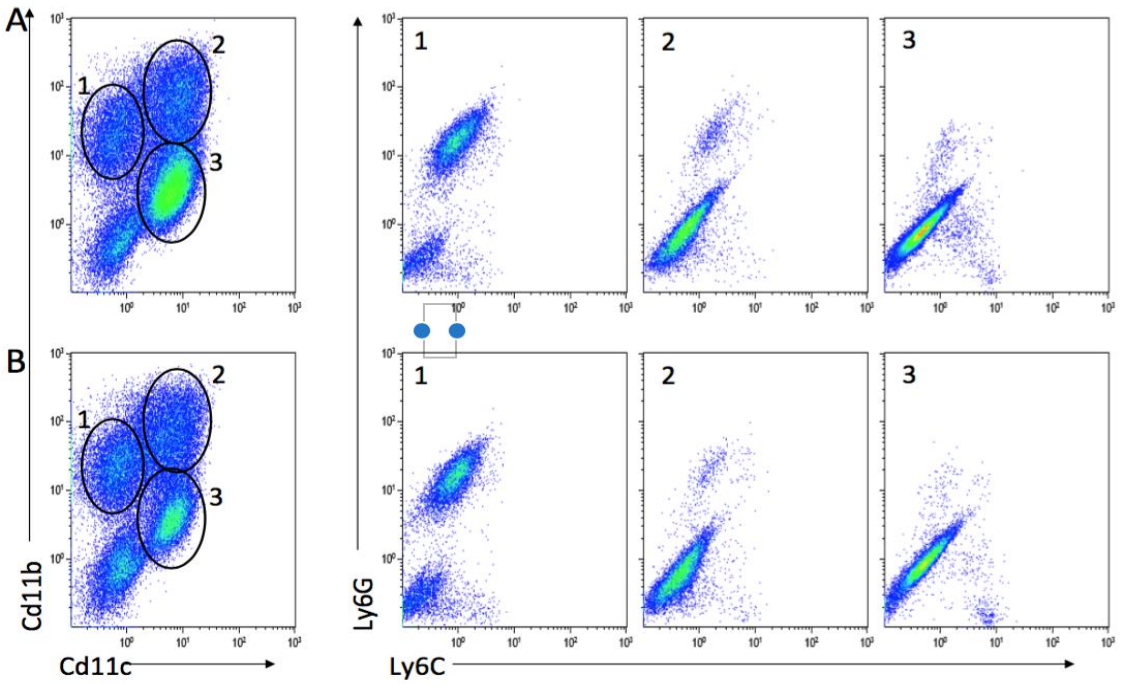

Figure 6-5

Figure 5. Immature activated macrophages (F4/80+ Cd11b+ Cd11c- Ly6G+ Ly6C+) are increased in iNOS chimeric mice. BAL cells were analyzed by flow cytometry and F4/80+ were phenotyped based on Cd11b, Cd11c, Ly6G and Ly6C expression. Cells were collected from wild type (A) and iNOS chimeric mice (B).

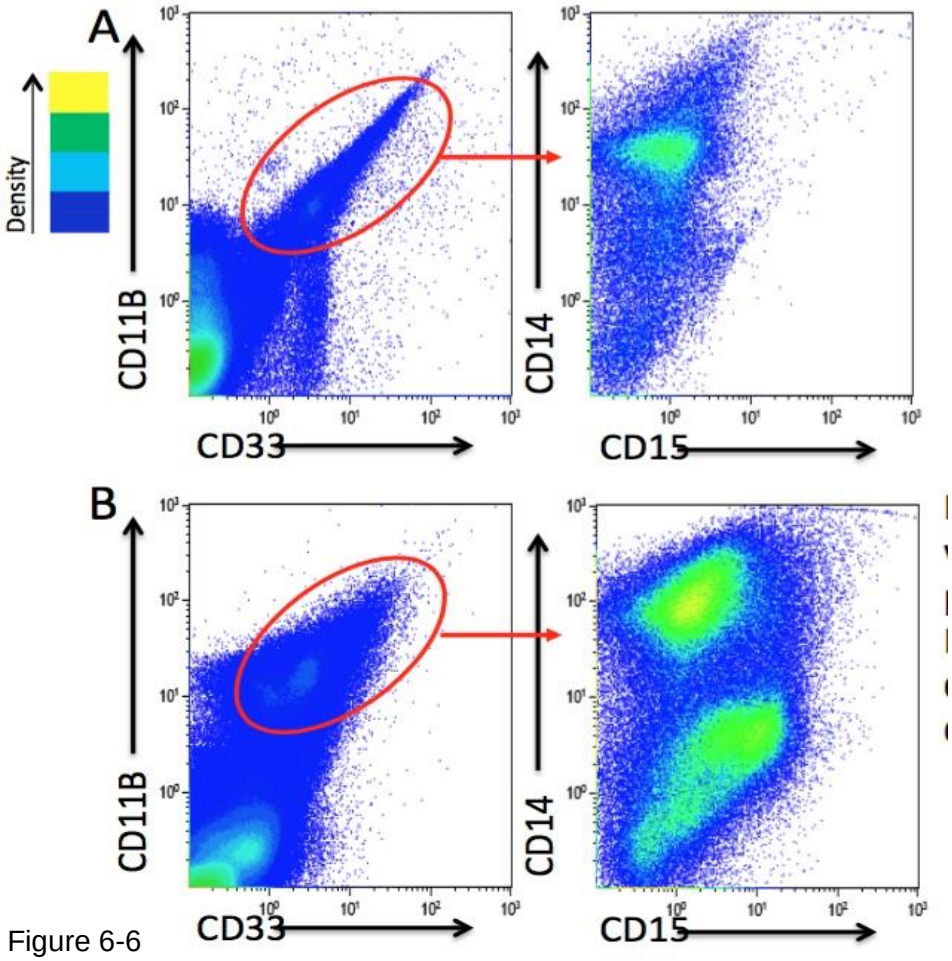

Figure 6-6

Figure 6. Blood (A) and chyle (B) cells were isolated from LAM patients and processed for flow cytometry. Expression of activation markers, CD15 and CD14, was assessed on CD11B and CD33 positive cells.

APPENDIX 2

In collaboration with Dr. Anant Madabhushi, Dr. Mirabela Rusu and Dr. Haibo Wang, we used in-vivo imaging techniques to construct a three dimensional model of the mouse lung from histological sectioning. This approach co-registered magnetic resonance imaging (MRI) of in-vivo lung with serially sectioned histology. In-vivo MRI was used to identify large blood vessels and airways and measure total lung volume at peak inspiration. After removal from the body and inflation with fixative solution, a MRI of ex-vivo lung was then taken. After fixation, lungs were embedded and sectioned along the transverse plane starting at the bottom of the lung and sectioning every 55 microns to the top. Histological sections were aligned and reconstruction was transformed, using the ex-vivo MRI, to match lung volume and location of large airways and blood vessels on in-vivo MRI using the methods described in the paper below.

We were also able to use the co-registered histological sections to identify a MRI signature for inflammation. Inflammation was identified on histological section and mapped onto in-vivo MRI using the co-registration techniques explained below. The MRI signature identified can be used in future experiments to analyze pulmonary inflammation. For instance, ITB causes diffuse and patchy inflammation as seen on histology. Using the MRI signature identified in this work, we can see the extent of inflammation throughout the whole lung. This approach also allows for longitudinal studies in the same mouse. For instance, mice could be analyzed by MRI 3, 8, 15 and 21 days post ITB thereby following the development and resolution of inflammation following ITB.

The co-registration of histological sections to in-vivo MRI also afforded us the opportunity to map the airway tree of a C57/BL6 mouse. Large airways were identified on in-vivo MRI and smaller airways on histology section. Using the reconstruction

approach for histology, the airway tree was also reconstructed from histological sections and transformed based on in-vivo MRI to actual dimensions at peak inhalation (Figure Appendix 2.1). Airways were visualized using Slicer software. Airway dimensions, including length and diameter, were measured using Slicer. 16 airway generations were identified with our approach.

Airway trees of rodents have been previously reported using other techniques. Dr. Gomes and colleagues, inflated airways with silicone rubber to create a cast of the conducting airways of a 6g harvest mouse (*Micromys minutus*) and 1.5kg African giant pouched rat (*Cricetomys gambianus*) (Gomes and Bates, 2002). Their work measured the length and diameter of airways and reported 33 generations in the African giant pouched rat and 18 generations in the harvest mouse. Dr. Thiesse and colleagues used micro-computed tomography (micro-CT) imaging technique to identify the airway tree of C57/BL6, A/J and BALB/C mice (Thiesse et al., 2010). They were able to identify and measure dimensions of 6 generations of airways.

The airway tree developed by in-vivo MRI and histology co-registration furthers our understanding of a commonly used in-bred mouse C57/BL6. Unlike the elegantly done work of Dr. Gomes and colleagues, the airway tree we developed is of a commonly used mouse strain. The C57/BL6 mouse airway tree was measured by Dr. Thiesse using micro-CT but our use of histological sections allowed for identification of lower airways.

It is our contention that by improving our understanding of the mouse airway tree, lung function measurements can be improved. Mathematical modeling of lung functional measurements from techniques like forced oscillation technique across increasing frequency rely on assumed parameters. One such assumed parameter is the branching pattern and dimensions of the airway tree. It is possible that by adding actual airway measurements, lung function modeling can be improved.

Framework for 3D histologic reconstruction and fusion with *in vivo* MRI: Preliminary results of characterizing pulmonary inflammation in a mouse model

Mirabela Rusu[a)]
Department of Biomedical Engineering, Case Western Reserve University, Cleveland, Ohio 44106

Thea Golden
Department of Pharmacology and Toxicology, Rutgers University, Piscataway, New Jersey 08854

Haibo Wang
Department of Biomedical Engineering, Case Western Reserve University, Cleveland, Ohio 44106

Andrew Gow
Department of Pharmacology and Toxicology, Rutgers University, Piscataway, New Jersey 08854

Anant Madabhushi
Department of Biomedical Engineering, Case Western Reserve University, Cleveland, Ohio 44106

(Received 26 September 2014; revised 24 May 2015; accepted for publication 8 June 2015; published 27 July 2015)

Purpose: Pulmonary inflammation is associated with a variety of diseases. Assessing pulmonary inflammation on *in vivo* imaging may facilitate the early detection and treatment of lung diseases. Although routinely used in thoracic imaging, computed tomography has thus far not been compellingly shown to characterize inflammation *in vivo*. Alternatively, magnetic resonance imaging (MRI) is a nonionizing radiation technique to better visualize and characterize pulmonary tissue. Prior to routine adoption of MRI for early characterization of inflammation in humans, a rigorous and quantitative characterization of the utility of MRI to identify inflammation is required. Such characterization may be achieved by considering *ex vivo* histology as the ground truth, since it enables the definitive spatial assessment of inflammation. In this study, the authors introduce a novel framework to integrate 2D histology, *ex vivo* and *in vivo* imaging to enable the mapping of the extent of disease from *ex vivo* histology onto *in vivo* imaging, with the goal of facilitating computerized feature analysis and interrogation of disease appearance on *in vivo* imaging. The authors' framework was evaluated in a preclinical preliminary study aimed to identify computer extracted features on *in vivo* MRI associated with chronic pulmonary inflammation.

Methods: The authors' image analytics framework first involves reconstructing the histologic volume in 3D from individual histology slices. Second, the authors map the disease ground truth onto *in vivo* MRI via coregistration with 3D histology using the *ex vivo* lung MRI as a conduit. Finally, computerized feature analysis of the disease extent is performed to identify candidate *in vivo* imaging signatures of disease presence and extent.

Results: The authors evaluated the framework by assessing the quality of the 3D histology reconstruction and the histology—MRI fusion, in the context of an initial use case involving characterization of chronic inflammation in a mouse model. The authors' evaluation considered three mice, two with an inflammation phenotype and one control. The authors' iterative 3D histology reconstruction yielded a 70.1% ± 2.7% overlap with the *ex vivo* MRI volume. Across a total of 17 anatomic landmarks manually delineated at the division of airways, the target registration error between the *ex vivo* MRI and 3D histology reconstruction was 0.85 ± 0.44 mm, suggesting that a good alignment of the *ex vivo* 3D histology and *ex vivo* MRI had been achieved. The 3D histology-*in vivo* MRI coregistered volumes resulted in an overlap of 73.7% ± 0.9%. Preliminary computerized feature analysis was performed on an additional four control mice, for a total of seven mice considered in this study. Gabor texture filters appeared to best capture differences between the inflamed and noninflamed regions on MRI.

Conclusions: The authors' 3D histology reconstruction and multimodal registration framework were successfully employed to reconstruct the histology volume of the lung and fuse it with *in vivo* MRI to create a ground truth map for inflammation on *in vivo* MRI. The analytic platform presented here lays the framework for a rigorous validation of the identified imaging features for chronic lung inflammation on MRI in a large prospective cohort. [http://dx.doi.org/10.1118/1.4923161]

Key words: framework, reconstruction, multimodal fusion, *in vivo* imaging signature, *in vivo* MRI, *ex vivo* MRI, histopathology, inflammation

1. INTRODUCTION

Pulmonary inflammation is a common condition associated with a variety of lung diseases such as asthma or chronic obstructive pulmonary disorder.[1] Manifestations of inflammation include hypertrophy of airway epithelial cells, infiltration and activation of leukocytes, and structural changes to the architecture of the lung.[2,3] The quantitative characterization of pulmonary inflammation on *in vivo* imaging holds the potential to facilitate improved and early characterization of lung diseases, as well as the investigation of anti-inflammatory drugs.[4]

Recent studies have investigated the ability of *in vivo* imaging, both computed tomography (CT)[5–7] and magnetic resonance imaging (MRI),[8–11] to identify pulmonary inflammation in preclinical models. These studies suggest that *in vivo* imaging may enable characterization of pulmonary inflammation. MRI is of particular interest in this regard as it is a nonradiation modality with a potentially better ability to image pulmonary soft tissue compared to CT.[8,9,11–14] There is however a need for computerized decision support and feature analysis tools to define and evaluate quantitative imaging signatures for pulmonary inflammation on *in vivo* MRI.

Currently, in most instances, the only way to definitively ascertain the presence and spatial extent of diseases is via pathologic examination of stained histology slices (Fig. 1). While surgically excised lung histopathology could serve not only for defining the precise extent and presence of disease, it could also serve as a conduit to map the extent of disease onto the corresponding *in vivo* imaging via coregistration. Such accurate mapping of disease extent on *in vivo* imaging paves the way for a rigorous comparison of imaging appearance of disease and normal regions. Furthermore, when image intensities alone are unable to discriminate disease from other confounding tissue regions, computerized feature analysis methods such as textural analysis could help prize out subtle cues to distinguish the similar appearing tissue regions.[15–18]

In this work, we introduce a novel analytic framework to facilitate imaging signature discovery for disease. Our framework was evaluated in the context of initial MRI based characterization of chronic inflammation in a mouse model. Specifically, the framework is comprised of three modules. First, the histology specimen is digitally reconstructed in 3D in order to facilitate its fusion with *in vivo* MRI. Such reconstruction is required as correspondences between lung histology and *in vivo* MRI slices may not be ascertainable due to different image viewing and histology cutting planes.

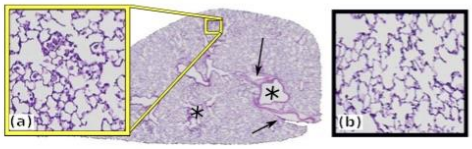

FIG. 1. Lung hematoxylin and eosin (H&E) stained slice showing regions of (a) inflammation and (b) normal tissue. Airways (*) and blood vessels (→) are visible.

Second, the 3D inflammation is mapped from the 3D reconstructed histology volume onto the *in vivo* MRI by coregistration of the 3D histology volume and the *in vivo* MRI using the *ex vivo* MRI as a conduit. Finally, image-derived features are extracted from the *in vivo* MRI of two mice with a phenotype of chronic pulmonary inflammation and the normal lung of five control mice. A comparison is performed between inflamed regions mapped from histology in two mice with an inflammation phenotype and normal lung from five control mice. By choosing these specific phenotypes, we can evaluate our framework to distinguish inflammation on *in vivo* MRI from normal lung tissue. The 3D histological reconstruction and its fusion with MRI were qualitatively and quantitatively evaluated in three mice, the two mice with an inflammation phenotype and one control mouse, while the preliminary textural analysis was performed on the latter three mice and an additional four control mice. While we do not claim in this paper to have identified the definitive computer extracted MRI features for diagnosis of pulmonary inflammation, the presented algorithmic pipeline paves the way for future discovery of validation of imaging signatures for diseases, including inflammation.

The remainder of the paper is organized as follows. First, we discuss previous work (Sec. 2) and provide an overview of our methodology (Sec. 3). A detailed methodological description of our framework is provided in Sec. 4, while the results are presented and discussed in Sec. 5. Finally, in Sec. 6, we present concluding remarks and future directions.

2. PREVIOUS WORK

In this paper, we present a pipeline of algorithmic steps in order to facilitate discovery of *in vivo* imaging signatures for disease. Specifically, in this paper, we evaluate this framework for the problem of identifying computer extracted MRI features associated with pulmonary inflammation in mice. Since our framework involves both 3D histologic reconstruction and radiology-pathology coregistration, we discuss previous related work in the context of these two areas.

Recently, a few approaches have been presented for coregistration of *ex vivo* histology and *in vivo* imaging data. Some approaches attempted to directly map the 2D histology slices onto the *in vivo* imaging by first determining and establishing slice[19–22] or landmark correspondences.[23] Alternative approaches inspired by the actual process of histology sample preparation have also been proposed.[24] Yet, when slice correspondences between the *ex vivo* histology and *in vivo* imaging datasets do not exist or are difficult to identify, 3D reconstruction techniques may allow for creation of a 3D histology volume and enable volumetric coregistration with corresponding *in vivo* imaging.[25] Such techniques are particularly useful in preclinical studies, where finely cut histologic sections corresponding to the *in vivo* imaging may be available. Some approaches have employed one-to-one registration[26–29] of histology slices by utilizing rigid[26,27] or deformable[28,29] transforms. However, one-to-one registration of adjacent slices is prone to propagation of registration errors

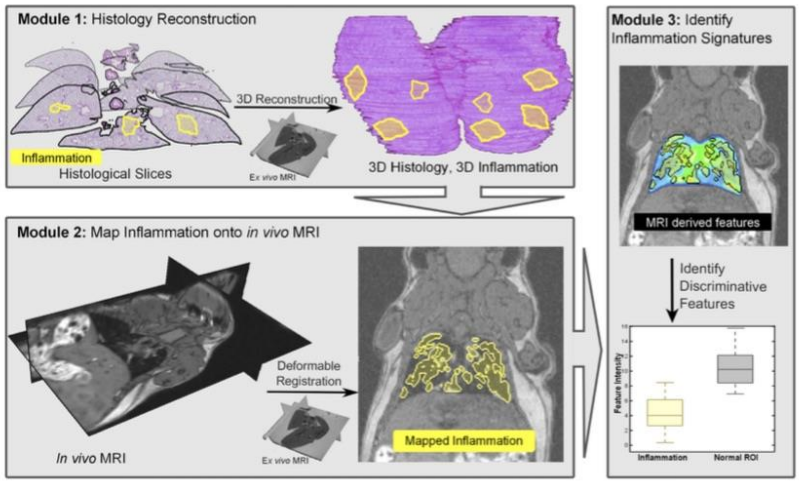

FIG. 2. Overview of our algorithmic pipeline for characterization of pulmonary inflammation. **Module 1:** 3D histology volume is reconstructed from the 2D histology sections using *ex vivo* MRI as a conduit; the reconstruction also results in the generation of a 3D map of inflammation (yellow). **Module 2:** Volumetric coregistration of 3D histology and *in vivo* MRI volumes allows for the mapping of inflammation onto *in vivo* imaging. **Module 3:** Computer extracted image features of inflammation can then be identified from the *in vivo* MRI.

between slices, resulting in a progressive shift along the Z-axis. Alternative approaches have included one-to-many[30,31] or many-to-many registration schemes[32] either using a coarse-to-fine deformable transforms[30] or natural gradients.[31] Yet these methods have not been applied in the context of a multibody registration of multiple objects relative to each other.

Once the coregistration of the histology volume and the *in vivo* MRI has been accomplished, mapping of disease extent on the *in vivo* imaging can be established. This then paves the way for application of computerized feature analysis to identify imaging features to distinguish disease presence from confounders. Such methods are needed as image intensity alone may be insufficient to capture subtle differences between normal and diseased regions.[15–18,33,34]

3. BRIEF OVERVIEW AND NOVEL CONTRIBUTIONS

The current study seeks to develop the algorithmic pipeline to pave the way for quantitative characterization of *in vivo* imaging signatures of disease. In this work, we specifically look at the use case of characterization of pulmonary inflammation on MRI in a mouse model for evaluating the framework. Figure 2 illustrates the three main modules of our framework and the novel aspects of our approach.

Module 1 (Sec. 4.B): The 3D histology volume $\mathcal{H}$ is reconstructed from the 2D histology sections using an iterative alignment scheme that progressively increases the optimization complexity from a single body registration to a multibody registration of individual lobes. This reconstruction scheme was designed to facilitate the alignment of slices between each other within the 3D volume, while simultaneously correcting for lobe movement relative to each other during histology sample preparation. Module 1 introduces a novel multiresolution reconstruction of the 3D histology volume based on a one-to-many multibody refinement of lung lobes. This approach involves making the individual lobes "spatially aware" of each other during the registration,[35] the spatial prior information coming from the *ex vivo* MRI.

Module 2 (Sec. 4.C): The 3D histology volume $\mathcal{H}$ is registered to the *in vivo* MRI using both an affine and deformable transform with the *ex vivo* MRI serving as a conduit for the registration (similar to Module 1). The registration of the histologically reconstructed volume with the *in vivo* MRI enables the mapping of the extent of lung inflammation from the 3D histology volume onto the *in vivo* MRI. This novel registration approach limits the influence of imaging artifacts, such as elastic deformations on account of the absence of neighboring organs, as well as tissue sample preparation that causes tissue shrinkage.

Module 3 (Sec. 4.D): Textural features[36–38] are extracted from *in vivo* MRI and compared between the inflamed and not inflamed regions. The preliminary feature analysis considered in this module serves as a means of showcasing how the presented framework can enable feature discovery.

4. METHODOLOGY

4.A. Data

Seven mice were included in this study: two surfactant protein D knockout ($Sftpd^{-/-}$) mice which have a demonstrated phenotype of chronic pulmonary inflammation and five C57BL/6J wild type (WT) mice (normal controls) (Table I).

TABLE I. Description of the acquisition and preparation protocols for the multimodal radiology and pathology datasets used for evaluating our analytic framework. The 3D reconstruction of the histology was performed at 0.5x, while the *in vivo* MRI was resampled to have consistent, close to isotropic voxels sizes of 250 μm^3 for feature analysis. The lungs of two Sftpd$^{-/-}$ mice and one WT mouse were fixed, carefully sliced, and had H&E staining. These histology images were utilized to assess the accuracy of the 3D histology reconstruction approach and the quality of the histology-MRI fusion. The remaining four WT mice were only used for the validation of the textural analysis module. Since the latter four mice are control animals without an inflammation phenotype, no mapping of histology onto the imaging is required and hence was not performed.

Mouse	Count	Modality	Sequence	Resolution (μm^3)	Voxels	Annotations
	2	*In vivo* MRI	*T*1 GRE	$M \times M \times 500$ $M \in \{156, 234\}$	$256 \times 256 \times N$ $N \in \{32, 34\}$	Lung, blood vessels
Sftpd$^{-/-}$	2	*Ex vivo* MRI	*T*1 GRE	$M \times M \times 500$ $M \in \{125, 156\}$	$M \times M \times N$ $M \in \{256, 512\}$ $N \in \{20, 34\}$	Lung, airways
	2	Histology		$0.75 \times 0.75 \times 110$	$M \times M \times N$ $M \in \{5000, 15\,000\}$ $N \in \{62, 74\}$	Lung, airways Blood vessels Inflammation
	1	*In vivo* MRI	*T*1 GRE	$234 \times 234 \times 500$	$256 \times 256 \times 32$	Lung
	1	*Ex vivo* MRI	*T*1 GRE	$156 \times 156 \times 500$	$256 \times 256 \times 34$	Lung, airways
WT	1	Histology		$0.75 \times 0.75 \times 110$	$M \times M \times 79$ $M \in \{5000, 15\,000\}$	Lung, airways Blood vessels
	4	*In vivo* MRI	*T*1 GRE	$M \times M \times N$ $M \in \{156, 500\}$ $N \in \{200, 500\}$	$M \times M \times N$ $M \in \{128, 256\}$ $N \in \{30, 128\}$	Lung

The mice allow us to compare image-derived features between inflamed and noninflamed regions. The lung MRI was acquired with a 1 Tesla (T) M2 High Energy Performance MRI System (Aspect Magnet Technologies Ltd.). A *T*1-weighted MR gradient recalled echo sequence was used. Imaging parameters include TE/TR = 3.5/15 ms, flip angle 30°, 0.55 mm slice thickness. MR images were taken from *in vivo* lungs of anesthetized mice, under isoflurane, gated for peak inspiration.

After the *in vivo* MRI acquisition, the mouse lung was extracted and the inflation was fixed to the same volume as the *in vivo* MRI lung with 4% paraformaldehyde and 2% sucrose. *Ex vivo* lungs were imaged using the same sequence protocol as the *in vivo* MRI (Table I). In order to use the *ex vivo* MRI as a conduit for the histology reconstruction, the *ex vivo* images were acquired after the lung was fixed (via inflation with fixative). Since the *ex vivo* scan shows an inflated lung and to facilitate the coregistration of *in vivo* and *ex vivo* MRI, we also used an inflated lung for the *in vivo* MRI acquisition. The fixed lung was then embedded in paraffin and 5 μm sections were cut with a spacing of 110 μm (Table I). These sections were stained with hematoxylin and eosin (H&E) (Fig. 1) and digitized at 10x magnification using the Olympus VS120-SL scanning microscopy system.

The specific physiologic characteristics captured by each of the acquired modalities are summarized below.

1. **Whole body 1 T *in vivo* MRI** shows the *in vivo* lung at a lower resolution, allowing for the visualization of arteries within the lung as hyperintense densities. Other organs, e.g., heart or liver, are spatially located in the proximity of the lung, resulting in its elastic compression.
2. ***Ex vivo* MRI** shows the lung at better resolution compared to the *in vivo* MRI and allows for the visualization of large bronchi (hypointense regions). The same protocol used for *in vivo* imaging was also used for *ex vivo* imaging. The *ex vivo* acquisition provides a conduit to coregister *in vivo* MRI with *ex vivo* histology as they share similar attributes.
3. ***Ex vivo* H&E stained histology slices** are obtained from the entire lung of three mice, two Sftpd$^{-/-}$ and one WT. The lungs of the remaining four WT mice did not undergo histology preparation, as they lack inflammation, and thus, they do not require histology mapping on *in vivo* imaging. The histology images have the highest resolution, allowing for the annotation of inflammation, blood vessels, and airways. Inflammation was identified as hypertrophy of airway epithelial cells and leukocyte infiltration[39] and was manually delineated by an expert with substantial expertise in lung pathology. Large airways, blood vessels, and lung lobes were identified using an automatic active contour approach,[40] parameterized to segment connected regions of interest. The results of the automated segmentation were then further manually partitioned into different anatomic classes: airways, blood vessels, or lung lobes. In spite of careful sample preparation, the histology slices may suffer from preparation artifacts, e.g., folding and shrinking. The histology slices were downsampled to a 0.5x magnification for further processing and reconstruction.

4.B. Module 1: Reconstruction of the 3D histology volume

The 3D reconstruction follows an iterative approach (Fig. 3), in which the complexity of the registration is progressively increased. See Table II for a summary of notation used in this manuscript and Secs. 4.C and 4.D.

The reconstruction involves optimization of the following scoring function for each histological slice $\mathcal{H}_i$, $i \in \{2,\ldots,N\}$, where N represents the total number of slices:

$$\psi(\mathcal{T},\mathcal{H}_i) = \psi_{\mathcal{H}}(\mathcal{T}(\mathcal{H}_i),k,k') + \tilde{w}\cdot\psi_{\mathcal{M}}(\mathcal{T},(\mathcal{H}_i),\widetilde{\mathcal{M}}_i), \quad (1)$$

where $\mathcal{T}$ is the rigid transformation of the slice $\mathcal{H}_i$. The term $\psi_{\mathcal{H}}$ quantifies the intrinsic alignment of $\mathcal{H}_i$ to neighboring k and k' slices located either lower and, respectively, higher in the Z stack. The Z stack refers to the third dimension in the reconstructed volume $\mathcal{H}$, where the first and second dimensions are defined relative to the 2D histology slice coordinate frame. The second term, $\psi_{\mathcal{M}}$, encodes the alignment of $\mathcal{H}_i$ with the corresponding slice in the *ex vivo* MRI, $\widetilde{\mathcal{M}}_i$, while $\tilde{w}$ represents the weight of the *ex vivo* term. Module 1 has four submodules.

1. **Module 1a. One-body backward intrinsic registration** ensures that each slice $\mathcal{H}_i$ is optimized within the reconstruction, $\forall i \in \{2,\ldots,N\}$, relative to the adjacent $k=7$, $\mathcal{H}_{i-j}$, $j \in \{1,\ldots,k\}$, $i-j>0$ slices located lower in the Z stack (backward registration). The *ex vivo* MRI is not considered in the scoring function as it has not yet been registered relative to the 3D histology reconstruction (i.e., $\tilde{w}=0$). Specifically, in Module 1a, Eq. (1) becomes

$$\psi(\mathcal{T},\mathcal{H}_i) = \sum_{j=1}^{k} w_j \cdot MI(\mathcal{T}(\mathcal{H}_i),\mathcal{H}_{i-j}), \quad (2)$$

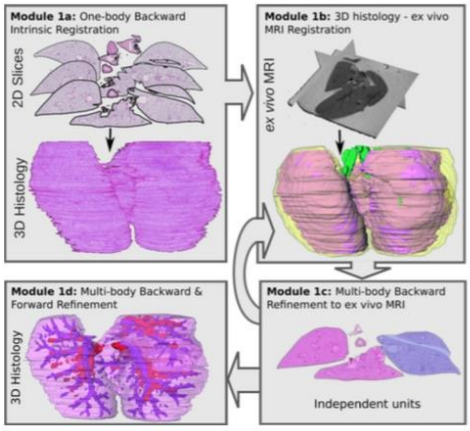

FIG. 3. Submodules of the histology reconstruction procedure (see Sec. 4.B for details).

TABLE II. Notations used in this paper.

Symbol	Definition
N	Number of histology slices
$\mathcal{H}$	3D histology volume
$\mathcal{H}_i$	Histology slice, $i \in \{1,\ldots,N\}$
$\mathcal{H}_i^m$	Unit m in $\mathcal{H}_i$
$\mathcal{A}$	Airways
$\widetilde{\mathcal{M}}$	*Ex vivo* MRI
$\widetilde{\mathcal{M}}_i$	*Ex vivo* MRI slice, $i \in \{1,\ldots,N\}$
$\mathcal{M}$	*In vivo* MRI
ψ	Optimized scoring function
$\psi_{\mathcal{H}}$	Histology scoring function
$\psi_{\mathcal{M}}$	*Ex vivo* MRI scoring function
MI	Mutual information
$\mathcal{T}$	Rigid transformation
w_j	Weight of the adjacent slice
$\tilde{w}$	Weight of *ex vivo* term

where $w_j = \exp(-(j^2/4))$ controls the influence of adjacent slices based on their proximity within the Z-stack.

2. **Module 1b. 3D histology-*ex vivo* MRI registration** ensures that the lung segmented from the *ex vivo* MRI is coregistered to the 3D histology volume, $\mathcal{H}$, using an affine transformation. A three-level pyramid registration scheme within the ITK-based package *elastix*[41] was used to optimize the normalized mutual information, employed as the scoring function.
3. **Module 1c. MultiBody backward refinement to *ex vivo* MRI** ensures that independent lobular units m are considered and their rigid transforms $\mathcal{T}^m$ are individually optimized. During histology sample preparation (fixing and staining), the five lobes may move relative to each other. The five lobes were split into two independent units, $m \in \{1,2\}$, the left and right lung, forming $\mathcal{H}_i^m$, $\forall i \in \{1,\ldots,N\}$, with their own optimized rigid transformation $\mathcal{T}_i^m$. More than two lobular units can be considered. Eq. (1) thus becomes

$$\psi(\mathcal{T}^m,\mathcal{H}_i^m) = \psi_{\mathcal{H}}(\mathcal{T}^m(\mathcal{H}_i^m),k) + \tilde{w}\cdot\psi_{\mathcal{M}}(\mathcal{T}(\mathcal{H}_i^m),\mathcal{H}_i^n,\widetilde{\mathcal{M}}_i), \quad (3)$$

TABLE III. Computer extracted MRI derived features capture different types of information, e.g., quantifying the smoothness, heterogeneity, or directional patterns. These features are not intended as a comprehensive compendium of textural features, but rather as an illustration of the types of feature interrogation of the diseased regions that can be facilitated via the newly presented histologic reconstruction and radiology–pathology coregistration pipeline.

Feature category	Number of features	Captured information
First order statistics (Ref. 36)	4	Smoothness
Second order statistics (Ref. 36)	13	Edges, heterogeneity
Haralick (Ref. 37)	13	Intensity co-occurrence
Gabor filter (Ref. 38)	48	Directional linear patterns

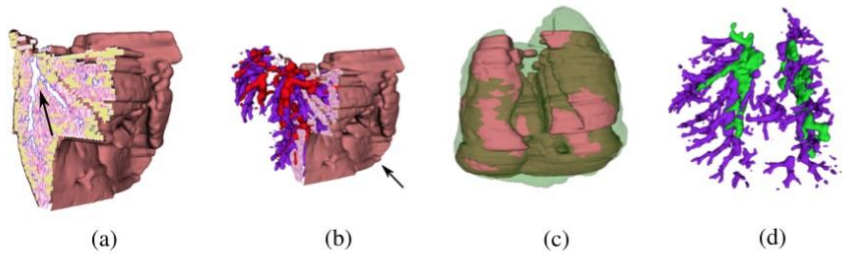

(a) (b) (c) (d)

FIG. 4. Histology volume reconstruction, $\mathcal{H}$; (a) cut through $\mathcal{H}$ shows the 3D continuity of the lung outline (brown), airways (blue outline, see arrow), and inflammation (yellow); (b) same as (a) with completely reconstructed airways (purple) and blood vessels (red); arrows point to reduced zig-zag pattern which is a qualitative indication of a good alignment; (c) overlay of $\mathcal{H}$ and *ex vivo* MRI, $\widetilde{\mathcal{M}}$ (green); (d) alignment of airways, histology (purple), *ex vivo* MRI (green).

where $m, n \in \{1,2\}$, $m \neq n$ represent independent units. $\psi_{\mathcal{H}}(\mathcal{T}(\mathcal{H}_i^m),k)$ is defined using Eq. (2) while $\psi_{\mathcal{M}}$ encodes the mutual information of the MRI slice, $\mathcal{M}_i$ and the entire histology slice, $\mathcal{H}_i$ composed of the transformed unit $\mathcal{H}_i^m$ and not transformed units $\mathcal{H}_i^n$, where $n \neq m$, $\tilde{w} > 0$.

While only the optimized unit m is considered in $\psi_{\mathcal{H}}$, all independent units, $\mathcal{H}_i^m$, are considered in the second term, $\psi_{\mathcal{M}}$. This helps to ensure that each unit is aware of the location of the other units and thus helps to limit their overlap.

4. **Module 1d. Multibody backward and forward refinement** ensures that the independent units $\mathcal{H}_i^m$ are optimized relative to the lobular units in the adjacent slices $i+j$, $j \in \{-k,k'\}$, $j \neq 0$. As opposed to Module 1c, in Module 1d, we consider the lobular units of adjacent slices located not only lower but also higher in the Z stack. Specifically, Eq. (3) becomes

$$\psi_{\mathcal{H}}(\mathcal{T}(\mathcal{H}_i^m),k,k') = \sum_{j=-k}^{k',j\neq 0} w_j \cdot MI(\mathcal{T}(\mathcal{H}_i^m),\mathcal{H}_{i+j}^m). \quad (4)$$

Module 1 iterates between the different submodules 1a–d using the following scheme. In iteration 1, the procedures defined in submodule 1a are performed. In iteration 2, the procedures defined in submodules 1b, 1c are performed. In iteration 3, the procedures defined in submodules 1b, 1c are reiterated to refine the reconstruction relative to the *ex vivo* MRI. Finally, in iteration 4, the steps in submodule 1d are employed to refine the final reconstruction. At each iteration, the transformation of each histology slice $\mathcal{H}_i, i \in \{1,\ldots,N\}$, or respective lobular unit, is refined.

Module 1 is evaluated by assessing the accuracy of the 3D histology volume reconstruction and registration with *ex vivo* MRI via the following measures.

1. The intrinsic alignment of the histology slices: $\text{DSC}_{\mathcal{H}} = 1/(N-1) \times \sum_{i=1}^{N-1} D(\mathcal{H}_i,\mathcal{H}_{i+1})$, where the dice similarity coefficient (DSC) is defined as $D(A,B) = 2|A \cap B|/(|A|+|B|)$ and $|A|$ represents the cardinality of the set A.
2. Alignment of the reconstruction, $\mathcal{H}$, with the *ex vivo* MRI, $\widetilde{\mathcal{M}}$: $\widetilde{\text{DSC}} = D(\mathcal{H},\widetilde{\mathcal{M}})$.
3. The alignment of L landmarks corresponding to the airway tree divisions within histology, $\mathcal{A}_{\mathcal{H},l}$, and *ex vivo* MRI, $\mathcal{A}_{\mathcal{M},l}$, $l \in \{1,\ldots,L\}$,

$$\text{RMSD} = 1/L \times \sqrt{\sum_{l=1}^{L} |\mathcal{A}_{\mathcal{H},l},\mathcal{A}_{\mathcal{M},l}|^2}. \quad (5)$$

A good reconstruction and fusion are suggested by a large DSC (max value 1) and reduced RMSD (min value: 0).

4.C. Module 2: Map disease ground truth from histology onto *in vivo* MRI volume

The linear alignment of $\mathcal{H}$ and $\mathcal{M}$ was achieved using $\widetilde{\mathcal{M}}$ as a conduit in the affine registration. To maintain the higher resolution offered by the histology, the registrations were performed using an isotropically upsampled *in vivo* MRI. $\mathcal{H}$ is warped to $\mathcal{M}$ using a B-spline based free-form deformation in a three-level pyramid registration scheme that optimizes the normalized mutual information, where the finer pyramid has a grid spacing of 4 mm. The optimized deformable transformation that warps $\mathcal{H}$ onto $\mathcal{M}$ is also applied to project the 3D inflammation ground truth on to $\mathcal{M}$, thus creating the *in vivo* ground truth for inflammation. We evaluated the registration of $\mathcal{H}$ with $\mathcal{M}$ by quantifying the alignment via $\text{DSC} = D(\mathcal{H},\mathcal{M})$.

FIG. 5. Reconstruction viewed from different planes, including axial, sagittal, and coronal. (Multimedia view) [URL: http://dx.doi.org/10.1118/1.4923161.1]

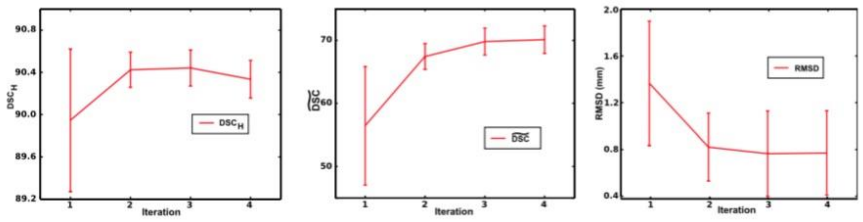

(a) (b) (c)

FIG. 6. Progression of 3D reconstruction quality per iteration shown for three mice: (a) $DSC_{\mathcal{H}}$, (b) $\overline{DSC}$, and (c) landmark RMSD; iteration 1 - Module 1a, iteration 2 - Modules 1b,1c; iteration 3 - Repeat Modules 1b, 1c; iteration 4 - Module 1d.

4.D. Module 3: Identify computer extracted features associated with inflammation

Following standardization of lung intensities via landmark-based histogram alignment,[42] 78 features were derived from the *in vivo* MRI in both Sftpd$^{-/-}$ and control mice after the *in vivo* MRI was resampled to a consistent 250 μm voxel size. The computer derived features extracted from $\mathcal{M}$ are summarized in Table III.

These features attempt to capture subtle subvisual differences in image intensity that may not be visibly discernible on the original MRI. For instance, Haralick features[37] capture co-occurring intensity statistics, while the Gabor filters[38] are steerable wavelets that emphasize and capture oriented gradient patterns in the image. First and second order statistics[36] are able to characterize image smoothness and identify edges.

As previously mentioned, the goal of this work was not so much to validate imaging signatures for lung inflammation, but so much as to pave the framework to facilitate feature discovery. With this in mind, we evaluated our framework with some well established image texture features to identify their association with inflammation in the lung. These features were largely drawn from classical textural operators including first and second order statistics,[36] steerable filters,[38] or Haralick features,[37] with the goal of being able to characterize the heterogeneous appearance of inflammation. Manifestations of inflammation include accumulation of foamy appearing alveolar macrophages and of peribronchial and perivascular infiltrates in the lung.[2,3] We expect that these accumulations modify the visible smoothness of the lung, which could be captured via first and second order statistical texture features.[36] Moreover, such infiltrates may appear with similar intensity patterns at different locations within the lung, suggesting the need of Haralick features to identify such correlated patterns. The discontinuous accumulation of leukocytes may result in the creation of heterogeneous patches with borders that may be emphasized by Gabor filter features.

In order to compare the appearance profiles of inflamed and noninflamed regions and identify those textural features that are most discriminating between inflammation and noninflammation, we evaluate the difference between feature value distributions via the Bhattacharyya distance[43]

$$Bh(p,q) = -\ln\left(\sum_{b=1}^{B}\left(\sqrt{p_b,q_b}\right)\right), \tag{6}$$

where p and q are the discrete probability density function of the image derived features for the inflammation and normal regions, respectively. B represents the number of bins, while p_b and q_b are the normalized frequency of textural feature responses within each bin B.

As inflammation has a discontinuous spatial distribution, we choose to compare image derived features within inflamed regions in the Sftpd$^{-/-}$ mice and with an anatomically

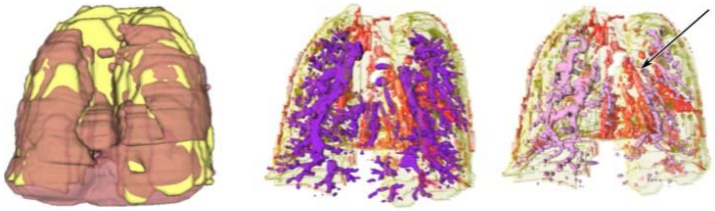

(a) (b) (c)

FIG. 7. Visualization of the 3D histology volume, $\mathcal{H}$ (brown), and *in vivo* MRI volume, $\mathcal{M}$ (yellow), alignment; (a) overlay of $\mathcal{H}$ and $\mathcal{M}$; (b) overlay of airways from $\mathcal{H}$ (dark purple) onto blood vessels from $\mathcal{M}$ (red). (c) Overlay of blood vessels from $\mathcal{M}$ (red) and blood vessels from $\mathcal{H}$ (pink). Arrow points to area of visually assessed close overlap.

TABLE IV. Mean and standard deviation of DSC between reconstructed histology volumes $\mathcal{H}$ and *in vivo* MRI lung volumes, $\mathcal{M}$.

Mice \ Registration	Affine	Deformable
Sftpd$^{-/-}$	56.0 (0.7)	73.7 (0.9)
Control	62.2 (8.3)	75.9 (5.4)

corresponding region of interest in the control mice. The regions of inflammation were identified in the Sftpd$^{-/-}$ mice as described in Secs. 4.B and 4.C.

5. EXPERIMENTAL RESULTS AND DISCUSSION

5.A. 3D histology reconstruction

Figure 4 depicts the final results of successfully aligning the 2D H&E slices into a 3D histology volume without introducing noticeable "drift" between slices. The exterior surface of the 3D reconstruction (brown in Fig. 4) appears to be smooth, without significant zig-zag patterns visible at the edges of the reconstruction [see arrow in Fig. 4(b)].

The airways appear as continuous 3D structures [arrow in Fig. 4(a) and Fig. 5 (Multimedia view)] within the histology reconstruction [purple in Figs. 4(b) and 4(d)], suggesting minimal alignment errors between slices as illustrated in Figs. 4(a)–4(c) and assessed quantitatively by $DSC_{\mathcal{H}}$ [Fig. 6(a)]. The extracted airways appear to closely overlap in 3D between the histology and the *ex vivo* MRI lung, as illustrated in Figs. 4(d). Moreover, the high degree of reconstruction accuracy is also reflected quantitatively in the low RMSD = 0.85 ± 0.44 mm between the 17 landmark points on the 3D histology reconstruction and *ex vivo* MRI of the three mice for which the reconstruction was performed.

The reconstruction approach was evaluated for the three mice (two Sftpd$^{-/-}$ mice and one control WT) at each iteration (Fig. 6). The reconstruction $\mathcal{H}$ shows a high $DSC_{\mathcal{H}}$ following Module 1a (first iteration), suggesting that the one-to-many registration without spatial constraints is able to closely coregister the histology slices. Yet, both the $\widetilde{DSC}$ and RMSD show their worse performance when the registration is not constrained by $\widetilde{\mathcal{M}}$.

TABLE V. Top five scoring features ranked according to the Bhattacharyya distance.

Feature	Parameters	Rank
Gabor	Angle: 0	1
Gabor	Angle: 2.74	2
Gabor	Angle: 0.39	3
Gabor	Angle: 0.78	4
Gabor	Angle: 2.35	5

Following the execution of Modules 1b, 1c (second iteration) in which the lobe units are simultaneously registered with constraints provided by *ex vivo* MRI, the intrinsic $DSC_{\mathcal{H}}$ and $\widetilde{\mathcal{M}}$ and landmark RMSD significantly improve, possibly reflecting the benefit of the second iteration.

In the third iteration, Modules 1b and 1c are rerun to refine the transformation of the *ex vivo* MRI and subsequently of the lobular units. Fig. 6 shows minimal improvement in $DSC_{\mathcal{H}}$, but substantial improvement of $\widetilde{DSC}$. Moreover, the decrease in RMSD suggests that the refinement of the *ex vivo* MRI transformation relative to the 3D histology reconstruction is required to further improve the reconstruction accuracy.

After Module 1d (fourth iteration), $\widetilde{DSC}$ reach their maxima, while the RMSD deviation is minimized to 0.85 ± 0.44 mm. $DSC_{\mathcal{H}}$ decreases slightly.

5.B. Fusion of 3D histology to *in vivo* MRI

Figure 7(a) shows the 3D histology volume, $\mathcal{H}$ (brown), overlaid onto *in vivo* MRI, $\mathcal{M}$ (yellow). The airway tree (purple) in Fig. 7(b) is shown relative to the blood vessels (red) extracted from $\mathcal{M}$ to depict the intertwining of the two systems. As expected, the two systems run in parallel to each other, without overlap as qualitatively seen in Fig. 7(b). Alignment accuracy is assessed qualitatively by visually investigating the blood vessel alignment, which in these figures appear to suggest close correspondences between blood vessels in $\mathcal{M}$ and $\mathcal{H}$ (pink) [see arrow in Fig. 7(c)].

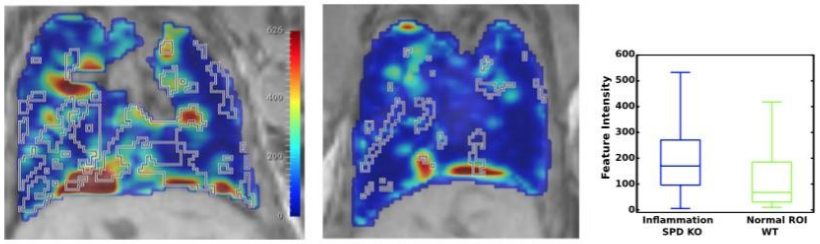

(a) (b) (c)

FIG. 8. Preliminary evaluation of the framework in characterizing imaging signatures of inflammation. The most discriminative feature (Gabor) is shown using the same colormap in (a) Sftpd$^{-/-}$ lung with mapped inflammation (outlined with the black and white line) from 3D histology reconstruction; (b) WT lung with volume of interest (outlined with the black and white line); (c) feature distributions show modest separation between the computer extracted features derived from the inflamed and noninflamed regions.

TABLE VI. Top three features within each feature group ranked according to the Bhattacharyya distance.

Feature	Parameters	Rank
Gabor	Angle: 0.00	1
	Angle: 2.75	2
	Angle: 0.39	3
Haralick	Energy	10
	Correlation	11
	IDM	12
First order	Median	8
	Range	13
	Mean	17
Second order	Gradient magnitude	38
	Gradient X	44
	Sobel X	56
MRI intensity		16

Table IV summarizes the quantitative evaluation via dice similarity coefficient, DSC, after each of the affine and deformable registration steps. DSC in the twoSftpd$^{-/-}$ mice is computed between $\mathcal{H}$ and $\mathcal{M}$ and not surprisingly shows an improvement in alignment following deformable registration. For the five control mice, DSC reflects the quality of registration that allows for the identification of the anatomically corresponding region of interest.

5.C. Feature characterization

Figure 8 illustrates a Gabor wavelet representation. This feature was ranked first according to the Bhatacharyya distance (Table V) reflecting the most substantial difference in distribution between the Sftpd$^{-/-}$ inflammation [Fig. 8(a)] and the corresponding volume of interest in the control mouse [Fig. 8(b)]. These differences are also reflected in the box and whiskers plot in Fig. 8(c). The statistical significance of these differences was not evaluated in this preliminary study due to the small sample size. The difference in Gabor features between inflamed and noninflamed regions appears to suggest that inflammation may influence the appearance of linear patterns within the *in vivo* MRI. Clearly, independent validation in a large cohort is needed to establish the statistical significance of these findings.

Table V shows the five-top ranked features according to the Bhattacharyya distance,[43] while Table VI shows the three-top ranked features, according to the same criterion, but within each feature class. Based on the Bhatacharyya distance criteria, the MRI intensity ranked 16 out of 79 features (Table VI), suggesting that several computer extracted features were more specific for identification of inflammation compared to the original signal intensity.

6. CONCLUDING REMARKS

We introduced a general analytic framework for 3D histologic reconstruction, multimodal fusion of radiology and pathology in order to facilitate computer based feature interrogation of disease appearance on *in vivo* imaging. The framework enables the mapping of disease extent from the histology onto the *in vivo* imaging, creating the disease ground truth required for further feature analysis. We evaluated our framework in a preliminary study aimed at characterizing the *in vivo* MRI signature of inflammation in a preclinical mouse model. Our evaluation showed that potential candidate *in vivo* imaging computer extracted MRI features of lung inflammation may be identified using our framework.

Our methodology comprised of multiple individual modules including (1) reconstruction of 3D histology volume using *ex vivo* MRI as a conduit, (2) coregistration of the 3D histology volume with the *in vivo* MRI, and (3) textural feature comparison between diseased and normal regions. Qualitative and quantitative results suggest that the individual modules have a high degree of accuracy. Our framework yielded (1) accurate intrinsic alignment of the 2D histologic slices within the reconstruction, (2) proper alignment of the 3D histology and *ex vivo* MRI, and (3) accurate alignment of the 3D histology and *in vivo* MRI on the three mice, two Sftpd$^{-/-}$ and one control, considered in our study. Despite the high variability in *in vivo* MRI imaging parameters, resolution, and field of view, our framework was able to identify preliminary textural features that appear to be associated with pulmonary inflammation in the seven mice, two Sftpd$^{-/-}$ and five controls in our evaluation cohort.

Some challenges may influence the accuracy of the fusion of 2D histology and *in vivo* MRI lung. First, the lung is a soft tissue which is prone to major elastic deformation caused by the neighboring organs within the *in vivo* MRI. Moreover, the histology preparation causes deformation and shrinkage of the tissue. In order to account for these challenges, we used the *ex vivo* MRI as a conduit in the registration and employed a pyramid anisotropic affine registration in the 3D histology reconstruction, and a deformable registration during the histology - *in vivo* MRI fusion. The reconstruction procedure is further complicated by the lung being composed of five lobes distributed between the left and right lungs. The lobes are not attached and thus are capable of moving relative to each other during tissue excise and histological preparation. Our multibody refinement approach used during the reconstruction was implemented to overcome the possible movements of the lobes relative to each other.

The framework described in this paper was evaluated in an established mouse model of chronic pulmonary inflammation. Inflammation was identified on histology and subsequently mapped onto *in vivo* MRI for two Sftpd$^{-/-}$ mice. A similar registration approach was used to define the volume of interest in the control mice, to generate a noninflamed volume of interest that corresponds anatomically and spatially to the regions of high inflammation likelihood, as shown by the Sftpd$^{-/-}$ mice. The noninflamed volume of interest could not have been mapped from histology, since the entire volume of the lung is normal in the control animals. We anticipate that the choice of the volume of interest is not essential as the entire volume is noninflamed in the control animals, yet we made every attempt to control for anatomical and interindividual

variations by considering elastic registrations within five animals. Although, as proof-of-concept and for evaluation purposes, we performed a 3D histology reconstruction and fusion with MRI in one control animal, we considered it unnecessary for the remaining four control mice.

A total of three animals were used to evaluate the 3D histology reconstruction and its fusion with MRI. The evaluation showed good landmark and/or volumetric alignment between the 3D reconstructed histology lung and the MRI-outlined lung, indicating a proper ground truth mapping of inflammation from histology onto MRI. MRI features were extracted from a total of seven mice and were utilized to evaluate differences between inflamed and noninflamed regions. While statistical significance was not evaluated due to the small sample size, the expression patterns of some of the features warrant a subsequent in depth feature analysis. Our initial results represent preliminary data and could potentially pave the way for the use of the fusion framework in interrogation of *in vivo* imaging signatures of lung inflammation. In future work, we intend to validate the image features identified in this preliminary study on a large, independent validation cohort.

We believe our unique reconstruction and image analysis framework may be extended to include additional histological stains, molecular biomarkers, or other imaging modalities, e.g., micro-CT, to enable a comprehensive study of inflammation and other lung conditions.

ACKNOWLEDGMENTS

The authors would like to thank Derek Adler and Dr. Ed Yurkow at the Rutgers Molecular Imaging Center for their imaging expertise. Research reported in this publication was supported by the Department of Defense (W81XWH-13-1-0487), National Institutes of Health under Award Nos. R01CA136535-01, R01CA140772-01, R21CA167811-01, GM108463, HL086621, ES005022, CA136535, CA140722, CA167811; the National Institute of Diabetes and Digestive and Kidney Diseases under Award No. R01DK098503-02, the DOD Prostate Cancer Synergistic Idea Development Award (No. PC120857); the QED award from the University City Science Center and Rutgers University, the Ohio Third Frontier Technology development Grant. The content is solely the responsibility of the authors and does not necessarily represent the official views of the National Institutes of Health.

[a]Author to whom correspondence should be addressed. Electronic mail: mirabela.rusu@gmail.com; Current address: GE Global Research Center, Niskayuna, New York 12309.

[1]P. K. Jeffery, "Remodeling in asthma and chronic obstructive lung disease," Am. J. Respir. Crit. Care Med. **164**, S28–S38 (2001).
[2]E. N. Atochina, M. F. Beers, S. Hawgood, F. Poulain, C. Davis, T. Fusaro, and A. J. Gow, "Surfactant protein-D, a mediator of innate lung immunity, alters the products of nitric oxide metabolism," Am. J. Respir. Cell Mol. Biol. **30**, 271–279 (2004).
[3]C. Botas, F. Poulain, J. Akiyama, C. Brown, L. Allen, J. Goerke, J. Clements, E. Carlson, A. M. Gillespie, C. Epstein, and S. Hawgood, "Altered surfactant homeostasis and alveolar type II cell morphology in mice lacking surfactant protein D," Proc. Natl. Acad. Sci. U. S. A. **95**, 11869–11874 (1998).
[4]J. Vogel-Claussen, J. Renne, J. Hinrichs, C. Schönfeld, M. Gutberlet, F. Schaumann, C. Winkler, C. Faulenbach, N. Krug, F. K. Wacker, and J. M. Hohlfeld, "Quantification of pulmonary inflammation after segmental allergen challenge using turbo-inversion recovery-magnitude magnetic resonance imaging," Am. J. Respir. Crit. Care Med. **189**, 650–657 (2014).
[5]D. L. Chen and D. P. Schuster, "Imaging pulmonary inflammation with positron emission tomography: A biomarker for drug development," Mol. Pharm. **3**, 488–495 (2006).
[6]B. N. Jobse, J. R. Johnson, T. H. Farncombe, R. Labiris, T. D. Walker, S. Goncharova, and M. Jordana, "Evaluation of allergic lung inflammation by computed tomography in a rat model in vivo," Eur. Respir. J. **33**, 1437–1447 (2009).
[7]V. Ntziachristos, "Optical imaging of molecular signatures in pulmonary inflammation," Proc. Am. Thorac. Soc. **6**, 416–418 (2009).
[8]N. Beckmann, B. Tigani, D. Ekatodramis, R. Borer, L. Mazzoni, and J. R. Fozard, "Pulmonary edema induced by allergen challenge in the rat: Noninvasive assessment by magnetic resonance imaging," Magn. Reson. Med. **45**, 88–95 (2001).
[9]B. Tigani, C. Cannet, H. Karmouty-Quintana, F.-X. Blé, S. Zurbruegg, E. Schaeublin, J. R. Fozard, and N. Beckmann, "Lung inflammation and vascular remodeling after repeated allergen challenge detected noninvasively by MRI," Am. J. Physiol. **292**, L644–L653 (2007).
[10]F.-X. Blé, C. Cannet, S. Zurbruegg, H. Karmouty-Quintana, R. Bergmann, N. Frossard, A. Trifilieff, and N. Beckmann, "Allergen-induced lung inflammation in actively sensitized mice assessed with MR imaging," Radiology **248**, 834–843 (2008).
[11]J. H. Holmes *et al.*, "Noninvasive mapping of regional response to segmental allergen challenge using magnetic resonance imaging and [F-18] fluorodeoxyglucose positron emission tomography," Magn. Reson. Med. **53**, 1243–1250 (2005).
[12]J. M. Wild, H. Marshall, M. Bock, L. R. Schad, P. M. Jakob, M. Puderbach, F. Molinari, E. J. R. Van Beek, and J. Biederer, "MRI of the lung (1/3): Methods," Insights Imaging **3**, 345–353 (2012).
[13]J. Biederer, M. Beer, W. Hirsch, J. Wild, M. Fabel, M. Puderbach, and E. J. R. Van Beek, "MRI of the lung (2/3). Why when how? Insights Imaging **3**, 355–371 (2012).
[14]J. Biederer, S. Mirsadraee, M. Beer, F. Molinari, C. Hintze, G. Bauman, M. Both, E. J. R. Van Beek, J. Wild, and M. Puderbach, "MRI of the lung (3/3)-current applications and future perspectives," Insights Imaging **3**, 373–386 (2012).
[15]S. E. Viswanath, N. B. Bloch, J. C. Chappelow, R. Toth, N. M. Rofsky, E. M. Genega, R. E. Lenkinski, and A. Madabhushi, "Central gland and peripheral zone prostate tumors have significantly different quantitative imaging signatures on 3 Tesla endorectal, in vivo T2-weighted MR imagery," J. Magn. Reson. Imaging **36**, 213–224 (2012).
[16]E. Segal, C. B. Sirlin, C. Ooi, A. S. Adler, J. Gollub, X. Chen, B. K. Chan, G. R. Matcuk, C. T. Barry, H. Y. Chang, and M. D. Kuo, "Decoding global gene expression programs in liver cancer by noninvasive imaging," Nat. Biotechnol. **25**, 675–680 (2007).
[17]O. Gevaert, J. Xu, C. D. Hoang, A. N. Leung, Y. Xu, A. Quon, D. L. Rubin, S. K. Napel, and S. Plevritis, "Non–small cell lung cancer: Identifying prognostic imaging biomarkers by leveraging public gene expression microarray data–methods and preliminary results," Radiology **264**, 387–396 (2012).
[18]P. Tiwari, J. Kurhanewicz, and A. Madabhushi, "Multi-kernel graph embedding for detection, Gleason grading of prostate cancer via MRI/MRS," Med. Image Anal. **17**, 219–235 (2013).
[19]J. Chappelow, A. Madabhushi, M. Rosen, J. Tomaszeweski, and M. Feldman, "Multimodal image registration of ex vivo 4 Tesla prostate MRI with whole mount histology for cancer detection," Proc. SPIE **6512**, S1–S12 (2007).
[20]J. Chappelow, B. N. Bloch, N. Rofsky, E. Genega, R. Lenkinski, W. DeWolf, and A. Madabhushi, "Elastic registration of multimodal prostate MRI and histology via multiattribute combined mutual information," Med. Phys. **38**, 2005–2018 (2011).
[21]E. Gibson, M. Gaed, J. A. Gómez, M. Moussa, S. Pautler, J. L. Chin, C. Crukley, G. S. Bauman, A. Fenster, and A. D. Ward, "3D prostate histology image reconstruction: Quantifying the impact of tissue deformation and histology section location," J. Pathol. Inf. **4**, 31 (2013).
[22]G. Nir, R. S. Sahebjavaher, P. Kozlowski, S. D. Chang, E. Jones, L. L. Goldenberg, and S. E. Salcudean, "Registration of whole-mount histology and volumetric imaging of the prostate using particle filtering," IEEE Trans. Med. Imaging **33**, 1601–1613 (2014).

[23]C. Orczyk, H. Rusinek, A. B. Rosenkrantz, A. Mikheev, F-M. Deng, J. Melamed, and S. S. Taneja, "Preliminary experience with a novel method of three-dimensional co-registration of prostate cancer digital histology and in vivo multiparametric MRI," Clin. Radiol. **68**, e652–e658 (2013).
[24]B. Turkbey, H. Mani, V. Shah, A. R. Rastinehad, M. Bernardo, T. Pohida, Y. Pang, D. Daar, C. Benjamin, Y. L. McKinney, H. Trivedi, C. Chua, G. Bratslavsky, J. H. Shih, W. M. Linehan, M. J. Merino, P. L. Choyke, and P. A. Pinto, "Multiparametric 3 T prostate magnetic resonance imaging to detect cancer: Histopathological correlation using prostatectomy specimens processed in customized magnetic resonance imaging based molds," J. Urol. **186**, 1818–1824 (2011).
[25]H. Park, M. R. Piert, A. Khan, R. Shah, H. Hussain, J. Siddiqui, and C. R. Meyer, "Registration methodology for histological sections and in-vivo imaging of human prostate," Acad. Radiol. **15**, 1027–1039 (2008).
[26]S. Ourselin, A. Roche, X. Subsol, G. Pennec, and N. Ayache, "Reconstructing a 3D structure from serial histological sections," Image Vision Comput. **19**, 25–31 (2001).
[27]A. Cifor, T. Pridmore, and A. Pitiot, "Smooth 3-D reconstruction for 2-D histological images," in *Information Processing in Medical Imaging* (Springer, Berlin Heidelberg, 2009), pp. 350–361.
[28]L. Alic, J. C. Haeck, K. Bol, S. Klein, S. T. van Tiel, P. A. Wielepolski, M. de Jong, W. J. Niessen, M. Bernsen, and J. F. Veenland, "Facilitating tumor functional assessment by spatially relating 3D tumor histology and in vivo MRI: Image registration approach," PLoS One **6**, e22835 (2011).
[29]J. Lotz, J. Berger, B. Müller, K. Breuhahn, N. Grabe, S. Heldmann, B. Homeyer, A. Lahrmann, H. Laue, J. Olesch, M. Schwier, O. Sedlaczek, and A Warth, "Zooming in: High resolution 3D reconstruction of differently stained histological whole slide images," Proc. SPIE **9041**, 904104-1–904104-7 (2014).
[30]P. Yushkevich, B. Avants, L. Ng, M. Hawrylycz, P. Burstein, H. Zhang, and J. Gee, "3D mouse brain reconstruction from histology using a coarse-to-fine approach," in *Biomedical Image Registration*, Lecture Notes in Computer Science (Springer, Berlin Heidelberg, 2006), pp. 230–237.
[31]H. Wang, J. W. Suh, S. R. Das, J. B. Pluta, C. Craige, and P. A. Yushkevich, "Multi-atlas segmentation with joint label fusion," IEEE Trans. Pattern Anal. Mach. Intell. **35**, 611–623 (2013).
[32]M. Feuerstein, H. Heibel, J. Gardiazabal, N. Navab, and M. Groher, "Reconstruction of 3-D histology images by simultaneous deformable registration," in *Medical Image Computing and Computer-Assisted Intervention* (Springer, Berlin Heidelberg, 2011), pp. 582–589.
[33]S. Ginsburg, P. Tiwari, J. Kurhanewicz, and A. Madabhushi, "Variable ranking with PCA: Finding multiparametric MR imaging markers for prostate cancer diagnosis and grading," in *Prostate Cancer Imaging. Image Analysis and Image-Guided Interventions* (Springer, Berlin Heidelberg, 2011), pp. 146–157.
[34]G. Litjens, O. Debats, J. Barentsz, N. Karssemeijer, and H. Huisman, "Computer-aided detection of prostate cancer in MRI," IEEE Trans. Pattern Anal. Mach. Intell. **33**, 1083–1092 (2014).
[35]M. Rusu and S. Birmanns, "Evolutionary tabu search strategies for the simultaneous registration of multiple atomic structures in cryo-em reconstructions," J. Struct. Biol. **170**, 164–171 (2010).
[36]J. C. Russ, *Image Processing Handbook*, 4th ed. (CRC, Inc., Boca Raton, FL, 2002).
[37]R. M. Haralick, K. Shanmugan, and I. Dinstein, "Textural features for image classification," IEEE Trans. Syst. Man Cybern. **SMC-3**, 610–621 (1973).
[38]A. C. Bovik, M. Clark, and W. S. Geisler, "Multichannel texture analysis using localized spatial filters," IEEE Trans. Pattern Anal. Mach. Intell. **12**, 55–73 (1990).
[39]D. G. Rudmann, A. M. Preston, M. W. Moore, and J. M. Beck, "Susceptibility to pneumocystis carinii in mice is dependent on simultaneous deletion of ifn-gamma and type 1 and 2 tnf receptor genes," J. Immunol. **161**, 360–366 (1998).
[40]S. Lankton and A. Tannenbaum, "Localizing region-based active contours," IEEE Trans. Pattern Anal. Mach. Intell. **17**, 2029–2039 (2008).
[41]S. Klein, M. Staring, K. Murphy, M. A. Viergever, and J. P. W. Pluim, "Elastix: A toolbox for intensity-based medical image registration," IEEE Trans. Med. Imaging **29**, 196–205 (2010).
[42]A. Madabhushi and J. K. Udupa, "New methods of MR image intensity standardization via generalized scale," Med. Phys. **33**, 3426–3434 (2006).
[43]A. Bhattacharyya, "On a measure of divergence between two multinomial populations," Indian J. Stat. **7**, 401–406 (1946).

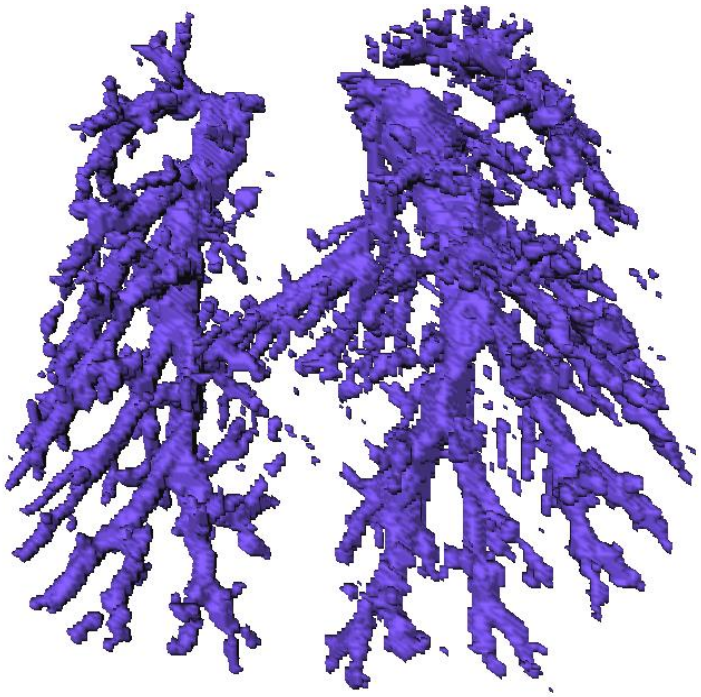

Figure 7-1

Figure 1. Airway tree of a C57/BL6 mouse. Airways were identified on MRI and histology sections and using co-registration techniques as reported in the paper below. Airway tree can be visualized with Slicer software and measurements made of dimensions.

REFERENCES

Adrie C, Monchi M, Dinh-Xuan AT, Dall'Ava-Santucci J, Dhainaut JF and Pinsky MR (2001) Exhaled and nasal nitric oxide as a marker of pneumonia in ventilated patients. *American journal of respiratory and critical care medicine* **163**:1143-1149.

Alp NJ and Channon KM (2004) Regulation of endothelial nitric oxide synthase by tetrahydrobiopterin in vascular disease. *Arteriosclerosis, thrombosis, and vascular biology* **24**:413-420.

Anderson CF and Mosser DM (2002) A novel phenotype for an activated macrophage: the type 2 activated macrophage. *Journal of leukocyte biology* **72**:101-106.

Anzueto A, Baughman RP, Guntupalli KK, Weg JG, Wiedemann HP, Raventos AA, Lemaire F, Long W, Zaccardelli DS and Pattishall EN (1996) Aerosolized surfactant in adults with sepsis-induced acute respiratory distress syndrome. Exosurf Acute Respiratory Distress Syndrome Sepsis Study Group. *The New England journal of medicine* **334**:1417-1421.

Arnold L, Henry A, Poron F, Baba-Amer Y, van Rooijen N, Plonquet A, Gherardi RK and Chazaud B (2007) Inflammatory monocytes recruited after skeletal muscle injury switch into antiinflammatory macrophages to support myogenesis. *The Journal of experimental medicine* **204**:1057-1069.

Ashbaugh DG, Bigelow DB, Petty TL and Levine BE (1967) Acute respiratory distress in adults. *Lancet* **2**:319-323.

Atochina-Vasserman EN, Beers MF, Kadire H, Tomer Y, Inch A, Scott P, Guo CJ and Gow AJ (2007) Selective inhibition of inducible NO synthase activity in vivo reverses inflammatory abnormalities in surfactant protein D-deficient mice. *Journal of immunology* **179**:8090-8097.

Auffray C, Fogg D, Garfa M, Elain G, Join-Lambert O, Kayal S, Sarnacki S, Cumano A, Lauvau G and Geissmann F (2007) Monitoring of blood vessels and tissues by a population of monocytes with patrolling behavior. *Science* **317**:666-670.

Austyn JM and Gordon S (1981) F4/80, a monoclonal antibody directed specifically against the mouse macrophage. *European journal of immunology* **11**:805-815.

Auten RL, Mason SN, Whorton MH, Lampe WR, Foster WM, Goldberg RN, Li B, Stamler JS and Auten KM (2007) Inhaled ethyl nitrite prevents hyperoxia-impaired postnatal alveolar development in newborn rats. *American journal of respiratory and critical care medicine* **176**:291-299.

Bates JHT (2009) *Lung Mechanics: An Inverse Modeling Approach*. Cambridge University Press, United Kingdom.

Bedoret D, Wallemacq H, Marichal T, Desmet C, Quesada Calvo F, Henry E, Closset R, Dewals B, Thielen C, Gustin P, de Leval L, Van Rooijen N, Le Moine A, Vanderplasschen A, Cataldo D, Drion PV, Moser M, Lekeux P and Bureau F (2009) Lung interstitial macrophages alter dendritic cell functions to prevent airway allergy in mice. *The Journal of clinical investigation* **119**:3723-3738.

Bernard GR, Artigas A, Brigham KL, Carlet J, Falke K, Hudson L, Lamy M, LeGall JR, Morris A and Spragg R (1994) Report of the American-European Consensus conference on acute respiratory distress syndrome: definitions, mechanisms, relevant outcomes, and clinical trial coordination. Consensus Committee. *Journal of critical care* **9**:72-81.

Bernard GR, Luce JM, Sprung CL, Rinaldo JE, Tate RM, Sibbald WJ, Kariman K, Higgins S, Bradley R, Metz CA and et al. (1987) High-dose corticosteroids in patients with the adult respiratory distress syndrome. *The New England journal of medicine* **317**:1565-1570.

Bland RD, Albertine KH, Carlton DP and MacRitchie AJ (2005) Inhaled nitric oxide effects on lung structure and function in chronically ventilated preterm lambs. *American journal of respiratory and critical care medicine* **172**:899-906.

Buckley BJ, Li S and Whorton AR (2008) Keap1 modification and nuclear accumulation in response to S-nitrosocysteine. *Free radical biology & medicine* **44**:692-698.

Burger RM, Peisach J and Horwitz SB (1981) Activated bleomycin. A transient complex of drug, iron, and oxygen that degrades DNA. *The Journal of biological chemistry* **256**:11636-11644.

Burke B, Ahmad R, Staples KJ, Snowden R, Kadioglu A, Frankenberger M, Hume DA and Ziegler-Heitbrock L (2008) Increased TNF expression in CD43++ murine blood monocytes. *Immunology letters* **118**:142-147.

Calfee CS, Eisner MD, Parsons PE, Thompson BT, Conner ER, Jr., Matthay MA, Ware LB and Network NARDSCT (2009) Soluble intercellular adhesion molecule-1 and clinical outcomes in patients with acute lung injury. *Intensive care medicine* **35**:248-257.

Calfee CS, Ware LB, Eisner MD, Parsons PE, Thompson BT, Wickersham N, Matthay MA and Network NA (2008) Plasma receptor for advanced glycation end products and clinical outcomes in acute lung injury. *Thorax* **63**:1083-1089.

Campbell S, Stone W, Whaley S and Krishnan K (2003) Development of gamma (gamma)-tocopherol as a colorectal cancer chemopreventive agent. *Critical reviews in oncology/hematology* **47**:249-259.

Cavarra E, Carraro F, Fineschi S, Naldini A, Bartalesi B, Pucci A and Lungarella G (2004) Early response to bleomycin is characterized by different cytokine and cytokine receptor profiles in lungs. *American journal of physiology Lung cellular and molecular physiology* **287**:L1186-1192.

Cohen PY, Breuer R, Zisman P and Wallach-Dayan SB (2015) Bleomycin-Treated Chimeric Thy1-Deficient Mice with Thy1-Deficient Myofibroblasts and Thy-Positive Lymphocytes Resolve Inflammation without Affecting the Fibrotic Response. *Mediators of inflammation* **2015**:942179.

Coleman JW (2001) Nitric oxide in immunity and inflammation. *International immunopharmacology* **1**:1397-1406.

Coleman MM, Ruane D, Moran B, Dunne PJ, Keane J and Mills KH (2013) Alveolar macrophages contribute to respiratory tolerance by inducing FoxP3 expression in naive T cells. *American journal of respiratory cell and molecular biology* **48**:773-780.

Crabtree MJ, Smith CL, Lam G, Goligorsky MS and Gross SS (2008) Ratio of 5,6,7,8-tetrahydrobiopterin to 7,8-dihydrobiopterin in endothelial cells determines glucose-elicited changes in NO vs. superoxide production by eNOS. *American journal of physiology Heart and circulatory physiology* **294**:H1530-1540.

Curry JM, Eubank TD, Roberts RD, Wang Y, Pore N, Maity A and Marsh CB (2008) M-CSF signals through the MAPK/ERK pathway via Sp1 to induce VEGF production and induces angiogenesis in vivo. *PloS one* **3**:e3405.

Dellinger RP, Zimmerman JL, Taylor RW, Straube RC, Hauser DL, Criner GJ, Davis K, Jr., Hyers TM and Papadakos P (1998) Effects of inhaled nitric oxide in patients with acute respiratory distress syndrome: results of a randomized phase II trial. Inhaled Nitric Oxide in ARDS Study Group. *Critical care medicine* **26**:15-23.

Dhaliwal K, Scholefield E, Ferenbach D, Gibbons M, Duffin R, Dorward DA, Morris AC, Humphries D, MacKinnon A, Wilkinson TS, Wallace WA, van Rooijen N, Mack M, Rossi AG, Davidson DJ, Hirani N, Hughes J, Haslett C and Simpson AJ (2012) Monocytes control second-

phase neutrophil emigration in established lipopolysaccharide-induced murine lung injury. *American journal of respiratory and critical care medicine* **186**:514-524.

Domenighetti G, Suter PM, Schaller MD, Ritz R and Perret C (1997) Treatment with N-acetylcysteine during acute respiratory distress syndrome: a randomized, double-blind, placebo-controlled clinical study. *Journal of critical care* **12**:177-182.

Doyle AG, Herbein G, Montaner LJ, Minty AJ, Caput D, Ferrara P and Gordon S (1994) Interleukin-13 alters the activation state of murine macrophages in vitro: comparison with interleukin-4 and interferon-gamma. *European journal of immunology* **24**:1441-1445.

Drazen JM, Gaston B and Shore SA (1995) Chemical regulation of pulmonary airway tone. *Annual review of physiology* **57**:151-170.

Dweik RA, Comhair SA, Gaston B, Thunnissen FB, Farver C, Thomassen MJ, Kavuru M, Hammel J, Abu-Soud HM and Erzurum SC (2001) NO chemical events in the human airway during the immediate and late antigen-induced asthmatic response. *Proceedings of the National Academy of Sciences of the United States of America* **98**:2622-2627.

Edwards JP, Zhang X, Frauwirth KA and Mosser DM (2006) Biochemical and functional characterization of three activated macrophage populations. *Journal of leukocyte biology* **80**:1298-1307.

Egawa M, Mukai K, Yoshikawa S, Iki M, Mukaida N, Kawano Y, Minegishi Y and Karasuyama H (2013) Inflammatory monocytes recruited to allergic skin acquire an anti-inflammatory M2 phenotype via basophil-derived interleukin-4. *Immunity* **38**:570-580.

Eisner MD, Parsons P, Matthay MA, Ware L, Greene K and Acute Respiratory Distress Syndrome N (2003) Plasma surfactant protein levels and clinical outcomes in patients with acute lung injury. *Thorax* **58**:983-988.

Erusalimsky JD and Moncada S (2007) Nitric oxide and mitochondrial signaling: from physiology to pathophysiology. *Arteriosclerosis, thrombosis, and vascular biology* **27**:2524-2531.

Flori HR, Ware LB, Glidden D and Matthay MA (2003) Early elevation of plasma soluble intercellular adhesion molecule-1 in pediatric acute lung injury identifies patients at increased risk of death and prolonged mechanical ventilation. *Pediatric critical care medicine : a journal of the Society of Critical Care Medicine and the World Federation of Pediatric Intensive and Critical Care Societies* **4**:315-321.

Flori HR, Ware LB, Milet M and Matthay MA (2007) Early elevation of plasma von Willebrand factor antigen in pediatric acute lung injury is associated with an increased risk of death and prolonged mechanical ventilation. *Pediatric critical care medicine : a journal of the Society of Critical Care Medicine and the World Federation of Pediatric Intensive and Critical Care Societies* **8**:96-101.

Fortis S, Spieth PM, Lu WY, Parotto M, Haitsma JJ, Slutsky AS, Zhong N, Mazer CD and Zhang H (2012) Effects of anesthetic regimes on inflammatory responses in a rat model of acute lung injury. *Intensive care medicine* **38**:1548-1555.

Fowler AA, Hamman RF, Good JT, Benson KN, Baird M, Eberle DJ, Petty TL and Hyers TM (1983) Adult respiratory distress syndrome: risk with common predispositions. *Annals of internal medicine* **98**:593-597.

Furchgott RF and Vanhoutte PM (1989) Endothelium-derived relaxing and contracting factors. *FASEB journal : official publication of the Federation of American Societies for Experimental Biology* **3**:2007-2018.

Gasse P, Mary C, Guenon I, Noulin N, Charron S, Schnyder-Candrian S, Schnyder B, Akira S, Quesniaux VF, Lagente V, Ryffel B and Couillin I (2007) IL-1R1/MyD88 signaling and the

inflammasome are essential in pulmonary inflammation and fibrosis in mice. *The Journal of clinical investigation* **117**:3786-3799.

Gaston B, Singel D, Doctor A and Stamler JS (2006) S-nitrosothiol signaling in respiratory biology. *American journal of respiratory and critical care medicine* **173**:1186-1193.

Gebistorf F, Karam O, Wetterslev J and Afshari A (2016) Inhaled nitric oxide for acute respiratory distress syndrome (ARDS) in children and adults. *The Cochrane database of systematic reviews*:CD002787.

Geissmann F, Manz MG, Jung S, Sieweke MH, Merad M and Ley K (2010) Development of monocytes, macrophages, and dendritic cells. *Science* **327**:656-661.

Genovese T, Cuzzocrea S, Di Paola R, Failla M, Mazzon E, Sortino MA, Frasca G, Gili E, Crimi N, Caputi AP and Vancheri C (2005) Inhibition or knock out of inducible nitric oxide synthase result in resistance to bleomycin-induced lung injury. *Respiratory research* **6**:58.

Gomes RF and Bates JH (2002) Geometric determinants of airway resistance in two isomorphic rodent species. *Respiratory physiology & neurobiology* **130**:317-325.

Gomez IG, Tang J, Wilson CL, Yan W, Heinecke JW, Harlan JM and Raines EW (2012) Metalloproteinase-mediated Shedding of Integrin beta2 promotes macrophage efflux from inflammatory sites. *The Journal of biological chemistry* **287**:4581-4589.

Gordon S (2003) Alternative activation of macrophages. *Nature reviews Immunology* **3**:23-35.

Gordon S and Martinez FO (2010) Alternative activation of macrophages: mechanism and functions. *Immunity* **32**:593-604.

Gordon S and Taylor PR (2005) Monocyte and macrophage heterogeneity. *Nature reviews Immunology* **5**:953-964.

Goss CH, Brower RG, Hudson LD, Rubenfeld GD and Network A (2003) Incidence of acute lung injury in the United States. *Critical care medicine* **31**:1607-1611.

Gow AJ, Farkouh CR, Munson DA, Posencheg MA and Ischiropoulos H (2004) Biological significance of nitric oxide-mediated protein modifications. *American journal of physiology Lung cellular and molecular physiology* **287**:L262-268.

Grasemann H, Gaston B, Fang K, Paul K and Ratjen F (1999) Decreased levels of nitrosothiols in the lower airways of patients with cystic fibrosis and normal pulmonary function. *The Journal of pediatrics* **135**:770-772.

Greene KE, Wright JR, Steinberg KP, Ruzinski JT, Caldwell E, Wong WB, Hull W, Whitsett JA, Akino T, Kuroki Y, Nagae H, Hudson LD and Martin TR (1999) Serial changes in surfactant-associated proteins in lung and serum before and after onset of ARDS. *American journal of respiratory and critical care medicine* **160**:1843-1850.

Groves AM, Johnston CJ, Misra RS, Williams JP and Finkelstein JN (2015) Whole-Lung Irradiation Results in Pulmonary Macrophage Alterations that are Subpopulation and Strain Specific. *Radiation research* **184**:639-649.

Guan F, Li G, Liu AB, Lee MJ, Yang Z, Chen YK, Lin Y, Shih W and Yang CS (2012) delta- and gamma-tocopherols, but not alpha-tocopherol, inhibit colon carcinogenesis in azoxymethane-treated F344 rats. *Cancer Prev Res (Phila)* **5**:644-654.

Guo C, Atochina-Vasserman E, Abramova H, George B, Manoj V, Scott P and Gow A (2016) Role of NOS2 in pulmonary injury and repair in response to bleomycin. *Free radical biology & medicine* **91**:293-301.

Guo CJ, Atochina-Vasserman EN, Abramova E, Foley JP, Zaman A, Crouch E, Beers MF, Savani RC and Gow AJ (2008) S-nitrosylation of surfactant protein-D controls inflammatory function. *PLoS biology* **6**:e266.

Guo FH and Erzurum SC (1998) Characterization of inducible nitric oxide synthase expression in human airway epithelium. *Environmental health perspectives* **106 Suppl 5**:1119-1124.

Guth AM, Janssen WJ, Bosio CM, Crouch EC, Henson PM and Dow SW (2009) Lung environment determines unique phenotype of alveolar macrophages. *American journal of physiology Lung cellular and molecular physiology* **296**:L936-946.

Hantos Z, Daroczy B, Csendes T, Suki B and Nagy S (1990) Modeling of low-frequency pulmonary impedance in dogs. *J Appl Physiol* **68**:849-860.

Hara MR, Agrawal N, Kim SF, Cascio MB, Fujimuro M, Ozeki Y, Takahashi M, Cheah JH, Tankou SK, Hester LD, Ferris CD, Hayward SD, Snyder SH and Sawa A (2005) S-nitrosylated GAPDH initiates apoptotic cell death by nuclear translocation following Siah1 binding. *Nature cell biology* **7**:665-674.

Hashimoto D, Chow A, Noizat C, Teo P, Beasley MB, Leboeuf M, Becker CD, See P, Price J, Lucas D, Greter M, Mortha A, Boyer SW, Forsberg EC, Tanaka M, van Rooijen N, Garcia-Sastre A, Stanley ER, Ginhoux F, Frenette PS and Merad M (2013) Tissue-resident macrophages self-maintain locally throughout adult life with minimal contribution from circulating monocytes. *Immunity* **38**:792-804.

Hattori Y, Nakanishi N, Kasai K, Murakami Y and Shimoda S (1996) Tetrahydrobiopterin and GTP cyclohydrolase I in a rat model of endotoxic shock: relation to nitric oxide synthesis. *Experimental physiology* **81**:665-671.

Hay J, Shahzeidi S and Laurent G (1991) Mechanisms of bleomycin-induced lung damage. *Archives of toxicology* **65**:81-94.

Hecht SM (2000) Bleomycin: new perspectives on the mechanism of action. *Journal of natural products* **63**:158-168.

Herold S, Tabar TS, Janssen H, Hoegner K, Cabanski M, Lewe-Schlosser P, Albrecht J, Driever F, Vadasz I, Seeger W, Steinmueller M and Lohmeyer J (2011) Exudate macrophages attenuate lung injury by the release of IL-1 receptor antagonist in gram-negative pneumonia. *American journal of respiratory and critical care medicine* **183**:1380-1390.

Herold S, von Wulffen W, Steinmueller M, Pleschka S, Kuziel WA, Mack M, Srivastava M, Seeger W, Maus UA and Lohmeyer J (2006) Alveolar epithelial cells direct monocyte transepithelial migration upon influenza virus infection: impact of chemokines and adhesion molecules. *Journal of immunology* **177**:1817-1824.

Hume DA, Pavli P, Donahue RE and Fidler IJ (1988) The effect of human recombinant macrophage colony-stimulating factor (CSF-1) on the murine mononuclear phagocyte system in vivo. *Journal of immunology* **141**:3405-3409.

Hung SI, Chang AC, Kato I and Chang NC (2002) Transient expression of Ym1, a heparin-binding lectin, during developmental hematopoiesis and inflammation. *Journal of leukocyte biology* **72**:72-82.

Hurshman AR, Krebs C, Edmondson DE, Huynh BH and Marletta MA (1999) Formation of a pterin radical in the reaction of the heme domain of inducible nitric oxide synthase with oxygen. *Biochemistry* **38**:15689-15696.

Ito S, Ingenito EP, Arold SP, Parameswaran H, Tgavalekos NT, Lutchen KR and Suki B (2004) Tissue heterogeneity in the mouse lung: effects of elastase treatment. *J Appl Physiol* **97**:204-212.

Jackson IL, Xu P, Hadley C, Katz BP, McGurk R, Down JD and Vujaskovic Z (2012) A preclinical rodent model of radiation-induced lung injury for medical countermeasure screening in accordance with the FDA animal rule. *Health physics* **103**:463-473.

Janssen WJ, Muldrow A, Kearns MT, Barthel L and Henson PM (2010) Development and characterization of a lung-protective method of bone marrow transplantation in the mouse. *Journal of immunological methods* **357**:1-9.

Jenkins SJ, Ruckerl D, Cook PC, Jones LH, Finkelman FD, van Rooijen N, MacDonald AS and Allen JE (2011) Local macrophage proliferation, rather than recruitment from the blood, is a signature of TH2 inflammation. *Science* **332**:1284-1288.

Jenkins SJ, Ruckerl D, Thomas GD, Hewitson JP, Duncan S, Brombacher F, Maizels RM, Hume DA and Allen JE (2013) IL-4 directly signals tissue-resident macrophages to proliferate beyond homeostatic levels controlled by CSF-1. *The Journal of experimental medicine* **210**:2477-2491.

Jensen JS, Fan X and Guidot DM (2013) Alcohol causes alveolar epithelial oxidative stress by inhibiting the nuclear factor (erythroid-derived 2)-like 2-antioxidant response element signaling pathway. *American journal of respiratory cell and molecular biology* **48**:511-517.

Ju J, Picinich SC, Yang Z, Zhao Y, Suh N, Kong AN and Yang CS (2010) Cancer-preventive activities of tocopherols and tocotrienols. *Carcinogenesis* **31**:533-542.

Kaczka DW, Hager DN, Hawley ML and Simon BA (2005) Quantifying mechanical heterogeneity in canine acute lung injury: impact of mean airway pressure. *Anesthesiology* **103**:306-317.

Katzenstein AL, Bloor CM and Leibow AA (1976) Diffuse alveolar damage--the role of oxygen, shock, and related factors. A review. *The American journal of pathology* **85**:209-228.

Kelleher ZT, Matsumoto A, Stamler JS and Marshall HE (2007) NOS2 regulation of NF-kappaB by S-nitrosylation of p65. *The Journal of biological chemistry* **282**:30667-30672.

Kelly B and O'Neill LA (2015) Metabolic reprogramming in macrophages and dendritic cells in innate immunity. *Cell research* **25**:771-784.

Kennedy DW and Abkowitz JL (1998) Mature monocytic cells enter tissues and engraft. *Proceedings of the National Academy of Sciences of the United States of America* **95**:14944-14949.

Kirby AC, Raynes JG and Kaye PM (2006) CD11b regulates recruitment of alveolar macrophages but not pulmonary dendritic cells after pneumococcal challenge. *The Journal of infectious diseases* **193**:205-213.

Kristof AS, Goldberg P, Laubach V and Hussain SN (1998) Role of inducible nitric oxide synthase in endotoxin-induced acute lung injury. *American journal of respiratory and critical care medicine* **158**:1883-1889.

Landsman L and Jung S (2007) Lung macrophages serve as obligatory intermediate between blood monocytes and alveolar macrophages. *Journal of immunology* **179**:3488-3494.

Landsman L, Varol C and Jung S (2007) Distinct differentiation potential of blood monocyte subsets in the lung. *Journal of immunology* **178**:2000-2007.

Lee TY, Chen YJ, Lu TC, Huang HD and Chen YJ (2011) SNOSite: exploiting maximal dependence decomposition to identify cysteine S-nitrosylation with substrate site specificity. *PloS one* **6**:e21849.

Liang J, Jung Y, Tighe RM, Xie T, Liu N, Leonard M, Gunn MD, Jiang D and Noble PW (2012) A macrophage subpopulation recruited by CC chemokine ligand-2 clears apoptotic cells in noninfectious lung injury. *American journal of physiology Lung cellular and molecular physiology* **302**:L933-940.

Lin HH, Faunce DE, Stacey M, Terajewicz A, Nakamura T, Zhang-Hoover J, Kerley M, Mucenski ML, Gordon S and Stein-Streilein J (2005) The macrophage F4/80 receptor is required for

the induction of antigen-specific efferent regulatory T cells in peripheral tolerance. *The Journal of experimental medicine* **201**:1615-1625.

Loke P, Nair MG, Parkinson J, Guiliano D, Blaxter M and Allen JE (2002) IL-4 dependent alternatively-activated macrophages have a distinctive in vivo gene expression phenotype. *BMC immunology* **3**:7.

Luce JM, Montgomery AB, Marks JD, Turner J, Metz CA and Murray JF (1988) Ineffectiveness of high-dose methylprednisolone in preventing parenchymal lung injury and improving mortality in patients with septic shock. *The American review of respiratory disease* **138**:62-68.

MacDonald KP, Palmer JS, Cronau S, Seppanen E, Olver S, Raffelt NC, Kuns R, Pettit AR, Clouston A, Wainwright B, Branstetter D, Smith J, Paxton RJ, Cerretti DP, Bonham L, Hill GR and Hume DA (2010) An antibody against the colony-stimulating factor 1 receptor depletes the resident subset of monocytes and tissue- and tumor-associated macrophages but does not inhibit inflammation. *Blood* **116**:3955-3963.

Mackaness GB (1962) Cellular resistance to infection. *The Journal of experimental medicine* **116**:381-406.

Malaviya R, Gow AJ, Francis M, Abramova EV, Laskin JD and Laskin DL (2015) Radiation-induced lung injury and inflammation in mice: role of inducible nitric oxide synthase and surfactant protein D. *Toxicological sciences : an official journal of the Society of Toxicology* **144**:27-38.

Malhotra D, Thimmulappa RK, Mercado N, Ito K, Kombairaju P, Kumar S, Ma J, Feller-Kopman D, Wise R, Barnes P and Biswal S (2011) Denitrosylation of HDAC2 by targeting Nrf2 restores glucocorticosteroid sensitivity in macrophages from COPD patients. *The Journal of clinical investigation* **121**:4289-4302.

Mantovani A, Sica A, Sozzani S, Allavena P, Vecchi A and Locati M (2004) The chemokine system in diverse forms of macrophage activation and polarization. *Trends in immunology* **25**:677-686.

Martinez FO and Gordon S (2014) The M1 and M2 paradigm of macrophage activation: time for reassessment. *F1000prime reports* **6**:13.

Martinez FO, Gordon S, Locati M and Mantovani A (2006) Transcriptional profiling of the human monocyte-to-macrophage differentiation and polarization: new molecules and patterns of gene expression. *Journal of immunology* **177**:7303-7311.

Martinez FO, Helming L, Milde R, Varin A, Melgert BN, Draijer C, Thomas B, Fabbri M, Crawshaw A, Ho LP, Ten Hacken NH, Cobos Jimenez V, Kootstra NA, Hamann J, Greaves DR, Locati M, Mantovani A and Gordon S (2013) Genetic programs expressed in resting and IL-4 alternatively activated mouse and human macrophages: similarities and differences. *Blood* **121**:e57-69.

Masri FA, Comhair SA, Koeck T, Xu W, Janocha A, Ghosh S, Dweik RA, Golish J, Kinter M, Stuehr DJ, Erzurum SC and Aulak KS (2005) Abnormalities in nitric oxide and its derivatives in lung cancer. *American journal of respiratory and critical care medicine* **172**:597-605.

Matthay MA and Zimmerman GA (2005) Acute lung injury and the acute respiratory distress syndrome: four decades of inquiry into pathogenesis and rational management. *American journal of respiratory cell and molecular biology* **33**:319-327.

Matute-Bello G, Downey G, Moore BB, Groshong SD, Matthay MA, Slutsky AS, Kuebler WM and Acute Lung Injury in Animals Study G (2011) An official American Thoracic Society workshop report: features and measurements of experimental acute lung injury in animals. *American journal of respiratory cell and molecular biology* **44**:725-738.

Matute-Bello G, Frevert CW and Martin TR (2008) Animal models of acute lung injury. *American journal of physiology Lung cellular and molecular physiology* **295**:L379-399.

Maus U, von Grote K, Kuziel WA, Mack M, Miller EJ, Cihak J, Stangassinger M, Maus R, Schlondorff D, Seeger W and Lohmeyer J (2002) The role of CC chemokine receptor 2 in alveolar monocyte and neutrophil immigration in intact mice. *American journal of respiratory and critical care medicine* **166**:268-273.

Maus UA, Janzen S, Wall G, Srivastava M, Blackwell TS, Christman JW, Seeger W, Welte T and Lohmeyer J (2006) Resident alveolar macrophages are replaced by recruited monocytes in response to endotoxin-induced lung inflammation. *American journal of respiratory cell and molecular biology* **35**:227-235.

McClintock D, Zhuo H, Wickersham N, Matthay MA and Ware LB (2008) Biomarkers of inflammation, coagulation and fibrinolysis predict mortality in acute lung injury. *Critical care* **12**:R41.

McNeill E, Crabtree MJ, Sahgal N, Patel J, Chuaiphichai S, Iqbal AJ, Hale AB, Greaves DR and Channon KM (2015) Regulation of iNOS function and cellular redox state by macrophage Gch1 reveals specific requirements for tetrahydrobiopterin in NRF2 activation. *Free radical biology & medicine* **79**:206-216.

McVean M and Liebler DC (1999) Prevention of DNA photodamage by vitamin E compounds and sunscreens: roles of ultraviolet absorbance and cellular uptake. *Molecular carcinogenesis* **24**:169-176.

Meduri GU, Headley AS, Golden E, Carson SJ, Umberger RA, Kelso T and Tolley EA (1998) Effect of prolonged methylprednisolone therapy in unresolving acute respiratory distress syndrome: a randomized controlled trial. *Jama* **280**:159-165.

Meduri GU, Kohler G, Headley S, Tolley E, Stentz F and Postlethwaite A (1995) Inflammatory cytokines in the BAL of patients with ARDS. Persistent elevation over time predicts poor outcome. *Chest* **108**:1303-1314.

Menzies FM, Henriquez FL, Alexander J and Roberts CW (2010) Sequential expression of macrophage anti-microbial/inflammatory and wound healing markers following innate, alternative and classical activation. *Clinical and experimental immunology* **160**:369-379.

Mert H, Yoruk I, Ertekin A, Dede S, Deger Y, Yur F and Mert N (2009) Vitamin levels in lung tissue of rats with bleomycin induced pulmonary fibrosis. *Journal of nutritional science and vitaminology* **55**:186-190.

Milberg JA, Davis DR, Steinberg KP and Hudson LD (1995) Improved survival of patients with acute respiratory distress syndrome (ARDS): 1983-1993. *Jama* **273**:306-309.

Mills CD, Kincaid K, Alt JM, Heilman MJ and Hill AM (2000) M-1/M-2 macrophages and the Th1/Th2 paradigm. *Journal of immunology* **164**:6166-6173.

Misharin AV, Morales-Nebreda L, Mutlu GM, Budinger GR and Perlman H (2013) Flow cytometric analysis of macrophages and dendritic cell subsets in the mouse lung. *American journal of respiratory cell and molecular biology* **49**:503-510.

Moore BB and Hogaboam CM (2008) Murine models of pulmonary fibrosis. *American journal of physiology Lung cellular and molecular physiology* **294**:L152-160.

Morris L, Graham CF and Gordon S (1991) Macrophages in haemopoietic and other tissues of the developing mouse detected by the monoclonal antibody F4/80. *Development* **112**:517-526.

Mosser DM and Edwards JP (2008) Exploring the full spectrum of macrophage activation. *Nature reviews Immunology* **8**:958-969.

Munson DA, Grubb PH, Kerecman JD, McCurnin DC, Yoder BA, Hazen SL, Shaul PW and Ischiropoulos H (2005) Pulmonary and systemic nitric oxide metabolites in a baboon

model of neonatal chronic lung disease. *American journal of respiratory cell and molecular biology* **33**:582-588.

Murphy J, Summer R, Wilson AA, Kotton DN and Fine A (2008) The prolonged life-span of alveolar macrophages. *American journal of respiratory cell and molecular biology* **38**:380-385.

Nakata K, Gotoh H, Watanabe J, Uetake T, Komuro I, Yuasa K, Watanabe S, Ieki R, Sakamaki H, Akiyama H, Kudoh S, Naitoh M, Satoh H and Shimada K (1999) Augmented proliferation of human alveolar macrophages after allogeneic bone marrow transplantation. *Blood* **93**:667-673.

Nathan C (2011) Is iNOS beginning to smoke? *Cell* **147**:257-258.

National Heart L, Blood Institute Acute Respiratory Distress Syndrome Clinical Trials N, Wiedemann HP, Wheeler AP, Bernard GR, Thompson BT, Hayden D, deBoisblanc B, Connors AF, Jr., Hite RD and Harabin AL (2006) Comparison of two fluid-management strategies in acute lung injury. *The New England journal of medicine* **354**:2564-2575.

Nau GJ, Richmond JF, Schlesinger A, Jennings EG, Lander ES and Young RA (2002) Human macrophage activation programs induced by bacterial pathogens. *Proceedings of the National Academy of Sciences of the United States of America* **99**:1503-1508.

Network TARDS (2000) Ventilation with lower tidal volumes as compared with traditional tidal volumes for acute lung injury and the acute respiratory distress syndrome. The Acute Respiratory Distress Syndrome Network. *The New England journal of medicine* **342**:1301-1308.

Orkin SH and Zon LI (2008) Hematopoiesis: an evolving paradigm for stem cell biology. *Cell* **132**:631-644.

Parsons PE, Eisner MD, Thompson BT, Matthay MA, Ancukiewicz M, Bernard GR, Wheeler AP and Network NARDSCT (2005) Lower tidal volume ventilation and plasma cytokine markers of inflammation in patients with acute lung injury. *Critical care medicine* **33**:1-6; discussion 230-232.

Perkins GD, McAuley DF, Thickett DR and Gao F (2006) The beta-agonist lung injury trial (BALTI): a randomized placebo-controlled clinical trial. *American journal of respiratory and critical care medicine* **173**:281-287.

Prieto J, Eklund A and Patarroyo M (1994) Regulated expression of integrins and other adhesion molecules during differentiation of monocytes into macrophages. *Cellular immunology* **156**:191-211.

Pugin J, Verghese G, Widmer MC and Matthay MA (1999) The alveolar space is the site of intense inflammatory and profibrotic reactions in the early phase of acute respiratory distress syndrome. *Critical care medicine* **27**:304-312.

Raes G, De Baetselier P, Noel W, Beschin A, Brombacher F and Hassanzadeh Gh G (2002) Differential expression of FIZZ1 and Ym1 in alternatively versus classically activated macrophages. *Journal of leukocyte biology* **71**:597-602.

Randolph GJ, Beaulieu S, Lebecque S, Steinman RM and Muller WA (1998) Differentiation of monocytes into dendritic cells in a model of transendothelial trafficking. *Science* **282**:480-483.

Ranieri VM, Suter PM, Tortorella C, De Tullio R, Dayer JM, Brienza A, Bruno F and Slutsky AS (1999) Effect of mechanical ventilation on inflammatory mediators in patients with acute respiratory distress syndrome: a randomized controlled trial. *Jama* **282**:54-61.

Razavi HM, Wang L, Weicker S, Quinlan GJ, Mumby S, McCormack DG and Mehta S (2005) Pulmonary oxidant stress in murine sepsis is due to inflammatory cell nitric oxide. *Critical care medicine* **33**:1333-1339.

Reeves PG, Nielsen FH and Fahey GC, Jr. (1993) AIN-93 purified diets for laboratory rodents: final report of the American Institute of Nutrition ad hoc writing committee on the reformulation of the AIN-76A rodent diet. *The Journal of nutrition* **123**:1939-1951.

Rivollier A, He J, Kole A, Valatas V and Kelsall BL (2012) Inflammation switches the differentiation program of Ly6Chi monocytes from antiinflammatory macrophages to inflammatory dendritic cells in the colon. *The Journal of experimental medicine* **209**:139-155.

Robbins RA, Sisson JH, Springall DR, Nelson KJ, Taylor JA, Mason NA, Polak JM and Townley RG (1997) Human lung mononuclear cells induce nitric oxide synthase in murine airway epithelial cells in vitro: role of TNFalpha and IL-1beta. *American journal of respiratory and critical care medicine* **155**:268-273.

Rosa AC, Pini A, Lucarini L, Lanzi C, Veglia E, Thurmond RL, Stark H and Masini E (2014) Prevention of bleomycin-induced lung inflammation and fibrosis in mice by naproxen and JNJ7777120 treatment. *The Journal of pharmacology and experimental therapeutics* **351**:308-316.

Roth MD and Golub SH (1993) Human pulmonary macrophages utilize prostaglandins and transforming growth factor beta 1 to suppress lymphocyte activation. *Journal of leukocyte biology* **53**:366-371.

Rubenfeld GD, Caldwell E, Peabody E, Weaver J, Martin DP, Neff M, Stern EJ and Hudson LD (2005) Incidence and outcomes of acute lung injury. *The New England journal of medicine* **353**:1685-1693.

Rudmann DG, Preston AM, Moore MW and Beck JM (1998) Susceptibility to Pneumocystis carinii in mice is dependent on simultaneous deletion of IFN-gamma and type 1 and 2 TNF receptor genes. *Journal of immunology* **161**:360-366.

Saederup N, Cardona AE, Croft K, Mizutani M, Cotleur AC, Tsou CL, Ransohoff RM and Charo IF (2010) Selective chemokine receptor usage by central nervous system myeloid cells in CCR2-red fluorescent protein knock-in mice. *PloS one* **5**:e13693.

Sangaletti S, Tripodo C, Cappetti B, Casalini P, Chiodoni C, Piconese S, Santangelo A, Parenza M, Arioli I, Miotti S and Colombo MP (2011) SPARC oppositely regulates inflammation and fibrosis in bleomycin-induced lung damage. *The American journal of pathology* **179**:3000-3010.

Santos-Silva MA, Pires KM, Trajano ET, Martins V, Nesi RT, Benjamin CF, Caetano MS, Sternberg C, Machado MN, Zin WA, Valenca SS and Porto LC (2012) Redox Imbalance and Pulmonary Function in Bleomycin-Induced Fibrosis in C57BL/6, DBA/2, and BALB/c Mice. *Toxicol Pathol*.

Schulz C, Gomez Perdiguero E, Chorro L, Szabo-Rogers H, Cagnard N, Kierdorf K, Prinz M, Wu B, Jacobsen SE, Pollard JW, Frampton J, Liu KJ and Geissmann F (2012) A lineage of myeloid cells independent of Myb and hematopoietic stem cells. *Science* **336**:86-90.

Seo SU, Kwon HJ, Ko HJ, Byun YH, Seong BL, Uematsu S, Akira S and Kweon MN (2011) Type I interferon signaling regulates Ly6C(hi) monocytes and neutrophils during acute viral pneumonia in mice. *PLoS pathogens* **7**:e1001304.

Singh B, Tiwari AK, Singh K, Singh SK, Ahmed A, Erwin PJ and Franco PM (2014) beta2 agonist for the treatment of acute lung injury: a systematic review and meta-analysis. *Respiratory care* **59**:288-296.

Singh D, Richards D, Knowles RG, Schwartz S, Woodcock A, Langley S and O'Connor BJ (2007) Selective inducible nitric oxide synthase inhibition has no effect on allergen challenge in asthma. *American journal of respiratory and critical care medicine* **176**:988-993.

Soroosh P, Doherty TA, Duan W, Mehta AK, Choi H, Adams YF, Mikulski Z, Khorram N, Rosenthal P, Broide DH and Croft M (2013) Lung-resident tissue macrophages generate Foxp3+

regulatory T cells and promote airway tolerance. *The Journal of experimental medicine* **210**:775-788.

Srivastava M, Jung S, Wilhelm J, Fink L, Buhling F, Welte T, Bohle RM, Seeger W, Lohmeyer J and Maus UA (2005) The inflammatory versus constitutive trafficking of mononuclear phagocytes into the alveolar space of mice is associated with drastic changes in their gene expression profiles. *Journal of immunology* **175**:1884-1893.

Starr A, Sand CA, Heikal L, Kelly PD, Spina D, Crabtree M, Channon KM, Leiper JM and Nandi M (2014) Overexpression of GTP cyclohydrolase 1 feedback regulatory protein is protective in a murine model of septic shock. *Shock* **42**:432-439.

Stein M, Keshav S, Harris N and Gordon S (1992) Interleukin 4 potently enhances murine macrophage mannose receptor activity: a marker of alternative immunologic macrophage activation. *The Journal of experimental medicine* **176**:287-292.

Steinberg KP, Hudson LD, Goodman RB, Hough CL, Lanken PN, Hyzy R, Thompson BT, Ancukiewicz M, National Heart L and Blood Institute Acute Respiratory Distress Syndrome Clinical Trials N (2006) Efficacy and safety of corticosteroids for persistent acute respiratory distress syndrome. *The New England journal of medicine* **354**:1671-1684.

Stroes E, Hijmering M, van Zandvoort M, Wever R, Rabelink TJ and van Faassen EE (1998) Origin of superoxide production by endothelial nitric oxide synthase. *FEBS letters* **438**:161-164.

Strosing KM, Faller S, Gyllenram V, Engelstaedter H, Buerkle H, Spassov S and Hoetzel A (2016) Inhaled Anesthetics Exert Different Protective Properties in a Mouse Model of Ventilator-Induced Lung Injury. *Anesthesia and analgesia* **123**:143-151.

Stuber F, Wrigge H, Schroeder S, Wetegrove S, Zinserling J, Hoeft A and Putensen C (2002) Kinetic and reversibility of mechanical ventilation-associated pulmonary and systemic inflammatory response in patients with acute lung injury. *Intensive care medicine* **28**:834-841.

Sunderkotter C, Nikolic T, Dillon MJ, Van Rooijen N, Stehling M, Drevets DA and Leenen PJ (2004) Subpopulations of mouse blood monocytes differ in maturation stage and inflammatory response. *Journal of immunology* **172**:4410-4417.

Suntres ZE and Shek PN (1997) Protective effect of liposomal alpha-tocopherol against bleomycin-induced lung injury. *Biomedical and environmental sciences : BES* **10**:47-59.

Tan SY and Krasnow MA (2016) Developmental origin of lung macrophage diversity. *Development* **143**:1318-1327.

Tanaka K, Ishihara T, Azuma A, Kudoh S, Ebina M, Nukiwa T, Sugiyama Y, Tasaka Y, Namba T, Sato K, Mizushima Y and Mizushima T (2010a) Therapeutic effect of lecithinized superoxide dismutase on bleomycin-induced pulmonary fibrosis. *Am J Physiol Lung Cell Mol Physiol* **298**:L348-360.

Tanaka K, Tanaka Y, Namba T, Azuma A and Mizushima T (2010b) Heat shock protein 70 protects against bleomycin-induced pulmonary fibrosis in mice. *Biochemical pharmacology* **80**:920-931.

Tarling JD and Coggle JE (1982) Evidence for the pulmonary origin of alveolar macrophages. *Cell and tissue kinetics* **15**:577-584.

Tarling JD, Lin HS and Hsu S (1987) Self-renewal of pulmonary alveolar macrophages: evidence from radiation chimera studies. *Journal of leukocyte biology* **42**:443-446.

Thiesse J, Namati E, Sieren JC, Smith AR, Reinhardt JM, Hoffman EA and McLennan G (2010) Lung structure phenotype variation in inbred mouse strains revealed through in vivo micro-CT imaging. *Journal of applied physiology* **109**:1960-1968.

Tighe RM, Liang J, Liu N, Jung Y, Jiang D, Gunn MD and Noble PW (2011) Recruited exudative macrophages selectively produce CXCL10 after noninfectious lung injury. *American journal of respiratory cell and molecular biology* **45**:781-788.

Toews GB, Vial WC, Dunn MM, Guzzetta P, Nunez G, Stastny P and Lipscomb MF (1984) The accessory cell function of human alveolar macrophages in specific T cell proliferation. *Journal of immunology* **132**:181-186.

Togeiro SM, Carneiro G, Filho FF, Zanella MT, Santos-Silva R, Taddei JA, Bittencourt LR and Tufik S (2012) Consequences of Obstructive Sleep Apnea on metabolic profile: a population-based survey. *Obesity (Silver Spring)*.

Tsou CL, Peters W, Si Y, Slaymaker S, Aslanian AM, Weisberg SP, Mack M and Charo IF (2007) Critical roles for CCR2 and MCP-3 in monocyte mobilization from bone marrow and recruitment to inflammatory sites. *The Journal of clinical investigation* **117**:902-909.

Tsoyi K, Nizamutdinova IT, Jang HJ, Mun L, Kim HJ, Seo HG, Lee JH and Chang KC (2010) Carbon monoxide from CORM-2 reduces HMGB1 release through regulation of IFN-beta/JAK2/STAT-1/INOS/NO signaling but not COX-2 in TLR-activated macrophages. *Shock* **34**:608-614.

van oud Alblas AB and van Furth R (1979) Origin, Kinetics, and characteristics of pulmonary macrophages in the normal steady state. *The Journal of experimental medicine* **149**:1504-1518.

Varol C, Landsman L, Fogg DK, Greenshtein L, Gildor B, Margalit R, Kalchenko V, Geissmann F and Jung S (2007) Monocytes give rise to mucosal, but not splenic, conventional dendritic cells. *The Journal of experimental medicine* **204**:171-180.

Vasquez-Vivar J, Martasek P, Whitsett J, Joseph J and Kalyanaraman B (2002) The ratio between tetrahydrobiopterin and oxidized tetrahydrobiopterin analogues controls superoxide release from endothelial nitric oxide synthase: an EPR spin trapping study. *The Biochemical journal* **362**:733-739.

Vasquez-Vivar J, Whitsett J, Martasek P, Hogg N and Kalyanaraman B (2001) Reaction of tetrahydrobiopterin with superoxide: EPR-kinetic analysis and characterization of the pteridine radical. *Free radical biology & medicine* **31**:975-985.

Villar J and Slutsky AS (1989) The incidence of the adult respiratory distress syndrome. *The American review of respiratory disease* **140**:814-816.

von Garnier C, Filgueira L, Wikstrom M, Smith M, Thomas JA, Strickland DH, Holt PG and Stumbles PA (2005) Anatomical location determines the distribution and function of dendritic cells and other APCs in the respiratory tract. *Journal of immunology* **175**:1609-1618.

Ware LB, Conner ER and Matthay MA (2001) von Willebrand factor antigen is an independent marker of poor outcome in patients with early acute lung injury. *Critical care medicine* **29**:2325-2331.

Ware LB, Eisner MD, Thompson BT, Parsons PE and Matthay MA (2004) Significance of von Willebrand factor in septic and nonseptic patients with acute lung injury. *American journal of respiratory and critical care medicine* **170**:766-772.

Ware LB and Matthay MA (2000) The acute respiratory distress syndrome. *The New England journal of medicine* **342**:1334-1349.

Yang J, Zhang L, Yu C, Yang XF and Wang H (2014) Monocyte and macrophage differentiation: circulation inflammatory monocyte as biomarker for inflammatory diseases. *Biomarker research* **2**:1.

Yang Z, Wang ZE, Doulias PT, Wei W, Ischiropoulos H, Locksley RM and Liu L (2010) Lymphocyte development requires S-nitrosoglutathione reductase. *Journal of immunology* **185**:6664-6669.

Yona S, Kim KW, Wolf Y, Mildner A, Varol D, Breker M, Strauss-Ayali D, Viukov S, Guilliams M, Misharin A, Hume DA, Perlman H, Malissen B, Zelzer E and Jung S (2013) Fate mapping reveals origins and dynamics of monocytes and tissue macrophages under homeostasis. *Immunity* **38**:79-91.

Zaynagetdinov R, Sherrill TP, Kendall PL, Segal BH, Weller KP, Tighe RM and Blackwell TS (2013) Identification of myeloid cell subsets in murine lungs using flow cytometry. *American journal of respiratory cell and molecular biology* **49**:180-189.